

Modulating the inflammatory response to biomaterials by mechanical stimuli : implications for in situ cardiovascular tissue engineering

Citation for published version (APA):

Ballotta, V. (2014). *Modulating the inflammatory response to biomaterials by mechanical stimuli : implications for in situ cardiovascular tissue engineering*. [Phd Thesis 1 (Research TU/e / Graduation TU/e), Biomedical Engineering]. Technische Universiteit Eindhoven. <https://doi.org/10.6100/IR780925>

DOI:

[10.6100/IR780925](https://doi.org/10.6100/IR780925)

Document status and date:

Published: 01/01/2014

Document Version:

Publisher's PDF, also known as Version of Record (includes final page, issue and volume numbers)

Please check the document version of this publication:

- A submitted manuscript is the version of the article upon submission and before peer-review. There can be important differences between the submitted version and the official published version of record. People interested in the research are advised to contact the author for the final version of the publication, or visit the DOI to the publisher's website.
- The final author version and the galley proof are versions of the publication after peer review.
- The final published version features the final layout of the paper including the volume, issue and page numbers.

[Link to publication](#)

General rights

Copyright and moral rights for the publications made accessible in the public portal are retained by the authors and/or other copyright owners and it is a condition of accessing publications that users recognise and abide by the legal requirements associated with these rights.

- Users may download and print one copy of any publication from the public portal for the purpose of private study or research.
- You may not further distribute the material or use it for any profit-making activity or commercial gain
- You may freely distribute the URL identifying the publication in the public portal.

If the publication is distributed under the terms of Article 25fa of the Dutch Copyright Act, indicated by the "Taverne" license above, please follow below link for the End User Agreement:

www.tue.nl/taverne

Take down policy

If you believe that this document breaches copyright please contact us at:

openaccess@tue.nl

providing details and we will investigate your claim.

**Modulating the inflammatory response to
biomaterials by mechanical stimuli**

**Implications for *in situ* cardiovascular
tissue engineering**

Virginia Ballotta

Financial support by the Dutch Heart Foundation for the publication of this thesis is gratefully acknowledged.



A catalogue record is available from the Eindhoven University of Technology Library
ISBN: 978-90-386-3686-3

Copyright © 2014 by V.Ballotta

All rights reserved. No part of this book may be reproduced, stored in a database or retrieval system, or published, in any form or in any way, electronically, mechanically, by print, photo print, microfilm or any other means without prior permission by the author.

Cover design by Alberto Leopaldi and Anthal Smits

Printed by: Proefschriftmaken.nl || Uitgeverij BOXPress

This research forms part of the Project P1.01 iValve of the research program of the BioMedical Materials institute, co-funded by the Dutch Ministry of Economic Affairs.

The research described in this thesis was supported by a grant of the Dutch Heart Foundation (iValve – DHF 2008T089)

Modulating the inflammatory response to biomaterials by mechanical stimuli.

Implications for in situ cardiovascular tissue engineering.

PROEFSCHRIFT

ter verkrijging van de graad van doctor aan de Technische Universiteit Eindhoven, op gezag van de rector magnificus prof.dr.ir. C.J. van Duijn, voor een commissie aangewezen door het College voor Promoties, in het openbaar te verdedigen op maandag 29 september 2014 om 16:00 uur

door

Virginia Ballotta

geboren te Milaan, Italië

Dit proefschrift is goedgekeurd door de promotoren en de samenstelling van de promotiecommissie is als volgt:

voorzitter:	prof.dr. K. Nicolaij
1 ^e promotor:	prof.dr.ir. F.P.T. Baaijens
2 ^e promotor:	prof.dr. C.V.C. Bouten
copromotor(en):	dr. A. Driessen-Mol
leden:	Prof.Dr.med.Dr.rer.nat. S. Hoerstrup (University of Zurich) prof.dr. M.C. Verhaar (UMCU) prof.dr. K. Ito
adviseur(s):	dr. P.Y.W. Dankers

Dedicated to Alberto and to myself

“If we knew what we were doing, it wouldn't be called research”

(Attributed to Albert Einstein, physicist, 1879-1955)

Table of contents

SUMMARY	V
1 GENERAL INTRODUCTION	1
1.1 THE TARGET: CARDIOVASCULAR TISSUES	2
1.1.1 Semilunar heart valves	3
1.1.2 Small caliber blood vessels	5
1.1.3 New perspectives for cardiovascular tissue replacements	7
1.2 THE CHALLENGE: TUNING THE HOST RESPONSE TO BIOMATERIALS	8
1.2.1 The four phases of the host response	8
1.2.2 Critical role of macrophages	10
1.2.3 Modulation of macrophage polarization with biomaterial design	11
1.3 THE METHOD: ENGINEERED CONSTRUCTS TOWARDS <i>IN SITU</i> REGENERATION	13
1.3.1 Clinical and pre-clinical studies	13
1.3.2 Hemodynamics and tissue regeneration	15
1.3.3 Design of responsive scaffolds	15
1.4 RATIONALE, AIM AND OUTLINE OF THE THESIS	18
2 SHEAR FLOW AFFECTS SELECTIVE MONOCYTE RECRUITMENT INTO MCP-1- LOADED SCAFFOLDS	19
ABSTRACT	20
2.1 INTRODUCTION	21
2.2 MATERIALS AND METHODS	23
2.2.1 Electrospinning	23
2.2.2 MCP-1 loading	23
2.2.3 MCP-1 release	24
2.2.4 Cell isolation	24
2.2.5 Cell characterization	24
2.2.6 Chemotaxis assays	25
2.2.7 Flow experiments	26
2.2.8 Immunostainings	26
2.2.9 SEM	27
2.2.10 qPCR and gene expression analysis	27
2.2.11 Statistical analysis	27
2.3 RESULTS	29

Table of contents

2.3.1 Hybrid PCL/fibrin scaffolds demonstrate a burst-release of MCP-1	29
2.3.2 Baseline cell composition comprises biological inter-donor variations	29
2.3.3 MCP-1-loaded scaffolds induce highly specific chemotaxis of monocyte subsets	31
2.3.4 Flow experiments	33
2.4 DISCUSSION	37
ACKNOWLEDGEMENTS	40
3 STRAIN-DEPENDENT MODULATION OF MACROPHAGE POLARIZATION WITHIN SCAFFOLDS	41
ABSTRACT	42
3.1 INTRODUCTION	43
3.2 MATERIALS AND METHODS	45
3.2.1 Experimental layout	45
3.2.2 Scaffold preparation	45
3.2.3 Scaffold seeding and culture	46
3.2.4 Analyses	47
3.3 RESULTS	52
3.3.1 Scaffold characterization and strain validation	52
3.3.2 Gene expression analysis	53
3.3.3 Macrophage phenotype assessment and quantification via immunostaining	54
3.3.4 Quantitative analysis and immunostaining of extracellular matrix markers	57
3.4 DISCUSSION	59
3.5 CONCLUSION	62
ACKNOWLEDGMENTS	62
4 SYNERGISTIC PROTEIN SECRETION BY MESENCHYMAL STROMAL CELLS SEEDED IN 3D SCAFFOLDS AND CIRCULATING LEUKOCYTES IN PHYSIOLOGICAL FLOW	63
ABSTRACT	64
4.1 INTRODUCTION	64
4.2 MATERIALS AND METHODS	66
4.2.1 Cell culture and characterization	66
4.2.2 Scaffold preparation	66
4.2.3 Cell seeding	67
4.2.4 Strain experiments	68
4.2.5 Chemotaxis assay	69
4.2.6 Fluidics model	69
4.2.7 Flow cytometry and gating strategy	70

4.2.8 Multiplex ELISA	71
4.2.9 qPCR	72
4.2.10 Immunostainings	73
4.2.11 Statistical analysis	74
4.3 RESULTS	74
4.3.1 Scaffold and cell characterization	74
4.3.2 Cell-scaffold interactions statically and under cyclic strain	75
4.3.3 Chemotaxis assays	77
4.3.4 Cell behavior in pulsatile flow conditions	80
4.3.5 Synergistic protein secretion	83
4.4 DISCUSSION	85
ACKNOWLEDGMENTS	89
5 GENERAL DISCUSSION	91
5.1 SUMMARY AND MAIN FINDINGS	92
5.2 TOWARDS THE DESIGN OF IMMUNOMODULATORY SCAFFOLDS	95
5.2.1 Design of synthetic scaffolds	95
5.2.2 Synthetic scaffolds under mechanical forces	96
5.2.3 Unseeded vs seeded scaffold	99
5.3 STUDY LIMITATIONS AND FUTURE PERSPECTIVES	103
5.4 CONCLUSIONS	106
APPENDIX A	107
BIBLIOGRAPHY	109
NEDERLANDSE SAMENVATTING	123
ACKNOWLEDGEMENTS	125
CURRICULUM VITAE	127
LIST OF PUBLICATIONS	129

Summary

Several tissue engineering strategies were developed to obtain cardiovascular constructs able to integrate and regenerate within the body. A clinically relevant concept for replacement of cardiovascular defects proposes to implant either bare synthetic scaffolds or synthetic scaffolds seeded with autologous cells, entrusting the host inflammatory response to promote successful integration of the construct. The aim of this thesis is to provide a deeper insight into the modulation of the inflammatory response by mechanical forces acting on implanted load-bearing cardiovascular constructs, such as heart valves and arteries. More specifically, the effect of strain and shear stress on immune cell recruitment, differentiation, and signaling in synthetic scaffolds was investigated.

Monocyte chemoattractant protein-1 (MCP-1) is considered by others a key player in regeneration of synthetic scaffolds. The first part of this thesis aims at elucidating the response of subsets of circulating immune cells to a scaffold loaded with MCP-1. Using migration assays, we demonstrated that MCP-1 selectively attracts angiogenic and reparative circulating monocytes and fibrocytes. In conditions of pulsatile flow, on the other hand, a marked increase in immediate monocyte recruitment was observed, but without evident specificity in monocyte subsets. This suggests that the recruitment selectivity is dependent on the release kinetics of the MCP-1, as it is overruled by the effect of shear stress after the initial burst-release.

After investigating cell recruitment, we focused on the effect of cyclic strain on the adherent cells. We selected human peripheral blood mononuclear cells (PBMCs) as the immune cell source representative of the population of cells infiltrating into a synthetic scaffold *in vivo*. PBMCs were seeded into electrospun scaffolds of bisurea-modified polycaprolactone thermoplastic elastomers and subjected to a range of cyclic deformations in a FlexCell® tension system. We showed that PBMCs differentiate into macrophages upon contact with the scaffold and that moderate strain levels (below 7%) promote polarization of these macrophages toward an anti-inflammatory, pro-tissue-healing macrophage phenotype. These results suggest that macrophage polarization might be controlled by adapting the mechanical properties of the synthetic scaffolds, therefore tuning the resulting strain.

Monocyte-derived macrophage infiltration was shown to be enhanced by the incorporation of autologous cells into the synthetic scaffolds prior to implantation, but the underlying mechanism is not clear. In the final part of this thesis, we included pre-seeded cells into the synthetic scaffolds to identify the signaling factors involved in immune cell

Summary

recruitment and wound healing, which are secreted by the pre-seeded cells in the presence of physiological strain and shear flow. We demonstrated that human mesenchymal stromal cells (MSC) seeded onto PCL-based electrospun scaffolds are responsible for the synthesis of the immunomodulatory and trophic factors MCP-1, vascular endothelial growth factor (VEGF), and basic fibroblast growth factor (bFGF), and their release is not influenced by strain. On the other hand, a synergistic increase in bFGF protein production by MSC exposed to circulating PBMC in pulsatile flow was observed. Similarly, the gene expression of SDF-1 α factor, involved in tissue repair, was synergistically upregulated by MSC exposed to immune cells.

In conclusion, when aiming for acellular replacements, MCP-1, SDF-1 α , and bFGF are promising immunoregulatory and trophic factors, that may be included as bioactive components into the scaffolds, but their release kinetics at the site of implantation should be finely tuned to account for shear stress effects. Furthermore, mechanical properties of the scaffold should be designed as such that adherent cells are exposed to moderate strains (in the order of 7%). The results obtained in this thesis serve to tailor instructive scaffolds for *in situ* cardiovascular regenerative therapies.

1

General introduction

Cardiovascular tissue engineering aims at generating viable and autologous substrates capable of growing and remodeling *in vivo*, thus providing a functional alternative to current treatments for the repair of damaged or diseased tissues, including heart valves and blood vessels. The *in situ* approach of tissue engineering represents a promising route to deliver cell-free, off-the-shelf constructs able to restore functionality and provide living replacements, by harnessing the host inflammatory response or by selective recruitment of specific cell types. We hypothesized that circulating immune cells activated by the implant and recruited shortly after implantation play a crucial role in the long term tissue regeneration. The design of advanced biomaterials able to modulate the early immune response represents therefore the key challenge of such approach. Furthermore, cardiovascular tissues are exposed to a complex hemodynamic environment, involving a wide range of loads, that can significantly affect cell recruitment and fate, and influence extra cellular matrix formation. The aim of the present work is to elucidate the impact of biophysical cues, such as shear and tensile stress, on the interactions between cells and scaffolds. The acquired knowledge could serve to design constructs able to tune the early immune response and guide later tissue formation towards final regeneration.

1.1 The target: cardiovascular tissues

The cardiovascular system enables the blood circulation through the body, thus providing transport of oxygen, nutrients and hormones, removal of waste products, signalling for the immune system and heat distribution. The central organ of the human cardiovascular system is the heart, a hollow muscle consisting of two pumps that work synchronously, but in series, to direct the blood through the pulmonary and the system circulation. Unidirectional blood flow during the cardiac cycle is ensured by four heart valves, classified as atrio-ventricular or inflow (tricuspid and mitral) and semilunar or outflow (pulmonary and aortic) valves (Butcher *et al.*, 2011). The vascular system distributes the blood to the tissues through a dense network of vessels, organized in arteries, capillaries and veins. During each cardiac cycle, the pumping action of the heart and the consequent blood flow result in a wide range of loads acting on the components of the cardiovascular system. The following paragraphs will provide a description of the basic anatomy and physiology of semilunar heart valves and small caliber blood vessels. These structures represent relevant targets for cardiovascular tissue engineering, due to the severe risks connected to their failure and the lack of optimal substitutes (Bouten *et al.*, 2011).

1.1.1 Semilunar heart valves

Essential anatomy and physiology

Semilunar heart valves consist of three half-moon shaped leaflets with a layered architecture. The outflow side (fibrosa) is composed by dense collagen fibers oriented circumferentially, that provide mechanical strength to the valve. The preferred orientation of the collagen fibers result in anisotropic behavior: the leaflet can withstand high tensile stresses in the circumferential direction, thus preventing prolapse and retrograde flow, and the high compliance in the radial direction allows for proper coaptation of the orifice area (Schoen, 2012). The central core of the leaflets (spongiosa) consists of loosely arranged connective tissue rich in highly hydrated glycosaminoglycans (GAGs) that lubricate the adjacent layers and cushion compressive forces during the cardiac cycle. GAGs also play a role in sequestration of soluble compounds, serving as a reservoir for cell signaling molecules (Sacks *et al.*, 2009; Franz *et al.*, 2011). The inflow layer (ventricularis) consists of an organized network of elastin that ensures leaflet flexibility and guides collagen fiber reorientation during valve unloading (Vesely, 1998). The valve surface in contact with the blood is covered by a monolayer of endothelial cells, while most of the cellular component within the leaflet is represented by valvular interstitial cells.

Biomechanical environment

The aortic and the pulmonary valves prevent retrograde blood flow into the ventricle during the diastolic phase and are exposed to stresses of different amplitude, as result of the different downstream environments. The aortic valve opens during the systolic phase in response to the ventricular contraction and blood flows through the leaflet with a peak velocity of 1.2 m/s, generating laminar shear stresses on the ventricular surfaces (Figure 1.1A) (Otto, 2001). In presence of a flow rate of 5 l/min and a heart rate of 70 beats/min, the ventricular side is subjected to a unidirectional, pulsatile shear stress with a sinusoidal waveform, varying from 0 to 7,1 Pa , while the aortic surface is exposed to oscillatory shear stresses with a peak of 2 Pa (Yap *et al.*, 2012). During diastole, the ventricle relaxes and the valve closes, being exposed to a pressure difference of 80 mmHg, that induces strains of 10-20% in the circumferential direction and 40-60% in the radial direction (Figure 1.1B) (Guyton & Hall, 2000; Choon Hwai Yap , Hee-Sun Kim , Kartik Balachandran , Michael Weiler , Rami Haj-Ali, 2010; Butcher *et al.*, 2011). The pulmonary valve is exposed to a similar profile, but to a significantly lower transvalvular pressure (10 mmHg).

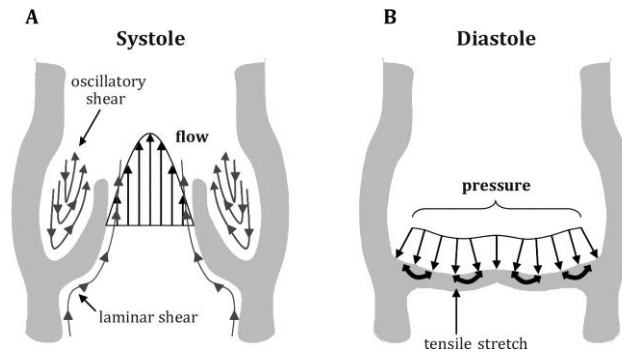


Figure 1.1 Semilunar valves kinematics. A) During the systolic phase, the blood flow induces shear stresses on the surfaces of the open leaflets. B) During the diastole, the blood pressure applied on the closed leaflets generates local deformations. Adapted from (Arjunon *et al.*, 2013)

Disease and replacements

Heart valve diseases represent a major health problem worldwide. The number of valvular replacements needed every year is in constant growth, as result of the increased incidence of valve degeneration inevitably connected to the rise in life expectancy (d'Arcy *et al.*, 2011). Besides the progressive valve stiffening related to aging, valves can be affected by congenital defects, nodular calcification, fibrous thickening or endocarditis (Schoen, 2012). When valvular functions are severely impaired, stenosis or insufficiency occur and the valve requires surgical repair or replacement. Aortic and pulmonary valves are often not suitable for valvuloplasty, therefore replacement remains the most common procedure for their treatment (Friedewald *et al.*, 2007).

Currently available prostheses are classified as mechanical and biological. Mechanical valves offer long-term durability, but their tendency to induce thromboembolic complications imposes to the recipients a daily anticoagulation therapy. Bioprostheses of human or animal origin do not require anticoagulant treatment, but are prone to degeneration and calcification, that lead to the need for reoperation (Mol *et al.*, 2009). Beyond their specific limitations, a fundamental problem related to the mechanical and biological valves is their incompetence to repair, remodel and grow. The inherent lack of these capabilities makes the current prostheses suboptimal, especially for pediatric patients, that need to undergo stages interventions during their childhood.

1.1.2 Small caliber blood vessels

Essential anatomy and physiology

The blood vessels are tubular structures organized in three concentric layers. The luminal side is covered by confluent endothelial cells residing on a basal membrane and oriented in the direction of the main flow. The endothelium absorbs the nutrient from the circulating blood and is involved in the control of vasomotor tone, blood cell trafficking, hemostatic balance and immune response. The intermediate layer consists of smooth muscle cells oriented circumferentially that set the vascular tone and regulate the blood flow, and of elastin fibers that provide for elastic recoil. The external layer is composed by a matrix of collagen fibers organized in the longitudinal direction, which supply mechanical strength to the vessel. Only the capillaries do not present a layered structure, as they consist exclusively of small endothelial linings that allow rapid exchange of products and gases between the blood and the tissues.

The anatomy of the blood vessels is strictly connected to their function and location in the vascular system. Moving distally from the heart, the decrease in blood pressure is reflected in a change of diameter and morphology of the vessels. Large arteries are compliant and elastic, to accommodate changes in blood volume, while in small muscular arteries ($\varnothing=0.3-6$ mm) a predominance of smooth muscle cells in the medial layers provides the contractile force to allow for continuous blood circulation. The coronary arteries, that supply the heart with nutrients and oxygen, typically exhibit a diameter of 3-4 mm and a wall thickness of 1 mm and are therefore considered as small arteries. The veins carry the blood towards the heart with increasing diameter from the peripheral districts and display large internal lumen and limited presence of muscular components (Marieb, 2001).

Biomechanical environment

The pumping action of the heart generates a pulsatile blood flow, that results in cyclic stresses acting on the arteries (Figure 1.2 A). In particular, the hydrostatic pressure induces radial deformations of the vessel and circumferential tensile strain in the wall (Figure 1.2B), while the flow causes shear stresses on the endothelium (Figure 1.2C). Moreover, the physiological pre-stretch of the vessels results in a longitudinal elongation.

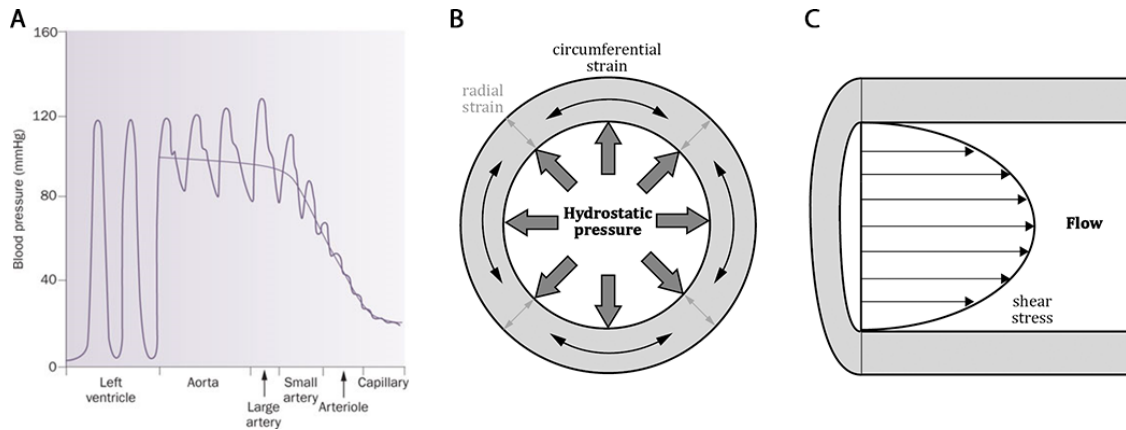


Figure 1.2 Hemodynamics of the small caliber arteries. A) Pulsatile blood pressure in the arteries is induced by the periodic contraction of the left ventricle. Adapted from (Safar, 2010). B-C) Schematic representation of the force acting on small caliber arteries: the hydrostatic pressure of the blood causes cyclic strains on the vessel walls in radial and circumferential direction, while the blood flow induces wall shear stresses.

Small arteries are exposed to high pressures (70-120 mmHg) that induce circumferential strain of 10-15% in the medial layer, while the axial pre-stretch is approximately around 30% (van Andel *et al.*, 2003). The laminar blood flow within the vessel generates a parabolic velocity profile and a wall shear stress of 1-2 Pa, that can be sensed by the endothelial cells (Soulis *et al.*, 2006).

Disease and replacements

Vascular diseases pose a great economic and social burden. Coronary artery disease alone requires 800,000 bypasses per year, while peripheral arterial disease affects 10% of the worldwide population, increasing to 30% for patients above 50 years of age (Tendera *et al.*, 2011; Mascarenhas *et al.*, 2014). The most common pathology affecting small arteries is atherosclerosis, an inflammatory process in which lipid rich plaques are deposited within the arterial walls. Large plaques or plaque ruptures can obstruct the lumen, causing hypoxia and ischemia of the downstream tissues with the associated vascular complications (Jaipersad *et al.*, 2014). Furthermore, atherosclerotic arterial walls are weakened and prone to aneurysmal dilation, which can lead to rupture of the vessel.

From a clinical point of view, reparative surgery, such as angioplasty or stent application, is preferred for the treatment of partially occluded arteries. When the obstruction of the lumen is severe, the artery section must be replaced or by-passed with a graft. Autologous grafts are not always available in diseased patients, while synthetic graft are susceptible to hyperplasia, coagulation and thrombogenesis when used to replace

small-diameter conduits (Huang & Niklason, 2014). The high incidence of small artery diseases combined with the limited availability of vascular substitutes results in the critical demand for off-the-shelf grafts with improved mechanical and biological properties.

1.1.3 New perspectives for cardiovascular tissue replacements

The lack of optimal replacements for cardiovascular tissues generated the need for functional and clinically relevant alternatives. Tissue engineering emerged as a new, evolving field that proposed to regenerate the damaged tissues by creating a living, autologous substitute. The traditional approach of tissue engineering comprises the isolation of cells from a patient, their culture *in vitro* on a scaffold until native-like tissue is formed, and the final implantation into the patient from whom the cells were obtained. The inherent shortcomings of the laboratory practice, e.g. time and economical resources required and entailed risk of infection, encouraged the pursuing of alternative approaches in which the *in vitro* step could be neglected. The concurrent development of advanced synthetic materials able to biodegrade and selectively interact with biomolecules and cells, encouraged the design of instructive substrates, intended to harness the regenerative potential of the body. The new *in situ* paradigm proposes to adopt such innovative biomaterials to elicit, upon implantation, a positive wound healing response, followed by integration and remodeling of the constructs. In order to tailor effective substrates for tissue regeneration, a profound awareness of the mechanisms that modulate the host response to the biomaterial is required. An overview of the current knowledge on immune response to implants will be presented in the following section.

1.2 **The challenge: tuning the host response to biomaterials**

The implantation of a biomaterial into the body is accompanied by the injury induced by the surgical procedure, that results in a physiological wound healing response. The damage provoked to a vascularized tissue initiates an hemostatic process, immediately followed by acute and chronic inflammation response and, lastly, by a foreign body reaction that will lead to fibrosis or regeneration. Each phase of the wound healing occurs in a sequential fashion and comprises cell migration, activation, differentiation and apoptosis, as well as complex interplays between the numerous cell populations involved (Figure 1.3) (Palsson & Bhatia, 2004).

1.2.1 **The four phases of the host response**

Hemostasis (seconds to minutes)

The first response to the injury is provided by the damaged vascular system, which covers the biomaterials with blood and proteins. This layer of proteins determines the activation of the coagulation cascade, complement system and platelets, and guides the formation of a fibrin clot, that serves as a provisional matrix. The platelets trapped in the provisional matrix release chemoattractants involved in immune cells recruitment, while several proteins absorbed onto the biomaterial surface, such as fibrinogen, fibronectin and vitronectin, offer binding sites for integrins, the major adhesion receptors of leukocytes (Hynes, 2002; Anderson *et al.*, 2008). A further mechanism to attract immune-competent cells consists in the release of alarmins, dangers signals secreted by cells dying in a “non-programmed way” following injury and capable of activating immune cells at the biomaterial surface (Bianchi, 2007).

Inflammation (minutes to days)

The first immune cells that migrate to the implant site during the acute phase of inflammation are the neutrophils, polymorphonuclear leukocytes able to phagocyte foreign particles up to 10 μm in diameter. In presence of larger implants, they respond by degranulation and release of proteolytic enzymes and reactive oxygen species (ROS), intended to undermine and corrode the surface of the biomaterial. Moreover, activated neutrophils secrete important chemokines, such as IL-8, that recruits additional neutrophils, but also MCP-1 and MIP- β 1, potent chemoattractants for monocytes, that

represent the second line of defense (Kobayashi *et al.*, 2005; Gonzalez-simon & Eniola-adeleso, 2012).

Monocytes arriving at the implantation site differentiate into macrophages, the phagocytic leukocytes that characterize the chronic inflammation stage. Macrophages can phagocytose wound debris and adhere to the surface of the biomaterial. Moreover, they secrete a wide range of pro- and anti-inflammatory factors that play a critical role towards the persistence of the inflammation, and therefore the failure of the implant, or the reparative proliferative phase. During chronic inflammation, also lymphocytes appear at the implant site and participate in macrophage activation and fusion into foreign body giant cells (Franz *et al.*, 2011). The role of macrophages and their interaction with lymphocytes will be further described in 1.2.2 and 1.2.3.

Proliferative phase (days to weeks)

The resolution of the chronic inflammation and initiation of the foreign body reaction is indicated by the infiltration of fibroblasts and endothelial cells. Macrophage and fibroblast participate to the deposition and remodeling of the granulation tissue to repair the wound and cover the implant. The granulation tissue consists in a loose matrix of fibronectin, collagen and hyaluronic acid, vascularized by endothelial cells and intended to restore structure and homeostasis at the inflammation site (Anderson & McNally, 2011). In this phase, macrophages fuse into foreign body giant cells to attempt the phagocytosis of larger particles and the degradation of the biomaterial, via oxidative and enzymatic processes.

Remodeling phase (weeks to year)

The granulation tissue deposited by fibroblast undergoes long-term remodeling. During this phase, the amount of newly formed blood vessels and infiltrated fibroblasts diminishes, in favor of repopulation by the tissue-resident cells and formation of the organized extracellular matrix. Restoration of the normal tissue architecture and function would be the ideal outcome of any implantation, but biomaterials are often associated with impaired wound healing and fibrous encapsulation.

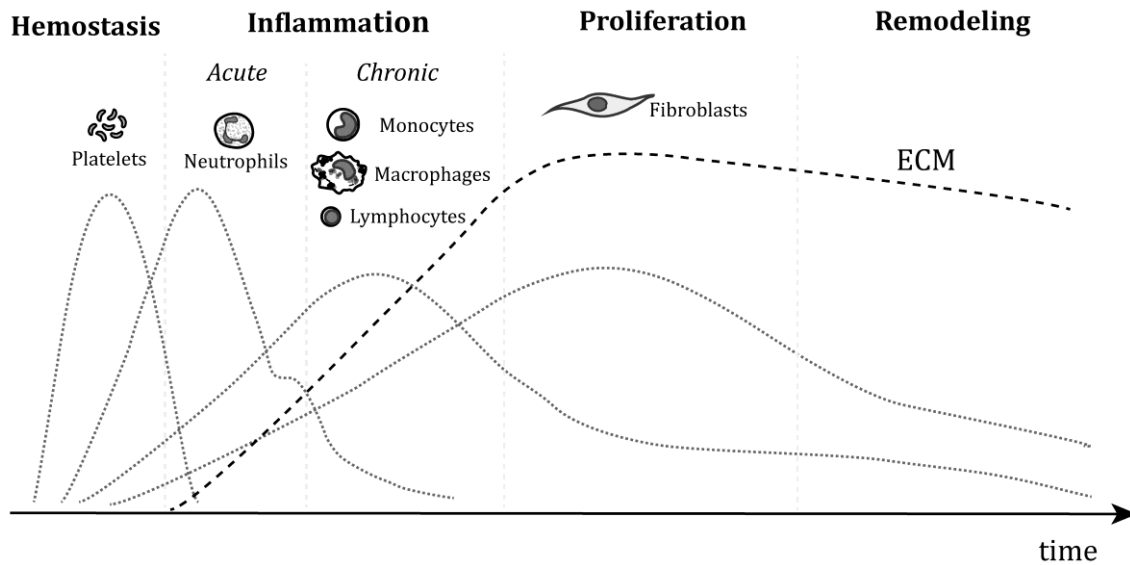


Figure 1.3 The four phases of wound healing. Adapted from (van Loon *et al.*, 2013).

1.2.2 Critical role of macrophages

Macrophages have been considered as prominent immune effector cells for long time. Il'ja Il'ič Mečnikov won the Nobel Prize in 1908 for discovering the phagocytic function of macrophages and suggested that the key to immunity was to “stimulate the phagocytes” (Nathan, 2008). Pioneering studies of the 1970s demonstrated that macrophages play a prominent role in wound healing through their ability of debridement and stimulation of fibroblast proliferation and angiogenesis (Leibovich & Ross, 1975; Poverini *et al.*, 1977). Recent analyses of the exceptional wound healing in salamanders, animals capable of self-regeneration, proved that systemic depletion of macrophages leads to failure of limb growth after amputation, but the full regenerative capacity can be restored by replenishment of the endogenous macrophage population (Godwin *et al.*, 2013).

To this day, macrophages have been identified as key players of the wound healing, but the underlying mechanisms of action remain incompletely understood. Regenerative potential of macrophages might lie in their remarkable plasticity, as they can exhibit different phenotypes and functionalities in response to varying environmental cues (Koh & DiPietro, 2011). A first classification of macrophage polarization states was based on the relative function and identified two main subsets, referred to as M1 and M2 and considered the extremes of a continuum (Figure 1.4).

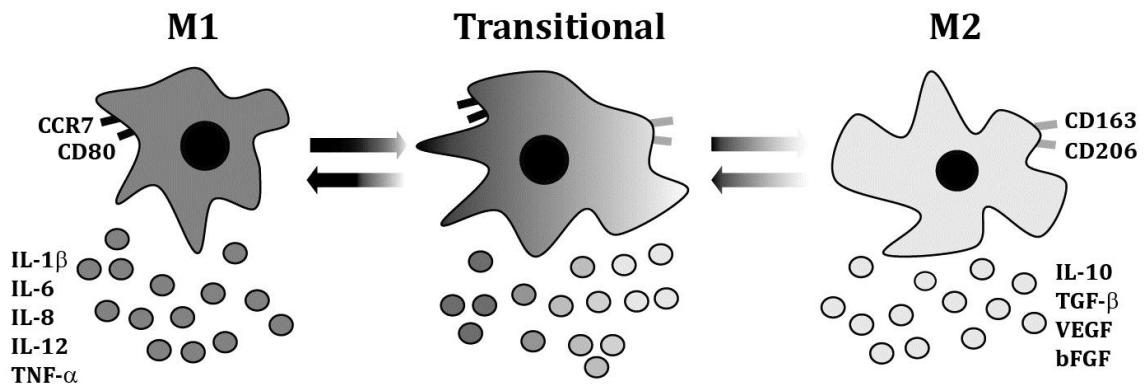


Figure 1.4 Plasticity of macrophages. The classically activated M1 macrophages exhibit CCR7 and CD80 surface markers and release inflammatory cytokines (dark grey circles). The M2 subset is an heterogeneous group of regulatory and wound-healing macrophages, expressing CD163 and CD206 surface markers and releasing factors towards inflammation resolution and tissue remodeling (light grey circles). The transition between M1 and M2 results in an intermediate polarization state, with characteristics and functions of both subsets (adapted from Brown & Badylak, 2013).

The M1 or “classically activated” macrophages exert phagocytic and degradative activity and secrete pro-inflammatory cytokines, such as IL-1 β , IL-6, IL-12 and TNF- α , as well as monocyte attractant factors, such as IL-8, MCP-1, and MIP-1 β . The “alternatively activated” M2 subset promotes immunoregulation and wound healing and releases high levels of anti-inflammatory cytokines, such as IL-10 (Mantovani *et al.*, 2004). Others have indicated classically activated (M1), wound-healing (M2a) and regulatory (M2b) subsets as three distinct categories, in which all intermediate states of polarization are conceivable, as macrophage can acquire transitional phenotypes with hybrid features (Mosser & Edwards, 2008). The ability of macrophages to switch phenotype from M1 to M2 and vice versa during the host response represents a protective mechanism to balance the host tissue response between pathogens removal and resolution of the inflammation, without inducing excessive local damage (Brown & Badylak, 2013).

1.2.3 Modulation of macrophage polarization with biomaterial design

The modulation of macrophage phenotype has been addressed by an increasing number of studies in the field of regenerative medicine as a potential mechanism to tune the immune response to biomaterials. During physiological wound healing, macrophage polarization is triggered by specific factors released by lymphocytes and neutrophils migrated to the site of injury. More specifically, M1 polarization is associated with the secretion of interferon

(IFN)- γ or TNF- α , while M2 phenotype arises in response to IL-4, IL-13 or IL-10 (Mantovani *et al.*, 2004). In addition to endogenous signaling, recent studies have investigated the influence of composition and geometry of implanted biomaterials on macrophage functional polarization, abandoning the concept of inert biomaterial (Franz *et al.*, 2011).

It was shown that biomaterials prepared by decellularization of living tissues, that mimic therefore the structure and biological composition of extracellular matrix, are capable of promoting constructive tissue remodeling. Scaffolds of biological origin were shown to induce infiltration of M1 macrophages immediately after implantation. A switch to an M2 cell population was observed after 1 week in response to specific ligand-receptor interactions between macrophages and the scaffold surfaces (Badylak *et al.*, 2008). Studies performed on synthetic biomaterials with different topography suggested that surface roughness and fiber diameter can affect macrophage adhesion and inflammatory cytokines release (Spiller *et al.*, 2009; Saino *et al.*, 2011). Ratner *et al.* demonstrated that cardiac implantation of hydrogel scaffolds with pores of 30-40 μm in diameter led to enhanced vascularization and limited fibrotic response, coupled with increased amount of M2 macrophages (Madden *et al.*, 2010). The correlation between fibrous scaffolds topography and macrophage polarization was further investigated *in vitro* by Garg *et al.*, who proved that increased fiber diameter and pore size shifts macrophage phenotype towards M2 (Garg *et al.*, 2013).

The intrinsic properties of the scaffold, such as composition and topography, can dictate immune response and must be, therefore, carefully selected, in order to promote functional outcome of the implant and avoid deleterious inflammation. Moreover, substrates for the repair of cardiovascular tissues will be exposed to significant hemodynamic forces that may interfere with crucial stages of the immune response, e.g. infiltration of monocyte or macrophage polarization. The potential interplay between scaffold and immune cells in presence of such forces must be further investigated and taken into consideration for the design of constructs able to promote site-appropriate tissue remodeling.

1.3 The method: engineered constructs towards *in situ* regeneration

1.3.1 Clinical and pre-clinical studies

The first clinical success of cardiovascular tissue engineering without *in vitro* cell expansion was obtained by implanting biodegradable vascular grafts pre-seeded with autologous bone marrow mononuclear cells (BM-MNCs). Such grafts replaced large vessels in high-flow, low-pressure environments in pediatric patients, demonstrating growth potential and long-term functionality (Matsumura, Hibino, *et al.*, 2003; Shinoka *et al.*, 2005; Hibino *et al.*, 2010). The promising results obtained by Shinoka's group paved the way for the first, FDA-sanctioned clinical trial of tissue engineered vascular grafts for pediatric cardiothoracic applications in the USA (Breuer, 2009). Additional insight into the process was provided by a murine model, which demonstrated that the autologous seeded cells were not directly involved in neotissue deposition, but elicited inflammation-mediated regeneration via a paracrine mechanism, in association with recruited host monocytes (Roh *et al.*, 2010). Upon contact with the scaffold, the monocytes differentiate into macrophages and initiate an immunomodulatory cytokine cascade that promotes the migration of smooth muscle and endothelial cells from adjacent tissues, resulting in tissue formation and remodelling. On the other hand, seeded BM-MNCs were shown to determine the initial amount and the polarization state of the infiltrating monocytes-macrophages and to attenuate the foreign body response to the scaffold. This process favoured enhanced tissue regeneration and diminished conduits stenosis, the primary graft complication in clinical trials (Hibino *et al.*, 2011). The exact signalling pathways induced by BM-MNCs and responsible for the regenerative mechanism might represent the key towards cell-free tissue engineering in human, but are yet to be identified. With this respect, promising results were achieved by implanting cell-free vascular grafts in animal models (Matsumura *et al.*, 2012, 2013; Wu *et al.*, 2012). The landmark study of Wu *et al.* showed that successful remodelling of small caliber rat arteries could be enabled by implanting unseeded, fast-degrading synthetic scaffold, with a highly porous structure that allowed for rapid monocyte infiltration. The translation of such approach from healthy rats to diseased human patients is not trivial and might require the enclosure of progenitor-cell homing signal into the scaffold, to allow for vascular cell infiltration.

Recently, cell-free, biodegradable vascular conduits designed to enable endogenous tissue growth have been implanted into pediatric patients within an ongoing and, to this date, successful clinical trial (Xeltis, 2014). The ground-breaking concepts and methods developed for *in situ* vascular regeneration have been recently adopted also for tissue engineering of heart valves, often in combination with minimally invasive surgical techniques. A proof of principle for this application was provided by Weber et al., who implanted synthetic valves pre-seeded with autologous BM-MNCs as pulmonary replacements in non-human primates. Evidence of host monocytic infiltration was observed within the first day and, after 4 weeks, the leaflets were covered by a confluent endothelium and adequate valvular functionality was retained during short-term follow up (Weber *et al.*, 2011). Alternative substrates prone to *in situ* repopulation and minimal invasive delivery are represented by decellularized matrices. Such substrates can be obtained through *in vitro* culture of homologous cells on biodegradable scaffolds and provide non-immunogenic, well-organized matrices capable of guiding tissue regeneration (Dijkman *et al.*, 2012; Meier *et al.*, 2014). Decellularized valvular substrates seeded with autologous BM-MNCs and implanted in sheep in the pulmonary district were shown to undergo rapid recellularization and to allow for functional tissue remodeling (Driessen-Mol *et al.*, 2013). The required *in vitro* step can prove a hindrance to the applicability of this approach. Nevertheless, decellularized substrates can be stored without incurring tissue alteration up to 18 months, therefore they still provide clinically relevant, off-the-shelf starter matrices for heart valve tissue engineering.

The translation of methods from animal studies into the clinical application represents a major challenge of regenerative medicine, due to the high inter-patients variability and the limited knowledge of complex biological processes, which often differ dramatically among species. Whereas blood vessels are currently involved in clinical trials, heart valve implantation remains extremely daunting, as result of the disastrous failures occurred in the past in pediatric patients, despite thorough preclinical testing in sheep (Simon, 2003). In order to ensure safe and effective clinical translation, a deep awareness of the human response to cardiovascular replacements is required. In particular, the effect of the hemodynamic environment on the implant should be investigated, in order to design scaffolds able to withstand the high mechanical forces, but also to modulate the inflammatory response.

1.3.2 Hemodynamics and tissue regeneration

Shear and tensile stress represent the principal loads acting on heart valves and blood vessels substitutes upon implantation. Such forces can interfere with cell recruitment and differentiation, thus affecting the outcome of the host response and tissue remodeling. During inflammation, shear stress enables leukocytes adhesion onto the endothelium by activating specific binding sites, the selectines (Ley *et al.*, 2007). Furthermore, endothelial cells can sense the variation of shear stress related to changes in the hemodynamics, and translate this information to the underlining cells, to induce remodeling of the tissue to adapt to the new environment (Langille & O'Donnell, 1986; Butcher & Nerem, 2006). In addition, multiple studies demonstrated that endothelial cells exposed to varying shear stress alter the expression of growth factors and chemokines important for *in situ* remodeling (Ando *et al.*, 1994; Bao *et al.*, 1999).

Cardiovascular tissues are subjected to continuous cyclic mechanical loading that can determine cellular phenotype and tissue remodeling. It was shown that stretch applied to smooth muscle cells can modulate their shape, cytoplasmic organization, and intracellular processes, leading to migration, proliferation, or contraction (Halka *et al.*, 2008). *In vivo* studies performed in baboons indicated that valves implanted above the native leaflets, and therefore unloaded, exhibited diminished tissue remodeling, as compared to their loaded counterparts (Weber *et al.*, 2011). However, in order to induce appropriate mechanotransduction, the mechanical properties of the scaffolds should be finely tuned, as a mismatch between scaffold and native tissue may result in impaired tissue formation (Wu *et al.*, 2012).

1.3.3 Design of responsive scaffolds

For a long time, biomaterials engineering aimed at the fabrication of inert scaffolds, able to minimize the inflammatory response to the implant. A material that was proven to be non-immunogenic, non-thrombogenic and non-toxic was considered “biocompatible” and, therefore, suitable for implantation. The growing need for biomaterials able to actively interact with the host and to degrade over time led, in 1987, to redefine the concept of biocompatibility as “the ability of a material to perform with an appropriate host response in a specific situation” (Williams, 1987). In his manifesto from 2011, Ratner suggested a more specific definition of biocompatibility, as “the ability of a material to locally trigger

and guide non-fibrotic wound healing, reconstruction and tissue integration” (Ratner, 2011). According to this definition, substrates for regeneration should be capable of evoking an appropriate host response, which may be influenced by the biochemical and biophysical cues specific for the anatomic site of implantation. Considering the high forces acting on valves and vessels and the complex biochemical milieu represented by the blood, the design of scaffolds for cardiovascular *in situ* repair poses several challenges. The selection of an appropriate biomaterial, processing method and functionalization of the scaffold are the main aspects to be addressed.

Synthetic polymers represent a valuable option due to their large availability and finely tunable chemical and mechanical properties by multiple processing methods. Some of the most widely used materials are biodegradable polyesters, such as polyglycolic acid (PGA), polylactic acid (PLA) and their copolymers, and poly (ϵ -caprolactone) (PCL). PCL represents an interesting candidate for cardiovascular applications, as it exhibits slow degradation rate (more than 24 months to resorb *in vivo*) and can provide excellent mechanical strength over time (de Valence *et al.*, 2012). Unfortunately, PCL has limited fatigue resistance preventing its use as heart valve scaffold. PCL is a highly versatile material, prone to be used in combination with other compounds to create reinforced structures (Wisse *et al.*, 2006). Another interesting elastomer is poly(glycerol sebacate) (PGS), which can be modified by adjusting the curing temperature and the concentration of the reactants to obtain fast degrading scaffolds, effectively used for rapidly remodeled vessels in animal models (Rai *et al.*, 2012). The degradation kinetics represents a critical parameter, as the loss of structural integrity and mechanical properties should be promptly compensated by the presence of a newly formed matrix. However, it was demonstrated that rapid degradation might limit the host exposure to the foreign material in small animal models, leading to a positive outcome of implanted vessels (Wu *et al.*, 2012). In conclusion, it is essential to choose a biomaterial that can be processed, either via chemical or physical methods, to obtain scaffolds that match the requirements of the intended application.

Several techniques for scaffold production have been proposed in the last decades. The most widely used for cardiovascular tissue engineering applications include electrospinning, knitting and salt leaching. Electrospinning represents a valid technology to process polymers into scaffolds with highly controllable mechanical and topographical properties. This technique allows for fabrication of three-dimensional fibrous structures with adjustable void space and fiber alignment, thus suitable for cardiovascular tissue engineering purposes (Figure 1.5) (Simonet *et al.*, 2014). A primary determinant of the

outcome of the implant is the initial porosity of the substrate, as increased void space can accelerate cellular infiltration and even harness macrophage polarization (Garg *et al.*, 2013). Moreover, by controlling the fiber size and orientation to simulate the native network of collagen and elastin fibrils, guidance of matrix deposition could be addressed (Jonge *et al.*, 2014). Mechanical performance of the scaffold represents another crucial factor for cardiovascular applications, since the substrate should be able to withstand high pressures immediately upon implantation. Furthermore, the micro-mechanical environment created by the scaffold profoundly affects cells viability and differentiation. Hence, appropriate transduction of constructive forces and shielding of daunting ones should be ensured by a rational scaffold design and manufacturing.

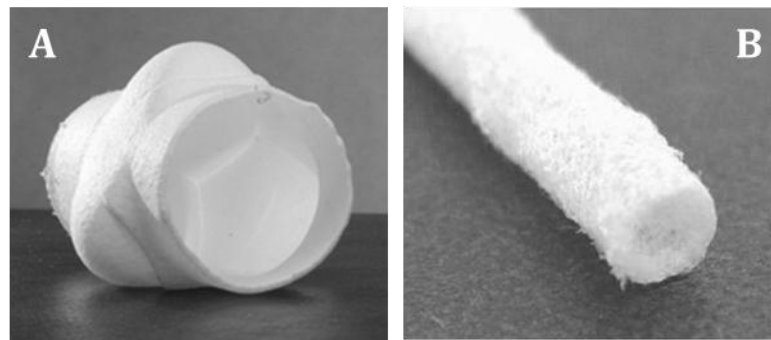


Figure 1.5 Photographs of electrospun scaffolds. 3D porous structures consisting of poly (ϵ -caprolactone) can be tailored in the shape of heart valves (A) and tubular vessels (B) by electrospinning (Courtesy of Marc Simonet).

A promising strategy to harness a positive outcome of the implant consists in activating the biomaterials to allow selective binding of cells and to guide their differentiation towards a specific phenotype. Strategies to develop bioactive materials by embedding functional molecules, such as antibodies, growth factors or RGD-peptides, range from simple coatings of the scaffold to more complex approaches that involve the covalent modification of the base material (Bouten *et al.*, 2011). An interesting option is provided by supramolecular polymers, which can be functionalized with bioactive molecules specifically modified with the same supramolecular units, thus offering a highly dynamic environment, analogous to the natural ECM (Dankers *et al.*, 2005). To this date, besides the ongoing clinical study with cell-free conduits mentioned in 1.3.1, the only method successfully applied to the clinics to create functionalized scaffolds remains the on-the fly seeding of autologous cells. Due to the wide range of signaling induced by cells *in vivo*, all the molecules responsible for the positive integration of the constructs have yet to be

identified. The disclosure of the molecules and pathways involved in the underlying mechanism will pave the way for the design of instructive, cell-free scaffolds capable of eliciting *in situ* cardiovascular tissue regeneration.

1.4 Rationale, aim and outline of the thesis

Mechanical loads acting on tissue engineered constructs *in vivo* were proven to influence the fate of implanted biomaterials. A deep understanding of the complex mechanism guiding cell recruitment, differentiation and signaling in presence of shear and tensile stress is a key challenge towards the design of instructive scaffolds for *in situ* cardiovascular regenerative therapies. We hypothesized that mechanical forces could exert significant influence on the final outcome of the implant by modulating the early phase of the inflammatory response. The aim of the present work is to provide a deeper insight into the interplay between immune cells and porous scaffolds subjected to mechanical stimuli. A systematic analysis of cell response to shear flow and cyclic strain within the physiological range was carried out with the aid of *in vitro* models.

In chapter 2, the role of shear stress on selective recruitment of human monocytes was elucidated using electrospun scaffolds, both bare and coated with a chemokine mediating the immune response, monocyte chemoattractant protein-1 (MCP-1). Upon adhesion onto the scaffold *in vivo*, the recruited monocytes-macrophages are exposed to local strain that can modulate their phenotype. The effect of different strain magnitudes on macrophage polarization towards an inflammatory (M1) and reparative (M2) phenotype is described in chapter 3. Finally, human mesenchymal stromal cells (hMSC), which participate to regeneration via a paracrine mechanism, were incorporated into the scaffolds, to provide an insight into the signalling involved in inflammation-mediated repair. Chapter 4 illustrates the results of an *in vitro* study investigating the interaction between hMSC and circulating immune cells in presence of biomechanical stimuli (i.e. strain and shear flow). Chapter 5 summarizes the main findings of the thesis and provides a general discussion of the presented results, highlighting some of the additional gaps that need to be bridged, towards effective *in situ* cardiovascular regeneration.

Shear flow affects selective monocyte recruitment into MCP-1-loaded scaffolds

This chapter is based on :

Ballotta V.*, Smits AIPM*, Driessen-Mol A, Bouten CVC, Baaijens FPT (2014) "Shear flow affects selective monocyte recruitment into MCP-1-loaded scaffolds". *Journal of Cellular and Molecular Medicine*. In press.

* these authors contributed equally to the study

Abstract

Novel cardiovascular replacements are being developed using degradable synthetic scaffolds, which function as a temporary guide to induce neotissue formation directly *in situ*. Priming of such scaffolds with fast-releasing Monocyte Chemoattractant Protein-1 (MCP-1) was shown to improve the formation of functional neoarteries in rats. However, the underlying mechanism has not been clarified. Therefore, the goal of this study was to investigate the effect of a burst-release of MCP-1 from a synthetic scaffold on the local recruitment of circulating leukocytes under hemodynamic conditions. Herein, we hypothesized that MCP-1 initiates a desired healing cascade by recruiting favorable monocyte subpopulations into the implanted scaffold. Electrospun poly(ϵ -caprolactone) scaffolds were loaded with fibrin gel containing various doses of MCP-1 and exposed to a suspension of human peripheral blood mononuclear cells in static or dynamic conditions. In standard migration assay, a dose-dependent migration of specific CD14⁺ monocyte subsets was observed, as measured by flow cytometry. In conditions of pulsatile flow, on the other hand, a marked increase in immediate monocyte recruitment was observed, but without evident selectivity in monocyte subsets. This suggests that the selectivity was dependent on the release kinetics of the MCP-1, as it was overruled by the effect of shear stress after the initial burst-release. Furthermore, these findings demonstrate that local recruitment of specific MCP-1-responsive monocytes is not the fundamental principle behind the improved neotissue formation observed in long-term *in vivo* studies, and mobilization of MCP-1-responsive cells from the bone marrow into the bloodstream is suggested to play a predominant role *in vivo*.

2.1 Introduction

Recognition of the role of monocytes in natural wound healing has been the basis of novel regenerative therapies, such as *in situ* cardiovascular tissue engineering. This approach aims at the regeneration of living cardiovascular substitutes directly within the body. Starting from the implantation of bare biodegradable constructs, these therapies rely on *in situ* colonization by host cells and subsequent neotissue formation as the original construct is degraded (Mol *et al.*, 2009; Bouten *et al.*, 2011).

Monocytes are circulating leukocytes that actively contribute to homeostasis and innate immune processes via phagocytosis and cytokine release (Auffray *et al.*, 2009). Originating from bone marrow precursor cells or from splenic reservoirs, they respond to inflammatory signals, migrating from the bloodstream into peripheral tissues, in which they differentiate into macrophages or dendritic cells (Robbins & Swirski, 2010). The diversity of physiological roles played by monocytes is reflected in their morphological heterogeneity (Gordon & Taylor, 2005). Three distinct populations were identified in humans, based on their expression of the surface markers CD14, CD16 and CCR2 (Ziegler-Heitbrock *et al.*, 2010; Shantsila *et al.*, 2011; Favre *et al.*, 2013). Classical CD14⁺/CD16⁻/CCR2⁺ monocytes represent the most abundant subset, consisting of highly versatile cells involved in phagocytic and pro-inflammatory activities, as well as in tissue repair and angiogenesis (Wong *et al.*, 2011). The non-classical CD14^{dim}/CD16⁺/CCR2⁻ population comprises monocytes with a patrolling function, exhibiting high motility in the local surveillance of tissues, which is attributed to an enriched expression of genes involving cytoskeletal rearrangement (Cros *et al.*, 2010; Wong *et al.*, 2011). Intermediate CD14⁺/CD16⁺/CCR2⁺ monocytes display enhanced expression of angiogenic and anti-inflammatory markers, which suggests their reparative potential (Skrzeczyńska-Moncznik *et al.*, 2008; Shantsila *et al.*, 2011). Monocyte mobilization and trafficking during homeostasis and inflammation occurs in response to local stimuli in conformity with the leukocyte adhesion cascade (Ley *et al.*, 2007). Chemokines, such as fractalkine (CX₃CL1) and stromal cell-derived factor-1 α (SDF-1 α or CXCL12), were shown to mediate migration and arrest of the non-classical and intermediate monocytes, which highly express the respective receptors CX₃CR1 and CXCR4 (Ancuta *et al.*, 2003). In contrast, monocyte chemoattractant protein-1 (MCP-1 or CCL2), mediates recruitment of CCR2⁺ monocytes (*i.e.* classical and intermediate monocytes), as well as related circulating progenitor species, such as CD34⁺/CD45⁺ fibrocytes, which are known to promote repair and remodeling (Moore *et al.*, 2005; Tsou *et al.*, 2007; Reilkoff *et al.*, 2011). In addition,

chemokine signaling can enhance monocyte anchorage to the endothelium, by inducing morphological changes in their α_4 - and β_2 -integrins, a pathway that is further influenced by physiological shear stresses exerted by the flowing blood (Maus *et al.*, 2002; Laudanna & Alon, 2006).

Recent progress in the field of *in situ* tissue engineering was achieved by Shinoka *et al.*, who successfully treated congenital cardiac defects in humans with synthetic vascular grafts, preseeded on-the-fly with autologous bone-marrow cells in a single operation (Shinoka *et al.*, 2005; Hibino *et al.*, 2010). The process that drove the transformation of the graft into a functional neovessel was explained via animal studies as a positive inflammatory response, induced by the scaffold, and stirred by infiltration of host monocytes. This process was enhanced by paracrine factors secreted by the preseeded cells, of which MCP-1 was identified as one of the principal mediators (Roh *et al.*, 2010). Additionally, it was suggested that a burst-release of MCP-1 from functionalized, acellular constructs prompted the enhanced recruitment of immune cells in the early phase, leading to long-term vascular remodeling (Roh *et al.*, 2010). However, a mechanistic understanding of the cellular events behind this process is lacking, which is fundamental for further clinical translation.

Our goal here was to elucidate the initial response of circulating immune cells to a MCP-1-loaded scaffold under physiological conditions of flow. We hypothesized that MCP-1 induces a favorable healing cascade at time of implantation by selectively attracting angiogenic and reparative circulating species, such as CCR2⁺ monocytes and fibrocytes. To test this, we developed a hybrid scaffold consisting of a highly porous electrospun poly(ϵ -caprolactone) (PCL) structure, combined with a fibrin gel containing rapidly-releasing MCP-1. We first established the chemotactic effect of our bioactive scaffolds, loaded with varying doses of MCP-1, on specific mononuclear cell populations using static chemotaxis assays. These scaffolds were subsequently placed in a previously validated *in vitro* flow setup to investigate its selectivity in recruiting cells in physiologically relevant conditions of pulsatile flow (Smits *et al.*, 2012).

2.2 Materials and Methods

2.2.1 Electrospinning

Fibrous PCL scaffolds were prepared by electrospinning using a climate-controlled electrospinning apparatus (EC-CLI, IME Technologies). A viscous polymer solution was prepared by dissolving PCL (Purasorb, Purac Biomaterials, Mw= 103 kDa, density $\rho_{PCL} = 1.15 \text{ kg/m}^3$) in chloroform (20% w/w). The solution was fed through a laterally translating nozzle (18 gauge), to which a high voltage of 16 kV was applied, at a flow rate of 25 $\mu\text{l}/\text{min}$. Polymer fibers were collected on a grounded rotating cylindrical drum ($\emptyset 32 \text{ mm}$) at 13 cm distance. Temperature and relative humidity were controlled at 23°C and 50%, respectively. Overall scaffold thickness was controlled via the total spinning time. The resulting PCL sheets were placed under vacuum overnight to remove any remaining solvent. The average scaffold thickness was measured per electrospun sheet (approximately 8-12 measurements at arbitrary locations per sheet; 10 sheets in total) using a digital microscope (VHX-500FE, Keyence). The overall density of the electrospun scaffolds ρ_0 was determined gravimetrically measuring the weight and the thickness of mesh samples over a defined area. The scaffold porosity was calculated using Equation (1):

$$\varepsilon = \left(1 - \frac{\rho_0}{\rho_{PCL}}\right) \cdot 100 \quad (1)$$

The fiber diameter and inter-fiber distance were measured using scanning electron microscopy (SEM) in high vacuum with an electron beam of 1.0-2.0 kV (Quanta 600F, FEI). Per sheet, three SEM images were taken at random locations (magnification 500X) and the respective averages were calculated from 25-30 measurements per image.

2.2.2 MCP-1 loading

Scaffolds were sterilized using 70% ethanol, followed by washing in phosphate-buffered saline (PBS), and overnight incubation in complete medium, consisting of RPMI (RPMI 1640, Gibco), supplemented with 10% fetal bovine serum (FBS Gold, PAA) and 1% penicillin/streptomycin (Lonza), to allow for adsorption of serum proteins and increase

the hydrophilicity of the scaffold. Recombinant human MCP-1 (Peprotech) was mixed into a sterile fibrinogen solution (10 mg fibrinogen/ml) at final concentrations of 2, 20, or 50 ng/ml. The fibrinogen, containing MCP-1 or PBS for controls, was mixed with thrombin (10 IU/ml) and immediately seeded into the scaffolds.

2.2.3 MCP-1 release

To measure the release rate of MCP-1, scaffolds were loaded with fibrin and MCP-1 to a final concentration of 20 ng/mL of medium and exposed to RPMI medium in both static and flow conditions. The applied flow conditions were similar to the conditions used in the cell experiments with a pulsatile flow of 1Hz, a peak pressure of 100 mmHg and peak shear stress of 1.6 Pa on the scaffold surface. Medium samples were collected at time points 20 minutes, 45 minutes, 90 minutes, 3 hours, 6 hours, and 24 hours. MCP-1 content was measured using an ELISA kit (RayBiotech), according to the manufacturer's protocol. The resulting release rate was determined cumulatively per scaffold (N=6 per group).

2.2.4 Cell isolation

Human peripheral blood buffy coats were obtained from 11 healthy donors (ages 21-60 years) under informed consent (Sanquin). Buffy coats were diluted in 0.6% sodium citrate in PBS, after which the mononuclear cell fraction (human peripheral blood mononuclear cells, hPBMC) was isolated using density gradient centrifugation on iso-osmotic medium with a density of 1.077 g/ml (Lymphoprep, Axis-Shield). After washing, the hPBMC were resuspended in freezing medium consisting of RPMI, supplemented with 20% FBS and 10% Dimethyl sulfoxide (Merck Millipore), and cryopreserved in the vapor phase of liquid nitrogen. Before use, cells were rapidly thawed, counted and resuspended in complete RPMI medium at a concentration of 5×10^6 cells/ml. For each donor, hPBMC were characterized with flow cytometry and qPCR as described below.

2.2.5 Cell characterization

Cells were double-stained for CD14/CD16, CD4/CD8, and CD34/CD45, using the following conjugated monoclonal antibodies: anti-CD14 (FITC, AbD Serotec); anti-CD16 (RPE-Cy5 or

Alexa 647, AbD Serotec); anti-CD4 (FITC, Diaclone); anti-CD8 (PE, Diaclone); anti-CD34 (PerCP-Cy5.5, BD Biosciences); anti-CD45 (FITC, BD Biosciences). Cell viability was assessed using 7-amino-actinomycin-D (7AAD; eBioscience). Unspecific binding was blocked using 0.5% bovine serum albumin (Sigma-Aldrich) in PBS. In order to increase the specificity for rare progenitor cell detection, an additional blocking step was performed using human FcR Blocking Reagent (Miltenyi Biotech). After washing, labeled cells were measured using a bench-top flow cytometer (Guava easyCyte 6HT, Merck Millipore) until 20,000 events per sample. Data analysis was performed using the Guava Express Pro software package, combined with FCS Express (De Novo Software). To accommodate for inter-donor variations within the relative fractions of the various cell populations, absolute cell numbers were normalized per donor on the specific baseline value of each cell type.

2.2.6 Chemotaxis assays

Cell migration was assessed using Boyden chambers in a 24-wells plate fitted with a transparent PET membrane with 3µm pores (ThinCerts, Greiner Bio-One). Seeded scaffolds were placed in the bottom compartment, with a MCP-1 concentration of 0, 2, 20, or 50 ng/ml, based on previous reports (Jay *et al.*, 2010; Roh *et al.*, 2010; Kränkel *et al.*, 2011) (N=8 per group). Unseeded electrospun PCL and fibrin only were included as controls (N=4 per group). Scaffolds were covered in 800 µl of complete medium. The chemotactic effects of the scaffolds were compared to the effects of MCP-1 directly dissolved in complete medium, at the same concentrations, but without scaffolds (N=8 per group). hPBMC were added to the top compartment at a concentration of 5×10⁶ hPBMC/ml in a total volume of 500 µl. After 4 hours of incubation (37°C; 5% CO₂), the migrated cells in the bottom compartment were analyzed with flow cytometry. The scaffolds were stained with 10 µM CellTracker Green (CTG; 5-Chloromethylfluorescein Diacetate, Molecular Probes) for immediate visualization of adherent cells. Three independent experiments were conducted, each using hPBMC from a different donor.

2.2.7 Flow experiments

Cell recruitment under conditions of pulsatile flow was studied using a previously developed mesofluidics setup (Smits *et al.*, 2012). In brief, scaffold strips seeded with 200 ng MCP-1 were placed in a custom parallel-plate flow chamber, in which they were exposed to a recirculating suspension of hPBMC in 10 ml of complete RPMI medium (5×10^6 hPBMC/ml). The total concentration of MCP-1 per flow chamber was therefore 20 ng/ml. Scaffolds seeded with fibrin only served as controls. A pulsatile flow of 1Hz was imposed, with a peak pressure of 100 mmHg and peak shear stress of 1.6 Pa on the scaffold surface, mimicking average physiological conditions for small-diameter arteries. Four independent experiments were conducted with hPBMC from 7 different donors (N=16 per group). Samples of the circulating cell suspension were taken aseptically, at time points 0, 1, 2.5, 6, 8, and 24 hours, without stopping the flow, via in-line Luer injection ports (ibidi GmbH). To focus on early effects, two independent experiments with hPBMC from 2 different donors (N=5 per group) were run for 4 hours and samples were taken at time points 0, 10, 30, 60, and 240 minutes. After 4 or 24 hours, the scaffolds were sacrificed for analysis and fixated overnight in 3.7% formaldehyde (Merck Millipore) for immunostainings or 2.5% glutaraldehyde (Grade I, Sigma-Aldrich) for SEM analysis, or snap-frozen in liquid nitrogen and stored at -80°C for qPCR analysis. To serve as gene expression controls, hPBMC from the initial suspension of each donor were stored at -80°C in lysis buffer (Buffer RLT, Qiagen). To accommodate for inter-donor variations in the gene expression levels, hPBMC from an external donor were stimulated with 1 $\mu\text{g}/\text{ml}$ lipopolysaccharide (LPS, *E.Coli*; Sigma-Aldrich) for 30 minutes to activate the cells to express inflammatory genes, which were used as reference values for normalization.

2.2.8 Immunostainings

Formaldehyde-fixated samples were washed in PBS and permeabilized in 0.5% Triton X-100 in PBS (Merck Serono). Non-specific binding was blocked by incubation in 10% horse serum (Invitrogen) in PBS. Cells were incubated overnight at 4°C with primary antibodies against CD68 (1:100, AbD Serotech), CCR7 (1:100, Abcam) and CD163 (1:100, AbD Serotech) in 1% bovine serum albumin in PBS. The scaffolds were then washed and incubated for 60 minutes with Alexa fluor 555 (1:300) for CD68, Alexa fluor 647 (1:300) for CCR7 and Alexa fluor 488 (1:300) for CD163. Scaffolds were subsequently stained with

4',6-diamidino-2-phenylindole (DAPI, Sigma-Aldrich). After washing steps, scaffolds were mounted on slides with Mowiol (Calbiochem) and observed with a confocal microscope (TCS SP5X, Leica Microsystems).

2.2.9 SEM

Glutaraldehyde-fixated samples were washed in PBS and dehydrated in a graded ethanol series, starting from 50% to 100% ethanol in 5 to 10% increments. Samples were visualized in high vacuum with an electron beam of 1.0-2.0 kV (Quanta 600F, FEI).

2.2.10 qPCR and gene expression analysis

Scaffolds were disrupted with a microdismembrator (Sartorius) and RNA was subsequently isolated with Qiagen RNeasy kit (Qiagen) according to the manufacturer's instructions. cDNA was synthesized with 50 ng RNA using M-MLV Reverse Transcriptase (Invitrogen). Expression levels of genes involved in the inflammatory process were evaluated with SYBR[®]Green Supermix (Bio-Rad) with CFX384 real-time detection system (Bio-Rad), and GAPDH was selected as reference gene. Primer sequences of selected genes are provided in Table 2.1. C_t values were normalized to the reference gene and to the LPS-treated hPBMC in order to obtain the relative gene expression. The expression levels of LPS-treated cells were set to a value of 1 for all genes, to serve as reference for the activated hPBMC state (Zgair, 2012).

2.2.11 Statistical analysis

Data collected with flow cytometry and qPCR are expressed as mean \pm standard error of the mean. When variances could not be considered equal (for the flow cytometry data), a logarithmic transformation was applied. An ANOVA with Bonferroni post-hoc testing was performed to detect statistical differences between the groups. Due to a non-normal distribution of the data from the gene expression analyses, these data were analyzed with Kruskal-Wallis tests followed by Dunn's multiple comparison tests. Statistical analyses were performed using Prism software (GraphPad) and differences were considered significant for P values < 0.05.

Table 2.1 Primer sequences encoding genes for qPCR analysis.

Primer	Symbol	Amplicon size (bp)	Accession number	Primer Sequence (5'-3')
monocyte chemoattractant protein-1	MCP-1	190	NM_002982	FW: CAGCCAGATGCAATCAATGCC RV: TGGAAATCCTGAACCCACTTCT
tumor necrosis factor	TNF	91	NM_000594	FW: GAGGCCAAGCCCTGGTATG RV: CGGGCCGATTGATCTCAGC
interleukin 10	IL10	112	NM_000572	FW: GACTTTAAGGGTTACCTGGGTTG RV: TCACATGCGCCTTGATGTCTG
chemokine (C-X-C motif) ligand 12	CXCL12	48	NM_000609	FW: ATTCTCAACACTCCAAACTGTGC RV: CTCAGCCGGGCTACAATCTG
chemokine (C-C motif) receptor 2	CCR2	100	NM_001123396	FW: TGCAAAAAGCTGAAGTGCTTG RV: CAGCAGAGTGAGCCACAAT
transforming growth factor, β 1	TGFB1	355	NM_000660	FW: GCAACAATTCCTGGCGATACCTC RV: AGTTCCTTCCGTGGAGCTGAAG
integrin, β 2	ITGB2	187	NM_000211	FW: TGCGTCCTCTCTCAGGAGTG RV: GGTCCATGATGTCTGTCAGCC
integrin, α 4	ITGA4	139	NM_000885	FW: CACAACACGCTGTTCGGCTA RV: CGATCCTGCATCTGTAAATCGC
chemokine (C-X3-C motif) receptor 1	CX3CR1	226	NM_001171174	FW: TCACCGTCATCAGCATTGATAGG RV: GTTTCACATTGCGGAGCAC
chemokine (C-X-C motif) receptor 4	CXCR4	130	NM_001008540	FW: GCCTTATCCTGCCTGGTATTGTC RV: GCGAAGAAAGCCAGGATGAGGAT
vascular endothelial growth factor A matrix metalloproteinase 9	VEGFA	213	NM_001025366	FW: GCAGAAATCATCAGGAAGTGG RV: GCATGGTGATGTTGGACTCC
	MMP9	224	NM_004994	FW: TGGGGGGCAACTCGGC RV: GGAATGATCTAAGCCAG
interleukin 6	IL6	45	NM_000600	FW: ACTCACCTCTTCAGAACGAATTG RV: GTCGAGGATGTACCGAATTTGT
interleukin 4	IL4	102	NM_000589	FW: CAGTTCTACAGCCACCATGAG RV: GTCGAGCCGTTTCAGGAATC
interleukin 13	IL13	121	NM_002188	FW: AGGCACACTTCTTCTTGGTCT RV: GAGTCTCTGAACCCTTGGCT
CD163 molecule	CD163	137	NM_004244	FW:CACTATGAAGAAGCCAAAATTACCT RV: AGAGAGAAGTCCGAATCACAGA
mannose receptor, C type 1	MRC1	114	NM_002438	FW: TGGGTTCTCTCTGGTTTCC RV: CAACATTTCTGAACAATCCTATCCA
chemokine (C-C motif) receptor 7	CCR7	106	NM_001838	FW: AAGCCTGGTTCCTCCCTATC RV: ATGGTCTTGAGCCTCTTGAATA

The primer pairs for IL4, IL13, CD163, MRC1, and CCR7 were sequenced by PrimerDesign.

2.3 Results

2.3.1 Hybrid PCL/fibrin scaffolds demonstrate a burst-release of MCP-1

Electrospinning resulted in isotropic fibrous PCL scaffolds with a fiber diameter distribution of $10.9 \pm 0.8 \mu\text{m}$ and an inter-fiber distance of $119 \pm 39 \mu\text{m}$ (Figure 2.1A).

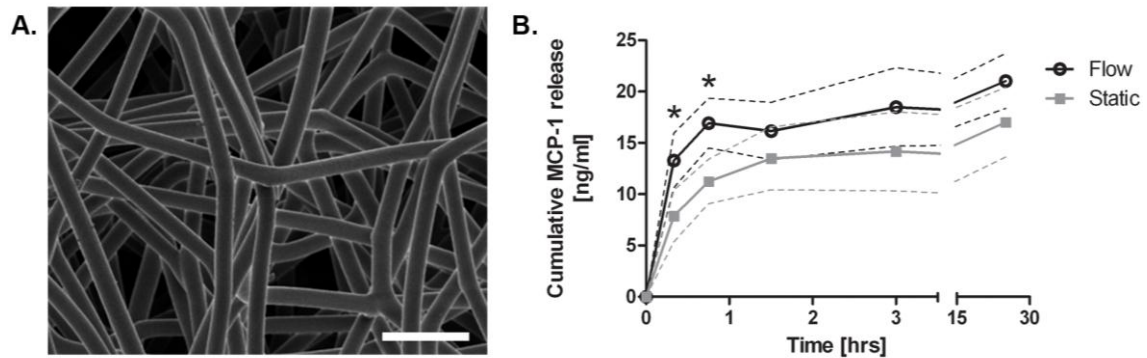


Figure 2.1 Scaffold characterization and MCP-1 release profile. (A) SEM image of an electrospun polycaprolactone scaffold with an average fiber diameter of $10.9 \pm 0.8 \mu\text{m}$. Scale bar represents $50 \mu\text{m}$. (B) Cumulative release of MCP-1 from the PCL/fibrin construct measured over 24 hours in static and pulsatile flow conditions. The results demonstrate a burst-release of MCP-1 in the first 45 minutes and 90 minutes for flow and static conditions, respectively. The data is plotted as mean \pm standard deviation; * $p < 0.05$.

For the chemotaxis experiments the average scaffold thickness was $392 \pm 36 \mu\text{m}$, to prevent direct contact with the membrane. For the flow experiments scaffold thickness was $507 \pm 79 \mu\text{m}$. The overall scaffold density ρ_0 was determined to be 0.12 kg/m^3 , from which the scaffold porosity was calculated to be approximately 90% (Equation 1). In static conditions, seeding the scaffolds with MCP-1 in fibrin gel resulted in a burst-release of MCP-1 in the first 90 minutes, followed by a gradual protein release up to 24 hours. In flow conditions, the protein release was significantly accelerated up to 45 minutes, after which the release rate showed a gradual increase similar to the static release (Figure 2.1B).

2.3.2 Baseline cell composition comprises biological inter-donor variations

Baseline values for the initial hPBMC population were determined for each donor using flow cytometry, as specified in Figure 2.2 (Bellini & Mattoli, 2007; Huenecke *et al.*, 2008; Reilkoff *et al.*, 2011; Shantsila *et al.*, 2011; Hristov *et al.*, 2012). The cellular composition displayed biological inter-donor variations, and baseline values of all specified cell types

fell within physiological values for healthy adults, as reported elsewhere (Table 2.2) (Abe *et al.*, 2001; Huenecke *et al.*, 2008; Shantsila *et al.*, 2011; Hristov *et al.*, 2012).

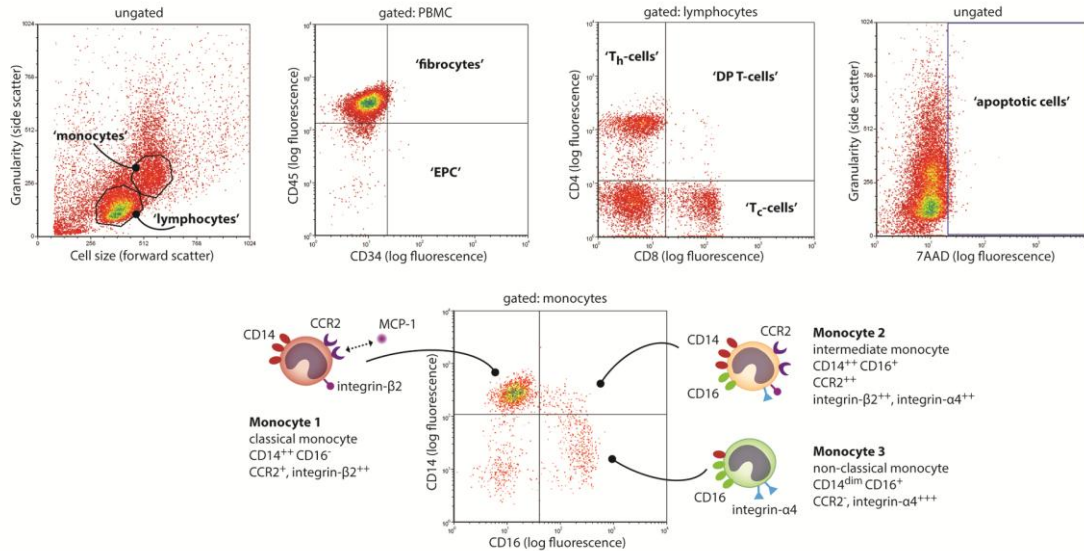


Figure 2.2 Gating strategy adopted to characterize hPBMC populations. (A) Cell populations were quantified by gating the lymphocyte and monocyte clouds in the forward scatter-side scatter plots, which combined formed the total hPBMC gate. (B) Within this gate, CD34⁺/CD45⁻ and CD34⁺/CD45⁺ cells were classified as 'endothelial progenitor cells' (EPC) and 'fibrocytes', respectively (Bellini & Mattoli, 2007; Reilkoff *et al.*, 2011; Hristov *et al.*, 2012). (C) Lymphocytes were further characterized for the presence of helper T-cells (T_H-cells; CD4⁺/CD8⁻), cytolytic T-cells (T_C-cells; CD4⁻/CD8⁺), and double-positive T-cells (DP T-cells; CD4⁺/CD8⁺) (Huenecke *et al.*, 2008). (D) Overall cell viability was quantified via 7AAD labeling. (E) Characterization of monocytes subsets based on CD14 and CD16 labeling, with cartoons illustrating the specific surface receptors and integrins. Monocytes subsets were specified as monocyte 1 (Mon1; CD14⁺/CD16⁻), monocyte 2 (Mon2; CD14⁺/CD16⁺), monocyte 3 (Mon3; CD14^{dim}/CD16⁺) (Shantsila *et al.*, 2011).

Table 2.2 Baseline cell composition of the hPBMC

	Mean \pm st.dev.	Range (min-max)
PBMC [μL^{-1}]	2,666 \pm 927	1,443 – 4,736
Monocytes [% of PBMC]	21.9 \pm 10.5	7.9 – 37.5
Mon1 [% of monocytes]	81.0 \pm 8.4	67.2 – 94.2
Mon2 [% of monocytes]	5.2 \pm 3.0	1.2 – 10.2
Mon3 [% of monocytes]	13.8 \pm 5.8	4.6 – 22.6
Lymphocytes [% of PBMC]	78.1 \pm 10.5	62.5 – 92.1
T_h-cells [% of lymphocytes]	39.2 \pm 13.6	18.0 – 58.5
T_c-cells [% of lymphocytes]	27.1 \pm 8.2	17.1 – 39.1
DP T-cells [% of lymphocytes]	1.2 \pm 0.7	0.6 – 2.5
CD4/CD8 ratio [-]	1.6 \pm 0.8	0.5 – 2.8
Fibrocytes [% of PBMC]	1.7 \pm 0.4	1.0 – 2.4
EPC [% of PBMC]	0.13 \pm 0.05	0.05 – 0.22

Mean values of initial cell populations among 11 donors obtained via flow cytometry. All values fell within physiological ranges.

2.3.3 MCP-1-loaded scaffolds induce highly specific chemotaxis of monocyte subsets

After 4 hours, the migrated cell population contained an increased fraction of monocytes compared to the initial hPBMC suspension in all groups (Figure 2.3B, D, F). CTG-staining demonstrates increased adhesion of migrated cells onto the scaffolds loaded with MCP-1, as compared with scaffolds containing only fibrin (Figure 2.3C, E). Incorporation of MCP-1 into the PCL/fibrin scaffolds led to a significant increase in migrated monocytes for concentrations of 20 and 50 ng/ml MCP-1, while overall lymphocyte migration was less than 1% of the initial lymphocytes for all conditions (Figure 2.3G, H). No significant effect of MCP-1 loading was observed on the migration of fibrocytes and EPC (Figure 2.3I, J). Monocyte subsets mon1 and mon2 were highly responsive to MCP-1 at concentrations of 20 and 50ng/ml, while overall migration of mon3 was very limited for all conditions tested (Figure 2.3K-M). In comparison to the fibrin-seeded control scaffolds, mon2 showed the most enhanced migration with over 6-fold increase in mon2 cell counts over the 0 ng/ml

scaffolds, compared to a nearly 4-fold increase in mon1 for MCP-1 concentrations of 20 and 50 ng/ml. The presence of PCL or fibrin alone did not lead to any changes in cell migration compared to the controls with 0 ng/ml MCP-1 (Figure 2.3G-M). Overall, the migration profile towards the MCP-1-loaded scaffolds was similar to results obtained by direct addition of MCP-1 to culture medium (data not shown).

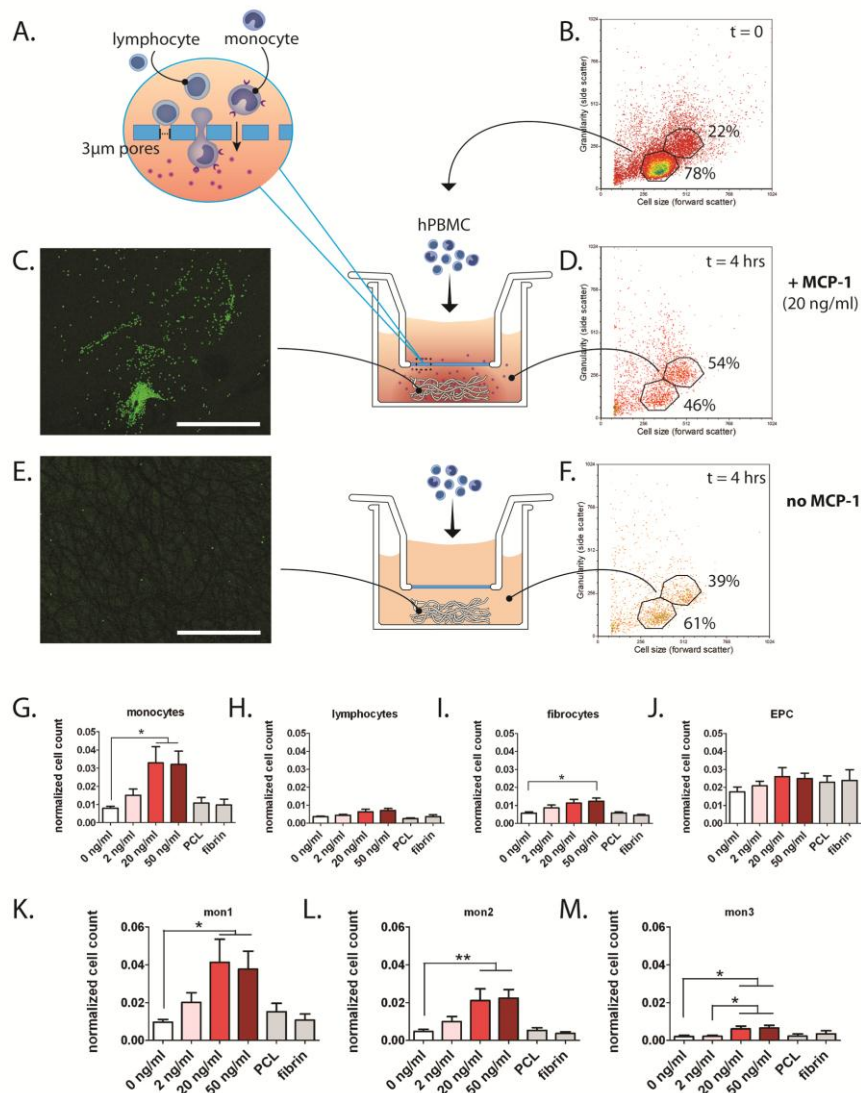


Figure 2.3 Chemotaxis assays revealed enhanced migration of Mon1 and Mon2 subsets toward MCP-1 concentrations of 20 and 50 ng/ml. (A) Schematic of monocyte migration through 3 μm pores of a Thincert™ membrane. (B) Flow cytometry showing the initial hPBMC composition, seeded into the upper compartment. (C-D) Enhanced migration of monocytes toward MCP-1-loaded scaffolds after 4 hours as revealed by immunofluorescence of the construct (C) and by flow cytometry of migrated cells in the bottom compartment (D). (E-F) CTG-staining showing a limited adhesion of cells onto the scaffolds without MCP-1 (E), and relative flow cytometry revealing limited increase of monocyte fraction in the migrated population (F). (G-M) Quantification of migrated populations in response to various doses of MCP-1 incorporated into PCL/fibrin scaffolds. Cell counts were normalized per cell type on the initial cell count of that specific population. Scale bars represent 500 μm . * $P < 0.05$; ** $P < 0.01$.

2.3.4 Flow experiments

MCP-1 release does not result in selective recruitment under conditions of flow

Based on the results obtained from the chemotaxis assays, a MCP-1 concentration of 20ng/ml was selected for loading the scaffolds in the flow experiments. Flow cytometry of the remaining cell suspension revealed that after 24 hours the circulating hPBMC consisted almost exclusively of lymphocytes (Figure 2.4A,B). The analysis per cell type indicated that lymphocyte count remained relatively stable at approximately 65% of the original amount, while monocytes were rapidly depleted to 27% of the initial monocyte count within the first 2.5 hours of flow, and to 5% after 24 hours (Figure 2.4C,D). Fibrocytes and EPC demonstrated an immediate depletion within the first hour, to approximately 45% and 35% of their initial cell numbers respectively, after which their numbers gradually decreased (data not shown). Viability was not affected under any of the experimental conditions, with an overall viability of >90% throughout the course of the experiment (Figure 2.4E).

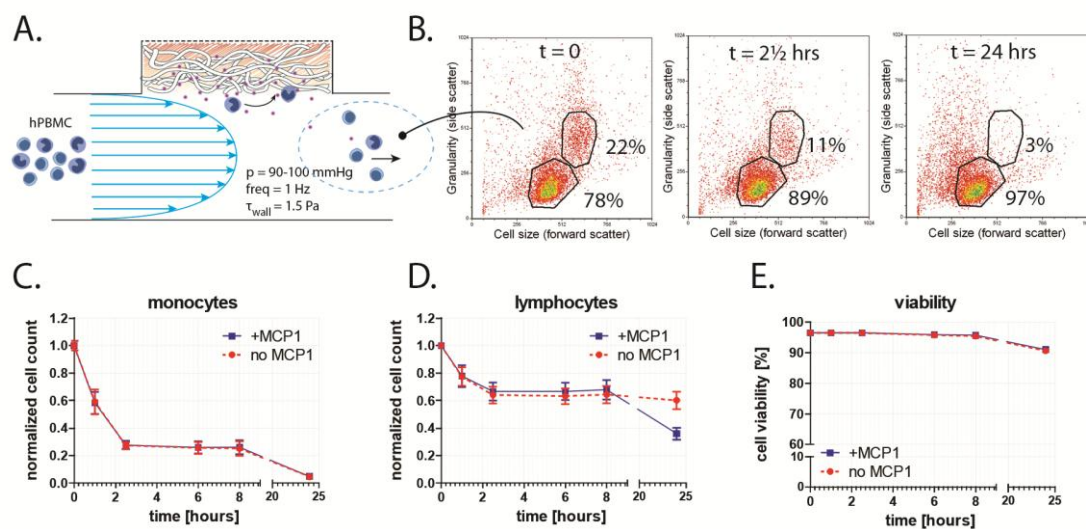


Figure 2.4 Cell recruitment by MCP-1 in scaffolds under physiological flow did not result in selective infiltration of monocytic subsets in response to MCP-1 at time points beyond 1 hour. (A) Drawing representing circulating hPBMC exposed to PCL/fibrin scaffolds with and without MCP-1 in conditions of physiological flow. (B) Flow cytometry of the circulating hPBMC suspension, showing monocyte depletion over time. (C-D) Analysis of circulating cell populations via flow cytometry revealing no differences between MCP-1 loaded scaffold and controls. Cell counts were normalized per cell type on the initial cell count of that specific population. (E) Viability of circulating cells was not affected by flow within the 24 hour follow-up.

Surprisingly, within this timeframe, no significant differences were observed between the MCP-1 and control groups for any of the cell types studied. Therefore, a second series of

experiments was conducted focusing on the immediate events in the first hour. These short-term follow-up experiments revealed an accelerated depletion of all monocytes after 10 and 30 minutes of flow in response to MCP-1 (Figure 2.5A-D). After 4 hours of flow, the remaining relative fractions of monocyte subsets mon2 and mon3 were lower compared to mon1, indicating a more pronounced depletion of mon2 and mon3 within this timeframe.

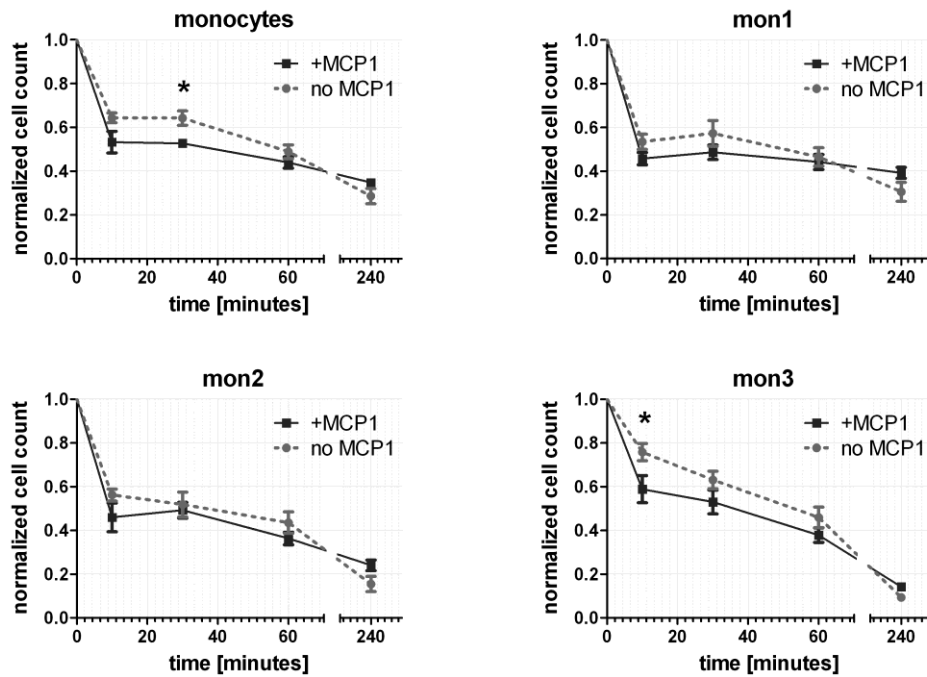


Figure 2.5 Accelerated monocyte recruitment by MCP-1-loaded scaffolds within the first 30 minutes of flow. (A-D) Flow cytometric analysis of monocyte subsets revealed a significantly enhanced depletion of total monocyte counts after 30 minutes of flow in response to MCP-1. All differences between the MCP-1-loaded scaffolds compared to the control scaffolds were negated beyond the 1 hour time point. * $P < 0.05$.

Scaffolds induce monocyte-to-macrophage differentiation with mixed phenotype

Analysis of the scaffolds after 24 hours of flow exposure revealed monocyte activation and adhesion to the scaffold (Figure 2.6A). Furthermore, macrophage differentiation was observed, represented by large, irregular-shaped cells, spreading along the PCL fibers, as visualized by SEM (Figure 2.6B). Consistently, immunofluorescent analysis demonstrated abundant infiltration of CD68⁺ macrophage into the scaffolds. Small, rounded, CD68⁻/CCR7⁺ lymphocytes were sparsely detected. Macrophages displayed a predominant M1 phenotype with strong, but not exclusive, expression of CCR7. In addition, macrophage

polarization towards the M2 phenotype was detected, characterized by CD163 expression (Figure 2.6C). This marker was mainly observed in morphologically larger or fused cells (Figure 2.6D). No apparent difference was observed between the MCP-1 and control groups.

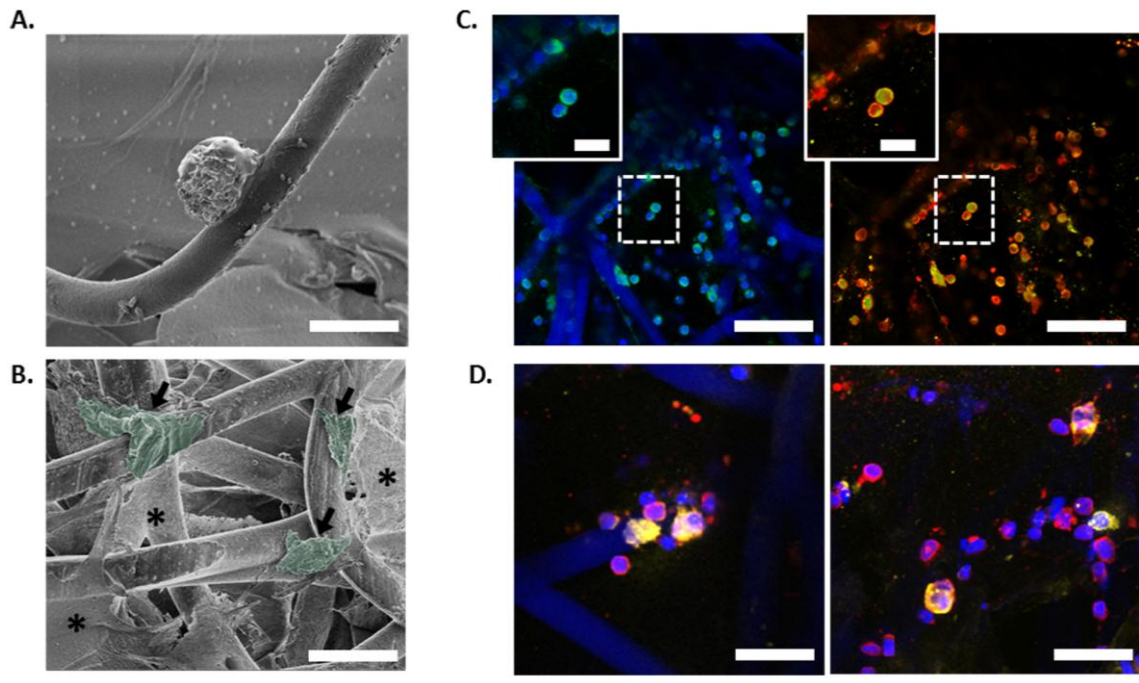


Figure 2.6 Monocytes were recruited to scaffold/fibrin constructs and resulted in M1 and M2 activated macrophages. Monocyte adherent on a PCL fiber (A) and activation of monocytes into macrophages (B) visualized with SEM. (C-D) Immunofluorescence of CD68⁺ macrophages (green), with expression of inflammatory (CCR7⁺; red) and wound healing features (CD163⁺, yellow). Cell nuclei are shown in blue (DAPI). (A-B) Scale bars represent 25 μ m; arrows indicate macrophages, artificial color overlay was added using Adobe Photoshop in post-processing to highlight macrophage morphology; * indicates fibrin. (C-D) Scale bars represent 50 μ m (C), 10 μ m (insets) and 25 μ m (D).

Gene expression of recruited cells in the scaffold after 4 and 24 hours of flow is depicted in Figure 2.7. Overall, MCP-1 loading did not have a significant effect on gene expression, with exception of CCR2 expression, which was significantly upregulated at 4 hours in the MCP-1-loaded scaffolds. Shear flow, on the other hand, generally resulted in an upregulation of immunomodulatory and angiogenic genes, compared to LPS-activated hPBMC, with increased expression at 4 hours compared to 24 hours. Furthermore, flow led to a decrease in integrin expression of ITGB2 over time, but not of ITGA4. Expression of the anti-inflammatory macrophage marker CD163 was significantly downregulated in response to flow, while the pro-inflammatory macrophage marker CCR7 was significantly upregulated. Expression of IL-4, IL-13, MRC-1, and CXCL12 was undetectable (data not shown).

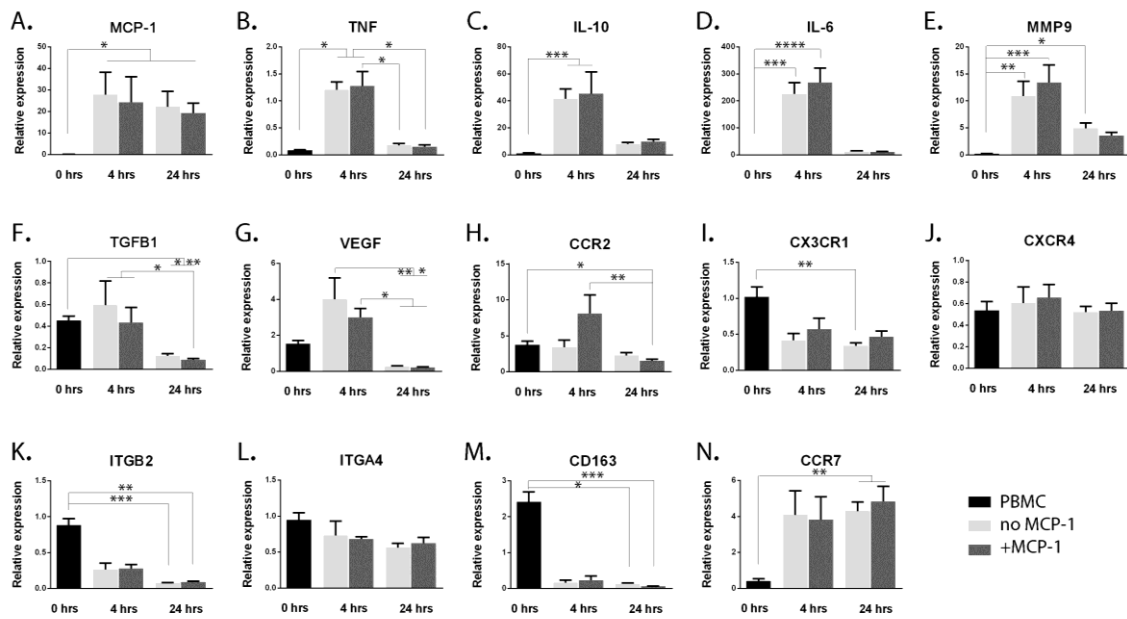


Figure 2.7 Gene expression of immunomodulating and angiogenic markers was upregulated in recruited hPBMC after 4 hours of flow. (A-E) Compared to LPS-stimulated cells, the initial hPBMC population showed low expression of genes involved in immunomodulation, such as MCP-1, TNF, IL10, IL6 and MMP9. Upregulation of these genes was observed at the 4 hours time point, followed by a decrease at 24 hours. MCP-1 was significantly upregulated for recruited cells at all time points. (F) TGFB1 expression was downregulated compared to the LPS control and no substantial changes were observed between the initial population and the cells recruited after 4 hours, while expression decreased significantly at 24 hours. (G) The angiogenic marker VEGF showed upregulation after 4 hours, followed by a significant decrease at 24 hours compared to 4 hours. (H-J) Gene expression of CCR2, CX₃CR1 and CXCR4 was evaluated, representing the receptors for the signaling molecules MCP-1, fractalkine, and SDF-1 α , respectively. CCR2 was upregulated in all groups, as compared to the LPS control, and exhibited increased expression in the MCP-1 group at 4 hours. CX₃CR1 was downregulated for recruited cells at both time points, while CXCR4 expression showed a decrease with respect to the LPS-treated cells, but no significant differences between the groups. (K, L) Concerning expression of integrins, no differences were detected between the controls and the initial hPBMC population, while recruited cells displayed a strong downregulation of ITGB2 at 4 and 24 hours. No differences were notable for ITGA4 in any group. (M) Expression of anti-inflammatory macrophage marker CD163 was high for cells at the initial time point compared to the LPS-treated reference cells, but its expression decreased significantly for infiltrating hPBMC. (N) Opposite behavior was observed for the pro-inflammatory marker CCR7, which showed a low expression by the initial cell population compared to the LPS-treated hPBMC, followed by a large increase in expression for recruited cells at both time points. * $P < 0.05$; ** $P < 0.01$; *** $P < 0.001$; **** $P < 0.0001$.

2.4 Discussion

Recent studies aimed at the *in situ* regeneration of cardiovascular tissues, have demonstrated *de novo* tissue formation on a degradable synthetic starter matrix, driven by the host immune response (Shinoka *et al.*, 2005; Yokota *et al.*, 2008; Hibino *et al.*, 2010; Roh *et al.*, 2010; Wu *et al.*, 2012). It was postulated that MCP-1 is one of the key mediators in the process and, as such, may be used as a therapeutic agent (Roh *et al.*, 2010). Concurrently, we recently demonstrated improved neotissue formation in MCP-1-loaded PCL/fibrin scaffolds in rats, but the underlying mechanism has not yet been clarified (Talacua *et al.*, 2014). Therefore, the goal of the present study was to elucidate the initial response of circulating human immune cells to a MCP-1-loaded scaffold under physiological conditions of flow. We hypothesized that local delivery of exogenous MCP-1 would induce specific recruitment of reparatory CCR2⁺ cells from the circulatory system. Our results demonstrate that a local gradient of MCP-1 resulted in highly specific recruitment of CD14⁺ monocytes in static migration assays, whereas released MCP-1 had no effect on circulating hPBMC in terms of cell recruitment and adhesion in conditions of pulsatile flow.

The role of MCP-1 and its primary receptor CCR2 *in vivo* can be considered rather ambiguous. While MCP-1 is implicated in many cardiovascular pathological conditions, such as atherosclerosis and intima hyperplasia, it is indispensable for physiological tissue homeostasis and angiogenesis (Schober *et al.*, 2004; Schober & Zerneck, 2007; Deshmane *et al.*, 2009; Melgarejo *et al.*, 2009; Niu & Kolattukudy, 2009). It was shown that the MCP-1-CCR2 axis is involved in monocyte emigration from the bone marrow, recruitment to the site of inflammation, and migration into damaged tissue, but its mode of action remains incompletely understood (Shi & Pamer, 2011). Therefore, we investigated the recruitment of monocytes towards MCP-1-loaded scaffolds in the current study, under static conditions as well as in flow. Considering the adverse effects of chronic overexpression of MCP-1, we opted for a short burst-release of MCP-1 from the scaffolds. We established the chemotactic potential of our hybrid MCP-1-loaded PCL/fibrin constructs after 4 hours of incubation, which is in correspondence with the determined release curve, showing a burst-release of the bulk of the loaded MCP-1 within the first 3 hours. A concentration of 20 ng/ml was sufficient to prompt specific migration. Capoccia *et al.* suggested that the angiogenic potential of monocytes is contained in the mon1 subset of circulating monocytes and they showed stimulation of angiogenesis in mice via CCR2-dependent signaling to the mon1 subset (Capoccia *et al.*, 2008). Correspondingly, Cochain *et al.*

suggested that an increase in the number of mon1 cells in circulation by MCP-1/CCR2 activation was the base of enhanced neovascularization in mice, while altered levels of mon3 had no effect on post-ischaemic neovascularization (Cochain *et al.*, 2010). Indeed we did observe a predominant migration of mon1 towards our MCP-1-loaded scaffolds in terms of absolute cell numbers. However, interestingly, in terms of relative migration compared to the fibrin-seeded scaffolds, the most pronounced migration was represented by the mon2 subset, which has been reported to accumulate in injured tissue typically in the proliferative phase of healing, leading to improved outcome (Tsujioka *et al.*, 2009; Shantsila *et al.*, 2013; van der Laan *et al.*, 2013).

When subjected to a suspension of hPBMC in pulsatile flow, there was a marked increase in immediate monocyte recruitment in the MCP-1-loaded scaffold compared to the control scaffold, without evident selectivity in monocyte subsets. The increase in monocyte recruitment correlates strongly with the MCP-1 release rate as measured in conditions of pulsatile flow. This was accompanied by an upregulation of CCR2 gene expression in the MCP-1-loaded scaffold group compared to the controls after 4 hours. After the initial burst-release of MCP-1, however, the specific chemotactic effect of the scaffold was negated and cell adhesion to the scaffolds was similar in both groups. Overall, there was a gradual depletion of monocytes but not lymphocytes. Monocyte adhesion is known to be influenced by shear stress (Ley *et al.*, 2007). Moreover, shear stress may have a differential effect on the specific monocyte subsets, as they exhibit distinctly different integrin presentation on their cell surface. Mon2 and mon3 mainly express integrin α_4 , while mon1 mainly express integrin β_2 . Since integrin α_4 is involved in the initial binding of monocytes to a substrate under influence of shear (Chan *et al.*, 2001; Hyduk & Cybulsky, 2009), this may explain the accelerated depletion of mon2 and mon3, compared to mon1, which we observed in flow cytometric analysis after 4 hours of flow. Concurrently, gene expression analysis revealed a downregulation of integrin β_2 , while integrin α_4 expression remained relatively stable over time.

Recruited monocytes displayed monocyte-to-macrophage differentiation induced by the hybrid construct, regardless of MCP-1 loading. Macrophages are of vital importance for *in situ* cardiovascular tissue engineering and early macrophage presence was shown to determine late-term outcome in neotissue formation (Hibino *et al.*, 2011). Further classification of macrophage polarization state revealed a mixed population of predominantly CCR7⁺ macrophages (M1) with limited presence of CD163⁺ macrophages (M2), which was reflected in the gene expression analyses. This combination of inflammatory and reparative factors, will determine the local microenvironment for host

cells colonizing the scaffold. This is in line with the recent findings by Willenborg *et al.*, who described a mixed macrophage population, dominated by M1 macrophages, in the early phase of tissue repair after skin wounding in mice (Willenborg *et al.*, 2012).

PCL was used as the scaffold material based on its excellent biocompatibility and ease of processing. As such PCL has numerous beneficial properties for large-scale use as vascular scaffold material and electrospun PCL grafts have been studied extensively in animal models (Pham *et al.*, 2006; Pektok *et al.*, 2008; de Valence *et al.*, 2012; Mrówczyński *et al.*, 2013). Apart from the material, the scaffold microstructure plays a profound role in cellular behavior. The fiber diameter and pore size of electrospun scaffolds are interdependent and as such, fiber diameter and alignment influence the cell infiltration depth into the scaffold. A fiber diameter of approximately 10 μm as used in this study was shown to accommodate homogenous cell infiltration (Balguid *et al.*, 2009; Smits *et al.*, 2012). The average fiber diameter and pore size have also been shown to influence (progenitor) cell orientation (Fioretta *et al.*, 2014) and macrophage differentiation (Garg *et al.*, 2013), respectively, as well as other processes that may impair or facilitate regeneration. Fibrin gel was employed here as a method to deliver the MCP-1 protein. Although we demonstrated that the fibrin itself does not have a chemotactic effect on the hPBMC subsets, *in vivo* the fibrin gel would likely act as a provisional matrix, offering important binding sites to circulating cells that adhere to and infiltrate into the scaffold.

The *in vitro* mesofluidics model used in the present study poses limitations in the sense that it does not include analogues for the bone marrow or splenic reservoirs. However, since the MCP-1-dependent extravasation of CCR2⁺ cells from the bone marrow has been well established (Serbina & Pamer, 2006; Tsou *et al.*, 2007), we opted for an *in vitro* model without cell replenishment that allows us to follow the response of the initially recruited cells to the scaffold, rather than cell mobilization. The role of local MCP-1/CCR2 in monocyte arrest still raises some discrepancies (Weber *et al.*, 1999; Maus *et al.*, 2002). As compared to the landmark study by Roh *et al.*, the released amount of MCP-1 per volume of blood/medium is lower in the current study (20 ng/ml vs 133 ng/ml). However, the absolute amount of MCP-1 (200 ng) is similar between studies, which implies that the local gradient of protein is comparable, at least initially. This is most relevant for local chemotaxis of the cells, which is the primary focus of the current study (Roh *et al.*, 2010). Moreover, in a recent study by our group, we demonstrated enhanced *in situ* matrix formation and organization in rats using MCP-1-loaded vascular grafts with similar release kinetics as used in the current study (Talacua *et al.*, 2014). Our results demonstrate that a local MCP-1 gradient resulted in recruitment of monocytes, whereas the protein no longer

had an effect after release into the circulatory medium in our model. This is in line with previous findings, which showed that systemic MCP-1 is scavenged by circulating monocytes without affecting the functional responsiveness of the cells (Volpe *et al.*, 2012). Furthermore, the results of the current study do not show evidence for enhanced monocyte adhesion with the addition of exogenous MCP-1 in the scaffolds. This suggests that the presence of endogenously produced MCP-1 is required to stabilize anchorage via other adhesion proteins, as previously demonstrated (Gerszten *et al.*, 1999; Green *et al.*, 2006), but that local increase of MCP-1 levels alone has no added value for monocyte arrest. We focused here on the role of hPBMC only, rather than whole blood. *In vivo*, other circulating cell types, such as neutrophils and/or platelets, may play indirect or synergistic roles in the MCP-1-mediated response, which are currently not taken into account. However, as monocytes are considered the principle mediators of the regenerative response, this model allows for mechanistic studies with a high level of control. Furthermore, one of the main advantages of our methodology for translational studies is the use of human cells. This is of particular importance when studying the monocyte subsets, as these cells are known to be functionally different between species (Gordon & Taylor, 2005; Ingersoll *et al.*, 2010; Robbins & Swirski, 2010; Ziegler-Heitbrock *et al.*, 2010).

We conclude that in conditions of pulsatile flow, specific recruitment of circulating CCR2⁺ subsets is not the fundamental principle behind the previously observed improved neotissue formation in MCP-1-loaded constructs. Although our scaffold was proven to be highly chemotactic toward CD14⁺ monocytes, this selectivity was dependent on the release kinetics of MCP-1, as it was overruled by the effect of shear stress after the initial burst. This suggests that a controlled release of MCP-1 is essential in hemodynamic conditions and, therefore, should be considered in novel scaffold designs for *in situ* tissue engineering applications. These results emphasize the importance of testing in bio-mimicking conditions for future clinical translation.

Acknowledgements

This research forms part of the Project P1.01 iValve of the research program of the BioMedical Materials institute, co-funded by the Dutch Ministry of Economic Affairs. The financial contribution of the Nederlandse Hartstichting is gratefully acknowledged.

3

Strain-dependent modulation of macrophage polarization within scaffolds

This chapter is based on :

Ballotta V., Driessen-Mol A, Bouten CVC, Baaijens FPT (2014) “Strain-dependent modulation of macrophage polarization within scaffolds”. *Biomaterials*, 35(18):4919-28.

Abstract

Implanted synthetic substrates for the regeneration of cardiovascular tissues are exposed to mechanical forces that induce local deformation. Circulating inflammatory cells, actively participating in the healing process, will be subjected to strain once recruited. We investigated the effect of deformation on human peripheral blood mononuclear cells (hPBMCs) adherent onto a scaffold, with respect to macrophage polarization towards an inflammatory (M1) and reparative (M2) phenotype and to early tissue formation. HPBMCs were seeded onto poly- ϵ -caprolactone bisurea strips and subjected to 0%, 7% and 12% cyclic strain for up to one week. After 1 day, cells subjected to 7% deformation showed upregulated expression of pro and anti-inflammatory chemokines, such as MCP-1 and IL10. Immunostaining revealed presence of inflammatory macrophages in all groups, while immunoregulatory macrophages were detected mainly in the 0 and 7% groups and increased significantly over time. Biochemical assays indicated deposition of sulphated glycosaminoglycans and collagen after 7 days in both strained and unstrained samples. These results suggest that 7% cyclic strain applied to hPBMCs adherent on a scaffold modulates their polarization towards reparative macrophages and allows for early synthesis of extracellular matrix components, required to promote further cell adhesion and proliferation and to bind immunoregulatory cytokines.

3.1 Introduction

A clinically relevant concept of cardiovascular regenerative medicine proposes to implant synthetic scaffolds seeded with autologous cells, entrusting the host response to promote successful integration of the construct. This method was effectively applied by Shinoka *et al.* to create tissue engineered vascular grafts (TEVG) with bone marrow mononuclear cells (BM-MNCs) for the treatment of congenital defects in children (Matsumura, Hibino, *et al.*, 2003; Hibino *et al.*, 2005; Shinoka *et al.*, 2005). The contribution of the cellular component to tissue regeneration *in vivo* was further investigated, suggesting that pre-seeded cells play a pivotal role as mediators for tissue remodeling via paracrine mechanisms (Roh *et al.*, 2010). Among the numerous cytokines involved in the process, monocyte chemoattractant protein 1 (MCP-1) secreted from cells upon implantation was identified by Roh *et al.* as a key player in early monocytic infiltration and subsequent TEVG remodeling. More specifically, a favorable neo tissue formation could be elicited by a relatively rapid release of the MCP-1 from the scaffold. In addition, early deposition of native-like extracellular matrix by seeded cells might promote host cell adhesion and proliferation and bind important immunoregulatory cytokines, such as interleukin-10 (Franz *et al.*, 2011).

Another factor that determines the integration of the construct and the remodeling outcome is represented by the early interaction between the biomaterial and circulating cells. Shortly after implantation, scaffolds are extensively infiltrated by immune cells, which can modulate this inflammatory response via paracrine and autocrine signaling. Among them, macrophages were shown to be actively involved in the resolution of the inflammation, due to their ability to shift from a pro-inflammatory polarization state (M1) towards a reparative and homeostatic profile (M2) (Anderson *et al.*, 2008; Mosser & Edwards, 2008). In particular, the delicate balance between M1 and M2 phenotypes might represent the key to functional regeneration *in vivo* (Brown *et al.*, 2012). Initially, the host response evoked at the implant site implies inflow of M1 macrophages, involved in tissue reorganization and in further recruitment of leukocytes via release of chemokines, such as MCP-1. At later stages, a predominance of M2 phenotype was shown to promote resolution of the inflammation and to result in successful remodeling of the construct (Brown *et al.*, 2009).

The influence of substrate composition and topography over M1/M2 polarization was demonstrated, addressing the type of scaffold material, fiber diameter and pore size as parameters able to impact macrophage phenotypic profile (Badylak *et al.*, 2008; Saino

et al., 2011; Garg *et al.*, 2013). We hypothesize that mechanical cues may additionally alter the evoked response. It is known that forces exerted on cells can directly affect their phenotype and their underlying genomic profile through mechanotransduction, causing the activation and inhibition of numerous pathways (Gieni & Hendzel, 2008; Throm Quinlan *et al.*, 2011). *In vivo*, synthetic substrates for the replacement of load-bearing structures, such as heart valves, are exposed to mechanical forces that result in local deformation, and thereby in the stimulation of pre-seeded and infiltrating cells.

The aim of the present study is to investigate the effect of mechanical strain on cells involved in the early immune response, in terms of phenotype polarization, expression of pro- and anti-inflammatory cytokines and matrix deposition. To obtain a mechanistic insight into this process, a pre-seeded electrospun scaffold was subjected to increasing strain levels. As scaffold material, a custom-made thermoplastic elastomer, i.e. poly- ϵ -caprolactone bisurea, PCL-U4U, was used (Wisse *et al.*, 2006). Human mononuclear cells from peripheral blood (hPBMCs) were selected as cell source. They are representative of the circulating mononuclear population activated by the biomaterial implant, and might therefore serve as an *in vitro* model to comprehend the response to strain by infiltrated host cells (Gonzalez-simon & Eniola-adeleso, 2012). In addition, hPBMCs are easier to isolate than bone marrow mononuclear cells (BM-MNCs) and may, therefore, provide a clinically interesting alternative for one-step interventions (Germani *et al.*, 2009).

3.2 Materials and Methods

3.2.1 Experimental layout

Scaffold strips seeded with human peripheral blood mononuclear cells (hPBMCs) were subjected to mechanical loading in two series of experiments. In the first series, the strips were subjected to moderate strain (7%), while, in the second series, high deformations (12%) were applied. Experiments of each series were conducted for up to 7 days and repeated 3 times. In all experiments, groups of scaffold strips seeded with hPBMCs (0% group) and with human vena saphena cells (hVSCs, control group) were cultured statically. For each experiment, hPBMCs were freshly isolated from different donors, whereas hVSCs were obtained from a single donor and included to account for inter-experimental differences.

Groups of 3 strips were sacrificed after 1, 2, 4, and 7 days. At every time-point, part of each strip was snap-frozen and stored at -80°C for gene expression analysis or biochemical assays, and the remainder was fixed in 3.7% formaldehyde solution (Sigma, St.Louis, MO, USA) for staining.

3.2.2 Scaffold preparation

Scaffold fabrication

A thermoplastic elastomer based on a poly- ϵ -caprolactone PCL2000 soft block and a 1,4-bis-ureido butane hard block (PCL-U4U) was supplied by SyMO-Chem (Eindhoven, the Netherlands), and this material was processed into microfibers organized in a porous isotropic scaffold. Specifically, a solution of 12.5% PCL-U4U was prepared dissolving the polymer in amylene stabilized chloroform (CHCl_3 ; Sigma) with 1% methanol. After being stirred overnight, the polymer solution was dispensed with the aid of a syringe pump (PHD 22/2000, Harvard Apparatus, Holliston, MA) to a moving 14G needle placed at 15 cm distance from the collecting mandrel ($\text{Ø}=29$ mm, length=100 mm) of an electrospinning device (EC-CLI, IME Technologies, Geldrop, The Netherlands). The solution flowed at 25 $\mu\text{l}/\text{min}$ in presence of 14 kV voltage, at constant temperature of 23°C and 30% relative humidity. A coaxial flow of CHCl_3 saturated air was applied around the needle to prevent excessive solvent evaporation (Larsen *et al.*, 2004). Randomly oriented fibers were

collected on the cylindrical drum rotating at 100 rpm to obtain electrospun scaffolds, which were kept under vacuum overnight to eliminate solvent remnants.

Scaffold characterization

For each scaffold, thickness and fiber diameter were measured with a digital microscope (VHX-500FE, Keyence, Mechelen, Belgium) and a scanning electron microscope (SEM; Quanta 600F, FEI, Eindhoven, The Netherlands) respectively. Measurements are expressed as mean \pm standard deviation. Biaxial tensile tests were performed with BioTester 5000 (CellScale, Canada) to evaluate scaffold mechanical performance and isotropy within the range of applied deformations (strain 0-12%). Constant strain rate of 1.6% per second was applied for strains up to 35% on a square patch. In order to simulate the experimental conditions, biaxial tests were performed on patches pre-seeded with fibrin gel and immersed in distilled water at 37°C. Cycles of stretching, resting and recovering were repeated 5 times on samples from 3 different electrospun sheets. Cauchy stresses and strains calculated for the last cycle of each measurement were averaged over the three samples and plotted with the relative standard deviations.

3.2.3 Scaffold seeding and culture

Scaffold strips preparation

For each experiment, scaffold strips of 25 x 5 mm (n=36) were cut out of 2 spun sheets and glued on their outer ends in wells of sterile non-coated BioFlex culture plates (Flexcell® International Corporation, NC, USA) with Silastic MDX4-4210 (Dow Corning, Michigan, USA). After silicon glue polymerization, sterilization was performed by incubation with 70% ethanol, followed by 2 washing steps of 30 min in sterile phosphate buffered saline (PBS). Strips for seeding with hPBMC (n=24) were incubated overnight in RPMI 1640 medium (Gibco, Grand Island, NY, USA) supplemented with 10% fetal bovine serum (FBS; Greiner Bio one, Frickenhausen, Germany) and 1% Penicillin/Streptomycin (p/s, Lonza, Basel, Switzerland). Strips for seeding with hVSCs (n=12), were incubated overnight in advanced Dulbecco's Modified Eagle Medium (DMEM, Invitrogen, Carlsbad, USA) supplemented with 10% FBS, 1% p/s and 1% GlutaMax (Invitrogen).

Cells isolation and seeding

HPBMCs were isolated from fresh buffy coats obtained by 6 healthy donors after informed consent (Sanquin Blood Supply Foundation, Nijmegen, The Netherlands). The buffy coat

was mixed with citrate buffer (6 g Sodium Citrate in 1000 ml phosphate buffer solution, Sigma) and mononuclear cells were isolated by centrifugation on an isosmotic medium with a density of 1.077 g/ml (Lymphoprep™, Axis-Shield, Scotland). For each experiment, cells from a single donor were seeded at a density of 4×10^5 cells/mm³ onto the PCL-U4U strips using fibrin gel as a cell carrier (Mol, van Lieshout, *et al.*, 2005). Human vascular-derived cells harvested from saphena magna vein (hVSCs) and previously characterized as myofibroblasts were used as control (Mol *et al.*, 2006). After being cultured for 7 days with advanced DMEM medium supplemented with 10% FBS, 1% p/s, 1% GlutaMax, cells were suspended in fibrin gel and seeded onto the PCL-U4U strips at a density of 1.5×10^4 cells/mm³. hVSCs were used at passage 7 in all experiments.

Application of cyclic loading

Immediately after seeding, hPBMCs seeded strips were subjected to cyclic stretch of moderate (7%) and high (12%) magnitude at frequency of 0.8 Hz with Flexcell® FX-5000™ Tension System (Flexcell® International Corporation, NC, USA) for up to 7 days. RPMI and DMEM enriched media prepared for strip incubation were used for hPBMCs and hVSCs groups respectively, additionally supplemented with L-ascorbic acid 2-phosphate (0.25 mg/ml; Sigma) and replaced every 3 days.

Strain distribution within a single strip was analyzed via digital imaging to correlate the applied stretch to the actual scaffold deformation, as previously described by Boerboom *et al.* (Boerboom *et al.*, 2008). Images at 60 frames/sec of randomly dotted strips strained at 7% or 12% were collected with a high speed camera (MotionScope, M5C; IDT, Tallahassee, USA) and subsequently analyzed with ARAMIS DIC software (Gom mbH, Braunschweig, Germany).

3.2.4 Analyses

Cells distribution

Cells distribution within the scaffold was evaluated 1 and 7 days after seeding. Slices of formaldehyde-fixed seeded scaffolds with a thickness of 10 µm were cut out of strips embedded in Tissue-Tek® O.C.T™ Compound (Sakura Finetek Europe B.V., Alphen aan den Rijn, The Netherlands) with a cryotome (Thermo Scientific™ HM 550 Cryostats, Thermo Fisher Scientific Inc, Waltham, MA). Cells nuclei were stained with 4', 6-diamidino-2-phenylindole (DAPI, Sigma) and examined with fluorescent microscopy (Axiovert 200M, Zeiss, Göttingen, Germany) with a 10X objective.

Gene expression

Seeded scaffolds, sacrificed after 1 and 2 days of straining and stored at -80°C were placed in Nalgene® cryogenic vials (Sigma) containing RNA-free metal beads and disrupted with a microdismembrator (Sartorius, Göttingen, Germany) 3 times for 30 s at 3000 rpm. RLT buffer with β -mercaptoethanol (Sigma) was added to lysate the cells and RNA was subsequently isolated with Qiagen RNeasy kit (Qiagen, Venlo, The Netherlands) according to manufacturer's instructions. RNA quantity and purity were determined with a spectrophotometer (NanoDrop®, ND-1000, Isogen Life Science, Ijsselstein, The Netherlands). cDNA was synthesized starting from 125 ng RNA in a 25 μ l reaction volume consisting of random primers (Promega, Madison, USA), dNTPs (Invitrogen), 5X first strand buffer (Invitrogen), DTT (Invitrogen), M-MLV enzyme (Invitrogen) and double autoclaved water (ddH₂O). cDNA synthesis was performed in a Thermal Cycler (C1000 Touch™, Bio-Rad, Hercules, CA, USA) heating the samples for 6 min at 72°C, 5 min at 37°C (with subsequent addition of M-MLV), 60 min at 37°C, and 5 min at 95°C. Control reactions without M-MLV were used to verify the absence of genomic contaminations. cDNA samples were stored at -20°C for qPCR use.

Glyceraldehyde-3-phosphate dehydrogenase (GAPDH) and adenosine-5'-triphosphate (ATP) were selected as reference genes, as they represented the most stable genes throughout different experimental conditions according to GeNorm algorithm (Vandesompele *et al.*, 2002). Expression level of genes involved in tissue formation and inflammatory processes (Table 3.1) was evaluated adding SYBR Green Supermix (Bio-Rad), 20 mM primer mix and ddH₂O to cDNA templates. All samples were analyzed in duplicates. The real time PCR reaction (CFX384 Touch Teal-Time PCR Detection System, Bio-Rad) was carried out for 3 min at 95°C, 40x(20 seconds at 95°C, 20 s at 60°C, 30 s at 72), 1 min at 95°C, 1 min at 65°C followed by melting curve analysis. $2^{-\Delta Ct}$ was calculated for each sample after normalization to the geometric mean of both reference genes. The obtained value was further normalized to hVSCs control group to account for inter-experimental differences. To limit the influence of patients variability, gene expression of strained hPBMCs in relation to the unstrained state of a representative donor's cells was determined. This procedure is based on the assumption that the absolute levels of gene expression may vary, but that the effect of straining is equal between donors.

Table 3.1 Primers used for qPCR

Primer	Symbol	Amplicon size (bp)	Accession number	Primer sequence (5'-3')
monocyte chemotactic protein-1	MCP1	190	NM_002982	FW:CAGCCAGATGCAATCAATGCC RV:TGGAATCCTGAACCCACTTCT
interleukin 6	IL6	45	NM_000600	FW:ACTCACCTCTTCAGAACGAATTG RV:GTCGAGGATGTACCGAATTTGT
tumor necrosis factor	TNF	91	NM_000594	FW:GAGGCCAAGCCCTGGTATG RV:CGGGCCGATTGATCTCAGC
interleukin 10	IL10	112	NM_000572	FW:ACTTTAAGGGTTACCTGGGTTG RV:TCACATGCGCCTTGATGTCTG
chemokine (C-X-C motif) ligand 12	SDF1- α	48	NM_000609	FW:TTCTCAACACTCCAAACTGTGC RV:CTTCAGCCGGCTACAATCTG
α-smooth muscle actin	α SMA	134	NM_001613.1	FW:CGTGTGGCCCTGAAGAGCAT RV:ACCGCTGGATAGCCACATACA
Collagen I	Col I	120	NM_000088.3	FW:AATCACCTGCGTACAGAACGG RV:TCGTCACAGATCACGTCATCG
Collagen III	Col III	140	NM_000090.3	FW:ATCTTGGTCAGTCCATATGC RV:TGGAATTTCTGGGTTGGG
Elastin	Ela	146	NM_000501	FW:CTGGAATTGGAGGCATCG RV:TCCTGGGACACCAACTAC
Fibrillin I	Fib I	124	NM_000138	FW:TGTTGGTTTGTGAAGATATTG RV:GTGGAGGTGAAGCGGTAG
Fibrillin II	Fib II	126	NM_001999	FW:ATCCCTGTGAGATGTGTC RV:TTCCCTCCTTGGCATATCC
matrix metalloproteinase 1	MMP1	101	NM_001145938	FW:CGCACAAATCCCTTCTACCC RV:CTGTCCGCAAATTCGTAAGC
matrix metalloproteinase 2	MMP2	174	NM_001127891	FW:ATGACAGCTGCACCACTGAG RV:ATTTGTTGCCAGGAAAGTG
matrix metalloproteinase 9	MMP9	224	NM_004994	FW:TGGGGGGCAACTCGGC RV:GGAATGATCTAAGCCAG

Immunocytochemistry and immunohistochemistry

Whole mount immunofluorescent staining was performed on formaldehyde-fixed strips sacrificed at 1, 2, 4 and 7 days. The samples were washed in phosphate saline buffer (PBS) and permeabilized in 0.5 Triton X-100 (Merck, Schiphol-riek, the Netherlands) in PBS for 10 min. Non-specific binding was blocked by 10% horse serum (Invitrogen) in PBS for 15 min. Finally, scaffolds were incubated overnight at 4°C with primary antibodies mix, diluted as reported in Table 3.2. Primary antibodies against CD68, CCR7 and CD163 or CD206 were used for strips sacrificed after 1, 2 and 4 days, while antibodies against Collagen type I, Collagen type III and α -smooth muscle actin were selected for strips sacrificed at day 7. The following day, scaffolds were washed and incubated for 60 min with secondary antibodies. After washing, cell nuclei were stained with DAPI. Samples

were mounted on slides with Mowiol (Calbiochem, San Diego, USA) and observed with confocal microscopy (TCS SP5X, Leica Microsystems, Wetzlar, Germany). The amount of CD68⁺, CD206⁺, CD163⁺ and CCR7⁺ cells was quantified with ImageJ software (U.S. National Institutes of Health, Bethesda, MD, USA), counting immune-positive cells on a minimum of 5 matched microscope images at 20X magnification per group. Macrophage polarization quantification was obtained dividing the number of CCR7⁺ cells and the number of CD206⁺ cells (or CD163⁺) by the number of CD68⁺, therewith determining M1 and M2 profile percentage, respectively.

Table 3.2 Markers selected for immunostaining and relative time points and antibodies, with concentrations indicated as volume/volume.

Marker	Function	Time point (days)	Primary antibody	Secondary antibody
CD68	macrophage marker	1, 2, 4	Mouse anti-human IgG2b; 1:100 v/v (AbD Serotech)	Alexa fluor 555 goat anti-mouse IgG2b; 1:300 v/v (Invitrogen)
CCR7 (aka CD197)	M1 marker	1, 2, 4	Rabbit anti-human IgG; 1:100 v/v (Abcam)	Alexa fluor 647 goat anti-rabbit IgG; 1:300 (Invitrogen)
CD206 (aka MRC1)	M2 marker (mannose receptor)	1, 2, 4	Mouse anti-human IgG1; 1:100 v/v (AbD Serotech)	Alexa fluor 488 goat anti-mouse IgG1; 1:300 v/v (Invitrogen)
CD163	M2 marker (scavenger receptor)	1, 2, 4	Mouse anti-human IgG1; 1:100 v/v (AbD Serotech)	Alexa fluor 488 goat anti-mouse IgG1; 1:300 v/v (Invitrogen)
Collagen type I		7	Rabbit anti-human IgG; 1:250 v/v (Abcam)	Alexa fluor 555 donkey anti-rabbit IgG; 1:300 v/v (Invitrogen)
Collagen type III		7	Rabbit anti-human IgG; 1:200 v/v (Abcam)	Alexa fluor 555 donkey anti-rabbit IgG; 1:300 v/v (Invitrogen)
αSMA	α-smooth muscle actin	7	Mouse anti-human IgG2a; 1:500 v/v (Sigma)	Alexa fluor 488 goat anti-mouse IgG2a; 1:300 v/v (Invitrogen)

Quantitative tissue assays

The amount of DNA, sulphated glycosaminoglycans (sGAG) and hydroxyproline (HYP) was quantified for strips sacrificed at day 7. After lyophilization, samples were digested in papain solution (100 mM phosphate buffer, 5 mM L-cystein, 5 mM ethylenediaminetetraacetic acid and 140 µg papain per ml, all from Sigma) overnight at 60°C. DNA content was determined with the Hoechst dye method, using calf thymus DNA (Sigma) to obtain the standard curve (Cesarone *et al.*, 1979). sGAG amount was measured via an adapted Dimethyl Methylene Blue (DMMB) assay, using shark cartilage chondroitin sulphate (Sigma) as reference (Farndale *et al.*, 1986). Briefly, 40 µl of diluted samples was

pipetted in duplo into a 96-well plate and 150 μ l of DMMB was added to each well and absorbance was measured at 540 nm. As a measure of collagen content, samples were hydrolyzed in 16 M Sodium Hydroxide (Sigma) and HYP concentration was quantified with Chloramin-T assay, using trans-4-hydroxyproline (Sigma) as reference (Huszar *et al.*, 1980). The amount of DNA, sGAG and HYP per mg of dry tissue was calculated and sGAG and HYP were normalized to DNA content.

Statistical analysis

All data from immunostaining quantification, qPCR and biochemical analyses are expressed as mean \pm standard error of the mean. HVSCs were used as a reference in qPCR analysis, with their expression level set to a value of 1 for all genes. The 12% group at day 2 was not included in statistical analysis of gene expression, due to the limited amount of RNA extracted from the samples. Statistical differences were analyzed with one-way ANOVA followed by Bonferroni multiple comparison test, using Prism software 5.0 (GraphPad Software, La Jolla, CA). Differences were considered significant for P values < 0.05.

3.3 Results

3.3.1 Scaffold characterization and strain validation

Electrospun PCL-U4U sheets with a thickness of $306 \pm 86 \mu\text{m}$ and average fiber diameter of $5.3 \pm 0.6 \mu\text{m}$ were obtained (Figure 3.1A, B). Mechanical testing of the scaffold showed absence of plastic deformation and no differences were detected between x and y direction for strain below 12% (Figure 3.1 C). For higher strain levels, a slight anisotropy of the construct was observed. DAPI staining revealed that the scaffold porosity allowed for hPBMCs infiltration and cells were evenly distributed throughout the strip thickness within 1 day after seeding (Figure 3.1D). Cyclic stretch applied to the scaffold with the Flexcell® Tension System induced strains between 7 and 8% for the intermediate strain level and between 12 and 13% for the high strain level (Figure 3.1E, F). The two strain sets were indicated as 7% and 12% group, respectively.

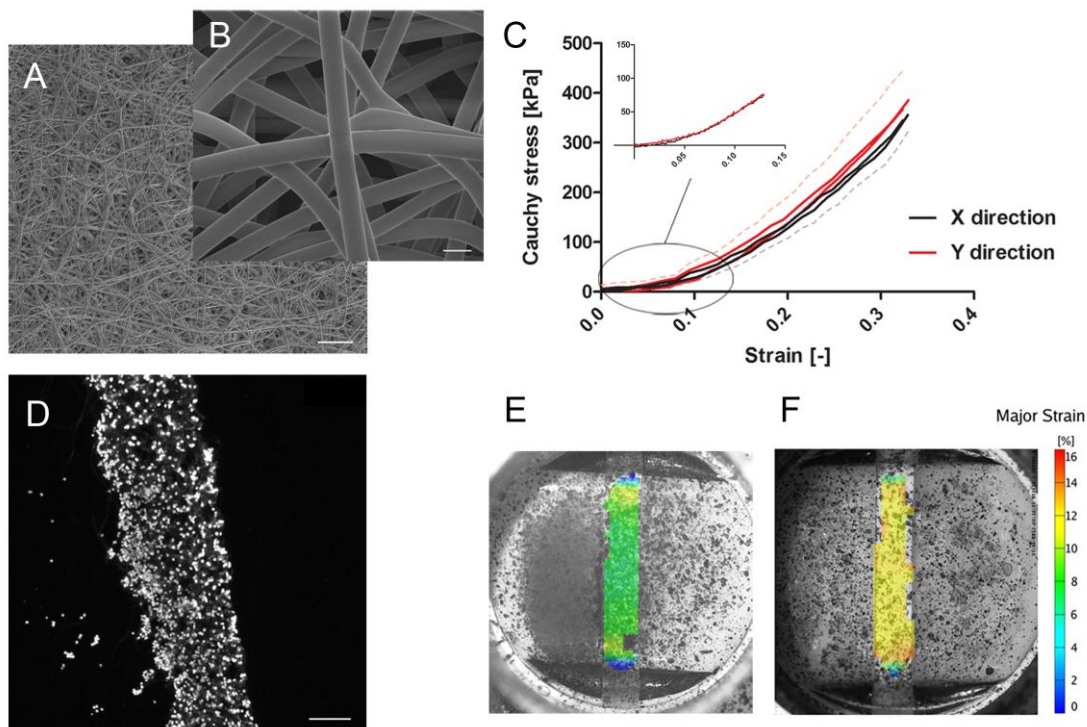


Figure 3.1 Scaffold characterization and strain validation. (A-B) SEM images revealing isotropic (A) and interconnected (B) PCL-U4U fibers. (C) Averaged ($n=3$) Cauchy stress vs strain curves with standard deviations (dashed lines) obtained with biaxial tensile test, indicating elastic behavior of the material. Inset: Cauchy stress vs strain curve of a representative sample, illustrating isotropy for mechanical strain below 12%. (D) Scaffold section stained with DAPI, showing hPBMCs infiltration throughout the thickness of the porous scaffold. (E-G) Scaffold subjected to different stretch magnitudes, resulting in 7% (E) and 12% (G) deformation. Scalebar: (A) $100 \mu\text{m}$, (B) $10 \mu\text{m}$, (D) $100 \mu\text{m}$.

3.3.2 Gene expression analysis

Expression of immune response markers was analyzed to investigate the response of hPBMCs to different strain magnitudes over time (Figure 3.2). Gene expression of the pro-inflammatory cytokines MCP-1, IL6 and TNF by hPBMCs was higher at day 1 and day 2 as compared to hVSCs (Figure 3.2A-C). At day 1, the expression of MCP-1 and IL6 showed significant increase for cells stimulated with 7% strain, compared to the other strain groups. The expression of anti-inflammatory markers IL10 and MMP9 showed similar behavior, with upregulation of all groups and significant increase for 7% strained cells, with respect to the control (Figure 3.2D-E). SDF1 α gene expression was downregulated for hPBMCs compared to hVSCs and showed significant increase for 12% group at day 1 (Figure 3.2F). For most genes, the expression of hPBMCs relative to hVSCs at day 2 was lower than its corresponding group at day 1, but the trend of expression at different strain levels remained consistent across the time points.

In comparison with hVSCs, hPBMCs showed low expression of genes involved in extracellular matrix synthesis, such as Collagen I and III, Elastin and Fibrillin I and II, MMP1 and MMP2 (data not shown). Expression of α SMA, marker for myofibroblasts and fibrocytes, was upregulated for hPBMCs after one day of strain at 7% and in static condition compared to the control (Figure 3.2G).

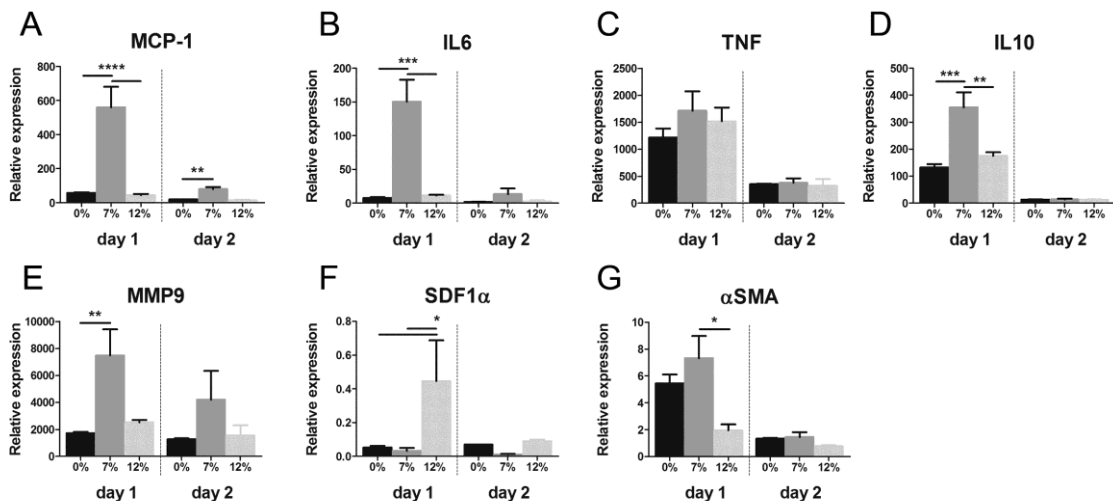


Figure 3.2. Gene expression analysis. Gene expression analysis of hPBMCs relative to hVSCs at day 1 and 2 for MCP-1 (A), IL6 (B), TNF (C), IL10 (D), MMP9 (E), SDF1 α (F), α SMA (G). *, **, ***, **** indicate significant difference for $P < 0.05$, 0.01 , 0.001 , 0.0001 respectively.

3.3.3 Macrophage phenotype assessment and quantification via immunostaining

Immunofluorescent staining showed that hPBMCs differentiated into macrophages with various phenotypes and revealed dissimilarities in cell distribution for scaffolds subjected to different strain conditions (Figure 3.3). After one day, all cells were adherent onto the scaffold fibers (Figure 3.3A). DAPI staining suggested that the 12% group was affected by cell depletion over time as compared to the other groups. A substantial fraction of cells exhibited the macrophage marker CD68, with no detectable differences between groups and time-points. Cell surface markers for the pro-inflammatory profile M1 (CCR7) and immunomodulatory and tissue remodeling profile M2 (CD206) revealed differential macrophage polarization among the different groups over time. A predominance of the M1 phenotype was observed for every experimental condition, with increasing presence of M2 cells at day 2 (Figure 3.3B) and 4 (Figure 3.3C) in 0% and 7% groups. Immunostaining for CD163 as M2 marker showed similar cell distribution and polarization (data not shown).

Figure 3.4 illustrates overall observed features of polarized macrophages in the different groups and time points. At day 1, macrophages exhibited a small size and round shape, with prevalence of CCR7 expression in each strain group. After 2 and 4 days, an increase of M2 marker expression was detected on the surface of cells exposed to 0% and 7% deformation, with frequent co-localization of CCR7 and CD206 on a single cell. Conversely, at day 2 and 4, macrophages subjected to 12% strain presented almost exclusively M1 phenotype. Cells positive to CCR7 only retained a small, round shape over time, while the majority of CD206⁺ cells displayed a more complex morphology and podosome-like protrusions development. Furthermore, the presence of cell clusters with marked M2 profile was detected in 0% and 7% strain groups at day 2 (Figure 3.5).

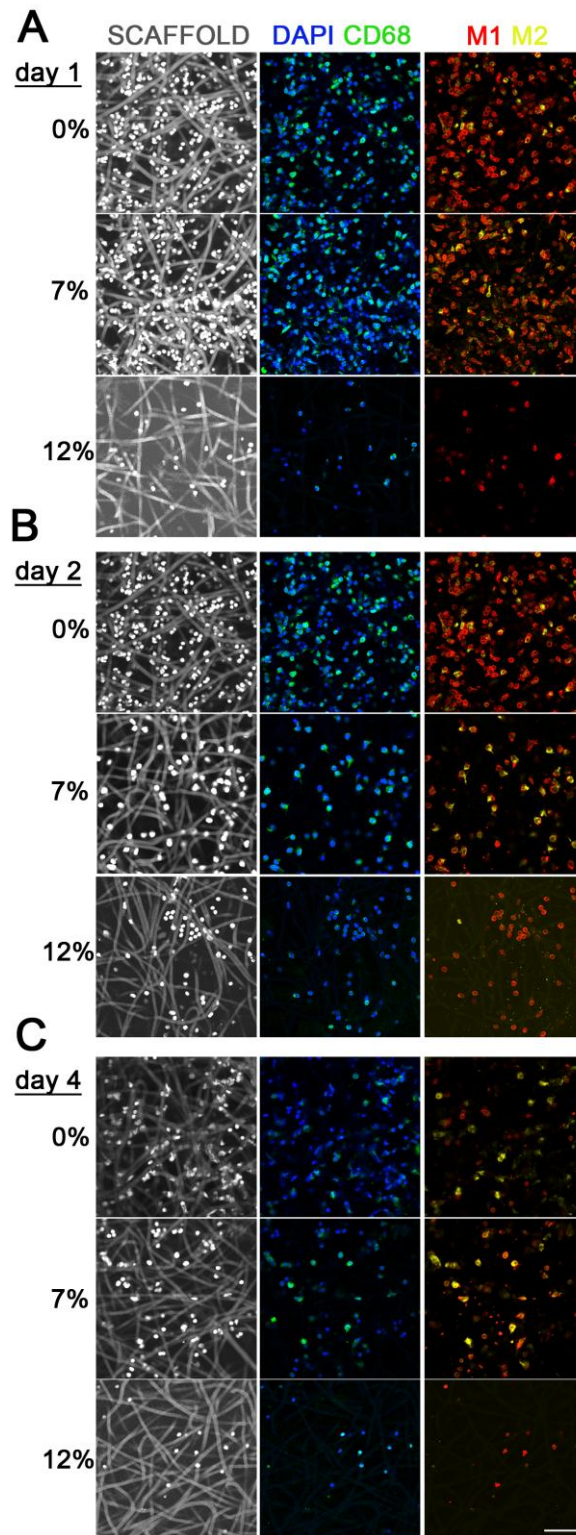


Figure 3.3 Cell distribution and phenotype within scaffolds subjected to different strain conditions. (A-C) DAPI staining (in blue) showing depletion of cells in 12% group over time, compared to 0% and 7% groups. CD68 staining (in green) proving monocyte differentiation into macrophages in all groups, with a prevalence of M1 phenotype (in red) compared to M2 (in yellow) in all groups at day 1. In time, increase of M2 is observed in 0% and 7% groups only. Scale bar: 50 μm .

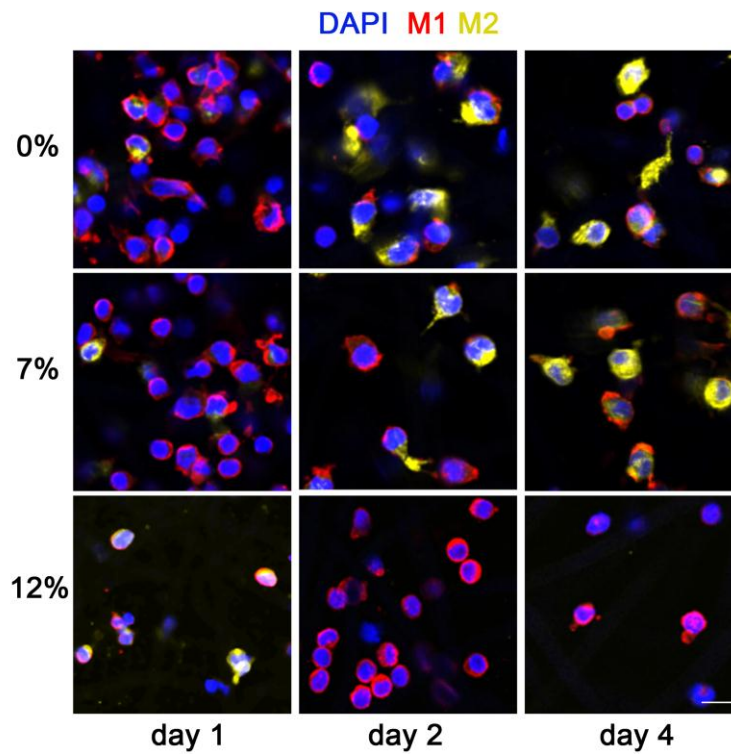


Figure 3.4 Macrophage phenotype assessment. *M1 (in red) and M2 (in yellow) staining, revealing increase of M2 macrophages over time in 0% and 7% groups, with co-localization of M1 and M2 markers. DAPI staining (in blue) indicates cell nuclei. Scale bar: 10 μ m.*

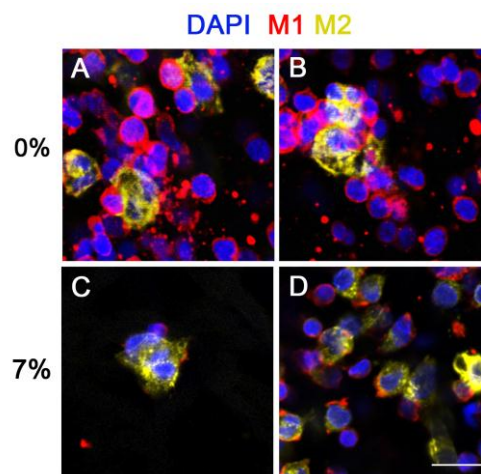


Figure 3.5 Cell clusters phenotype assessment. *Immunostaining for CCR7 (M1, in red) and CD163 (M2, in yellow) markers at day 2, revealing the presence of fused cells with preferred M2 phenotype both in 0% (A-B) and 7% (C-D) strain groups. Scale bar: 25 μ m.*

Quantitative analysis of the macrophage polarization status confirmed that the majority of macrophages were CCR7⁺ (M1), with no significant differences between groups and time

points (Figure 3.6A). A lower percentage of macrophages were CD206⁺ (M2), with diminished values for 12% groups at day 2 and 4. An M2/M1 (CD206⁺/CCR7⁺) ratio below 1 indicated that macrophage polarization was skewed towards M1 phenotype, but a significant increase towards M2 in the 7% strain group was observed over time (Figure 3.6B). In contrast, M2/M1 ratio remained stable for 0% group at day 2 and 4, but decreased substantially for 12% group, implying a limited presence of CD206⁺ cells. Data plotted per time point showed that the ratio of polarized macrophages was analogous for all groups after 1 day, whereas a significant decrease of M2/M1 was observed for 12% strain at day 2 and 4, as compared to other 2 groups (Figure 3.6C). Quantitative analyses performed with CD163 as M2 marker showed similar trend (data not shown).

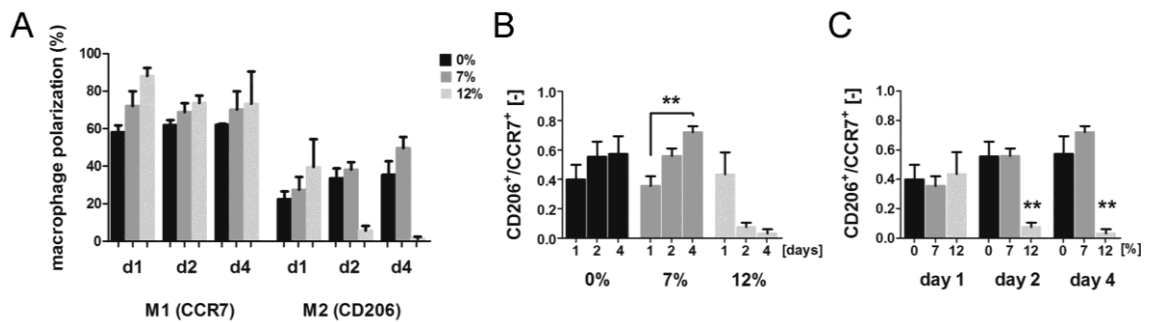


Figure 3.6 Macrophage phenotype quantification. (A) Macrophage polarization percentages calculated showing ratio of M1 and M2 to the total amount of CD68⁺ cells. (B) M2:M1 ratio revealing M2 phenotype increase in 7% group over time. Values below 1 indicate predominance of M1 macrophages. (C) A different representation of the same data showing decrease of M2 phenotype in 12% groups at day 2 and day 4. ** Denotes significant difference for $P < 0.01$.

3.3.4 Quantitative analysis and immunostaining of extracellular matrix markers

The presence of cells within the scaffold after 7 days and early tissue formation were visualized with immunostaining and evaluated via quantification of DNA and matrix components. DNA measurements confirmed the observations based on DAPI staining, revealing a decrease of the amount of cells for increasing strain levels, with more than 50% depletion in the 12% groups in comparison to the static control (Figure 3.7A). sGAG and HYP assays demonstrated the capacity of preseeded hPBMCs to synthesize and deposit sulphated glycosaminoglycans and hydroxyproline, but in lower amounts as

compared to hVSCs and with no significant differences between the strain levels (Figure 3.7B, C). sGAG and HYP amounts are reported normalized to DNA.

Immunostaining of collagen types showed deposition of Collagen type III in all groups, thus reflecting the results of HYP assay, but only limited amounts of Collagen type I was observed (Figure 3.7D). The staining for smooth muscle actin revealed the presence of spindle-shaped α SMA⁺ cells elongated along the polymer fibers in scaffolds subjected to 0 and 7% deformation.

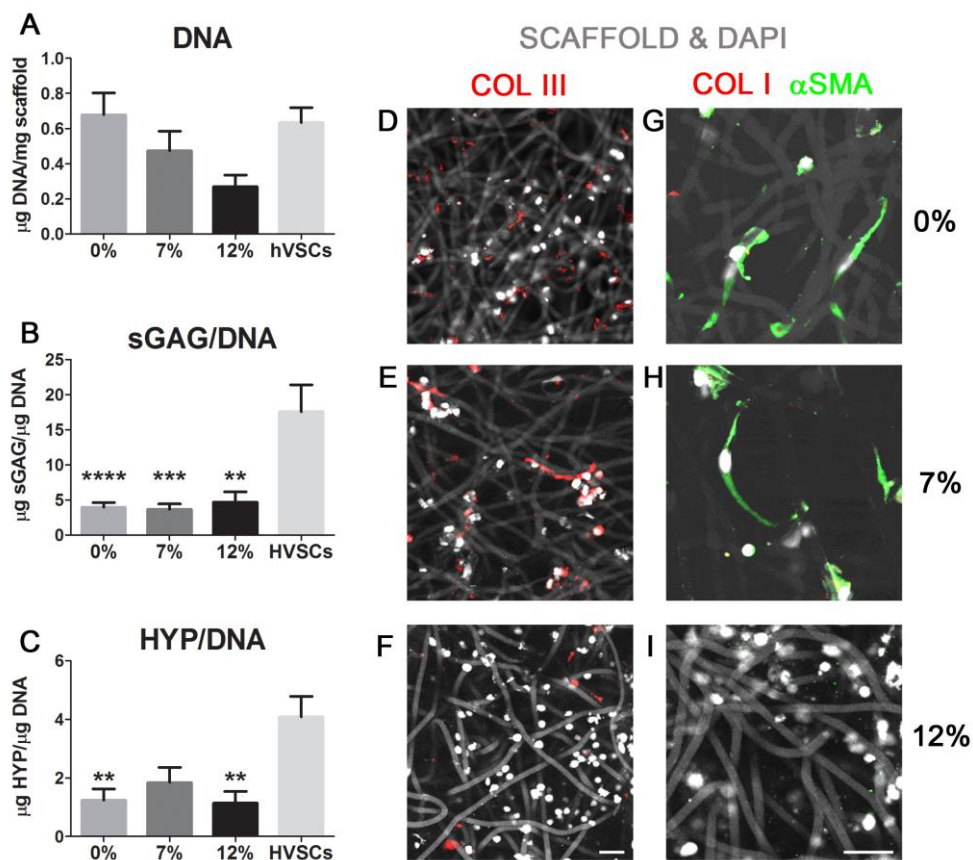


Figure 3.7 Analysis of extracellular matrix markers. (A-C) Quantitative analysis of DNA (A), sGAG (B) and HYP (C) of hPBMCs subjected to different deformations at day 7. sGAG and HYP are normalized on DNA content. (D-I) Immunostaining images revealing Collagen III deposition (D-F), absence of Collagen I and presence of α SMA⁺ spindle-shaped cells (G-I) after 7 days of cyclic loading. Scale bar: 25 μm . **, ***, **** indicate significant difference for $P < 0.01$, 0.001, 0.0001 respectively.

3.4 Discussion

Recent studies have shown that modulation of macrophage phenotype represents a critical determinant of functional integration or failure of implanted biomaterials (Brown *et al.*, 2012). Badylak *et al.* unveiled the correlation between the ratio of M1:M2 cells following implantation and the host response, suggesting that polarization towards an M2 phenotype might lead to constructive remodelling (Badylak *et al.*, 2008). The present study investigated the impact of mechanical cues on hPBMCs adherent on a fibrous scaffold *in vitro* and demonstrated that strain affects macrophage response in terms of signaling and differentiation. In particular, moderate strains (7%) elicit polarization towards a reparative M2 profile and enhance the expression of genes participating in the immune response, such as MCP-1, IL6, IL10, MMP9, while higher strains (12%) elicit a down-regulation of these genes.

Sensitivity of several cell types to cyclic stretch is well acknowledged, but there is only limited recognition of macrophage responsiveness to mechanical loading. Recently, it was proven that stretch affects elasticity and phagocytosis functionality of murine macrophages, in a process mediated by actin polymerization (Patel *et al.*, 2012). In the present study, human macrophages were shown to respond to cyclic strain amplitudes, selected among a range of deformations that can occur *in vivo* when load-bearing cardiovascular tissues are subjected to physiological forces (Bouten *et al.*, 2011). Moderate strain (7%) cyclically applied for one day remarkably altered the expression of genes, such as MCP-1, proven to expedite wound healing by early recruitment of cells from the circulation and adjacent tissues, when released with a short pulse (Jay *et al.*, 2010; Roh *et al.*, 2010). Furthermore, 7% deformation enhanced polarization of macrophages towards the M2 profile over time and did not result in cell loss within the scaffold. On the contrary, deformations around 12% resulted in cell loss over time and induced predominant transition towards the M1 profile, indicating that high strain magnitudes might discourage macrophage adhesion and interfere with differentiation towards tissue regenerative M2 phenotype. Variation of the genetic and phenotypic profile in response to different strain levels is an evidence of macrophage sensitivity to cyclic load that triggers mechanotransduction pathways. When cells are exposed to varying mechanical strain levels, forces acting on the cytoskeleton result in differential activation of multiple mechanosensors, such as stretch-sensitive ion channels and unfolding of actuated proteins (Throm Quinlan *et al.*, 2011). Identification of such sensors and related pathways for force transduction in macrophages is interesting, but beyond the scope of this study.

The mononuclear cell fraction of the seeded hPBMCs underwent differentiation into CD68⁺ macrophages upon contact with the PCL-U4U scaffold, irrespective of the applied deformation. At day 1, the CD68⁺ population was only partially polarized towards a M1 or M2 profile, therefore percentages of cells stained for CCR7 and CD206 or CD163 did not sum to 100%. At day 2 and 4, the sum of M1 and M2 percentages exceeded the total amount of CD68⁺ macrophages in 0 and 7% groups, as many cells exhibited concurrently both surface markers. This phenomenon might be justified by the presence of a transitional phenotype within the wide spectrum of macrophage activation described by Mosser and Edwards, reflected also in the concomitant expression of genes associated with both M1 (MCP-1, IL6, TNF) and M2 (IL10, MMP9) profiles (Mosser & Edwards, 2008).

Expression of inflammatory and immunoregulatory genes showed considerably high upregulation at day 1, as a result of the acute response prompted by the initial interaction between macrophages and the biomaterial. After 2 days, a decrease of gene expression of MCP-1, IL6, TNF and IL10 was observed, which might be connected to attenuation of the immune response, with potentially beneficial downstream implications, as it was shown that prolonged pro-inflammatory signaling can lead to deleterious consequences, such as chronic inflammation and scar tissue formation (Franz *et al.*, 2011). Gene expression of SDF-1 α , which was shown to contribute to inflammation resolution and recruitment of stem cells when incorporated into biomaterials, was downregulated for hPBMCs compared to hVSCs, indicating that adherent leukocytes might not represent a valid cell source for release of this chemokine (Thevenot *et al.*, 2010). α SMA gene expression was upregulated in 0 and 7% strained samples and spindle-like α SMA⁺ cells were detected in these groups after 7 days. The observed features are distinctive of fibrocytes, described as progenitor cells present in the hPBMCs fraction and involved in inflammation and matrix deposition (Reilkoff *et al.*, 2011). Extensive presence of fibrocytes may induce fibrosis, but their contribution to early collagen deposition and later differentiation into myofibroblasts might support graft remodeling (Thevenot *et al.*, 2011). Additional assessment needs to be carried out in future research to accurately identify the nature of these cells.

The presence of fused macrophages was observed in unstrained and 7% strained scaffolds at day 1 and 2. Their formation is probably triggered by the contact with 5 μ m diameter polymeric fibers, that hamper the phagocytosis capacity of macrophages (Anderson *et al.*, 2008). Formation of such multinucleated clusters is typically induced by anti-inflammatory cytokines and is associated with a transition to M2 phenotype, as confirmed by immunostaining (Anderson *et al.*, 2008).

The use of scaffolds pre-seeded with autologous cells for vascular regenerative medicine is currently under debate. Roh et al. could not detect the seeded BM-MNCs within the graft one week after implantation in a murine model, suggesting that seeded cells do not contribute to remodeling through direct tissue deposition, (Roh *et al.*, 2010). Further evidence of their limited contribution to vessel regeneration in small animals was provided by Wu et al., who obtained successful remodeling of a graft interposed in a rat abdominal aorta by means of a cell-free approach (Wu *et al.*, 2012). Brown et al indicated that acellular scaffolds were capable to elicit M2 polarization, but it was shown by Hibino et al. that pre-seeded grafts could significantly reduce infiltration of macrophages and M1 activation (Brown *et al.*, 2009; Hibino *et al.*, 2011). Rapid depletion of pre-seeded cells from implanted scaffolds was observed in small animal models, whereas persistence of pre-seeded cells was proved for up to 2 weeks in patches implanted in the arterial wall of ovine models (Sales *et al.*, 2007). These results suggest that the time before seeded cells are cleared might increase with the life span of the host, implying that they could survive several weeks within a human host, eventually supporting initial matrix deposition.

In the present study, hPBMCs were shown to contribute to ECM synthesis within a week from seeding, mainly by deposition of sGAG and Collagen III. In addition to offering additional mechanical support to the biodegradable construct, early matrix can support later tissue production by secondary infiltrating cells, by providing appropriate microenvironmental cues. In particular, sGAG have been identified to promote cell adhesion and proliferation and to bind cytokines involved in resolution of inflammation and angiogenesis, such as IL10 and IL8, preventing them from being cleaved (Franz *et al.*, 2011). Moreover, it was demonstrated that matrices based on collagen and sGAG support expression of CD163 and release of IL10 by adherent macrophages, signifying M2 activation (Kajahn *et al.*, 2012).

There are several limitations to this study. The model system allowed to study the effect of mechanical strain on adherent macrophages, without taking into account other immunoregulatory cells involved in M1/M2 polarization. Lymphocytes were present in the seeded leukocyte fraction, but they did not adhere to the scaffold, therefore their contribution to the study is considered irrelevant. A limited amount of markers and genes was selected to characterize activated populations of macrophages. Antibodies against CCR7 and CD163 or CD206 were used to discriminate between M1 and M2 respectively, as they are known to be highly indicative of polarized macrophages (Mantovani *et al.*, 2002). In order to provide a more exhaustive profiling of macrophages phenotype, the range of genes analyzed by qPCR could be widened and supplemented by quantification of cytokine

release at protein level. The role of other mechanical forces acting on implanted scaffolds, such as shear stresses induced by flow, was not included in this study, but is currently under investigation in our laboratory, to provide further insight into cell responses to mechanical cues.

The results of this study offer a first indication of a strain range that positively affects macrophages in terms of polarization and early matrix deposition. This information may be used to improve the remodeling outcome of an implant, by tuning the mechanical properties of the substrate in order to modulate the early response of pre-seeded and infiltrated macrophages upon implantation. With the aid of computational modeling, the design of scaffolds for the regeneration of load-bearing cardiovascular tissues can be optimized, in order to expose adherent cells to moderate strains when subjected to physiological loads.

3.5 Conclusion

This study indicates that the inflammatory response to a biomaterial can be modulated by mechanical strain. Deformations applied to adherent macrophages were shown to differentially affect their phenotype and gene expression. In particular, strain levels around 7% promote polarization towards the anti-inflammatory, reparative M2 profile. Furthermore, it was demonstrated that macrophages exposed to mechanical loads retain the capability to synthesize extracellular matrix. These results are instructive for the design and manufacturing of scaffolds intended as replacement for load-bearing cardiovascular tissues.

Acknowledgments

The authors are grateful to Serge H.M. Söntjens from SyMO-Chem for providing PCL-U4U material and for his help in revising the manuscript. Marc Simonet is gratefully acknowledged for his assistance with electrospinning. This research forms part of the Project P1.01 iValve of the research program of the BioMedical Materials institute, co-funded by the Dutch Ministry of Economic Affairs. The financial contribution of the Nederlandse Hartstichting is gratefully acknowledged.

Synergistic protein secretion by mesenchymal stromal cells seeded in 3D scaffolds and circulating leukocytes in physiological flow

This chapter is based on :

Ballotta V.*, Smits A.I.P.M.*, Driessen-Mol A, Bouten CVC, Baaijens FPT (2014) "Synergistic protein secretion by mesenchymal stromal cells seeded in 3D scaffolds and circulating leukocytes in physiological flow". *Biomaterials*, 35(33):9100-13.

*these authors contributed equally to the study

Abstract

Mesenchymal stromal cells (MSC) play an important role in natural wound healing via paracrine and juxtacrine signaling to immune cells. As such, MSC have been used in combination with biomaterials to function as natural producers of signaling factors upon implantation, in order to mediate regeneration of cardiovascular tissues *in situ*. The aim of this study was to identify the signaling factors secreted by preseeded cells in a biomaterial and their interaction with circulating leukocytes, in the presence of physiological biomechanical stimuli exerted by the hemodynamic environment (i.e. strain and shear flow). Electrospun poly(ϵ -caprolactone)-based scaffolds were seeded with human peripheral blood mononuclear cells (PBMC) or MSC, either adipose- or bone marrow-derived. The preseeded scaffolds were analyzed for the production of immunomodulatory and trophic proteins under static conditions and cyclic strain. Subsequently, the cross-talk between seeded cells and circulating leukocytes was addressed by exposing the scaffolds to a suspension of PBMC in static transwells and in pulsatile flow. Our results revealed that PBMC exposed to the scaffold consistently secreted a mix of immunomodulatory proteins, such as TNF α , IL-10 and MMP9, under all conditions tested. Preseeded MSC, on the other hand, secreted the trophic factors MCP-1, VEGF and bFGF. Furthermore, we observed a synergistic upregulation of CXCL12 gene expression and a synergistic increase in bFGF protein production by preseeded MSC exposed to PBMC in pulsatile flow. These findings indicate CXCL12 and bFGF as valuable targets for the development of safe and effective acellular instructive grafts for application in *in situ* cardiovascular regenerative therapies.

4.1 Introduction

Human multipotent mesenchymal stromal cells (MSC), are long-known for their multilineage differentiation potential (Pittenger *et al.*, 1999). In adult humans, MSC reside in local niches within various tissues throughout the body, such as the bone marrow and adipose tissue. Apart from their multipotency, MSC are well-recognized for their immunomodulatory potential (Aggarwal & Pittenger, 2005; Shi *et al.*, 2012). In addition, MSC contribute to tissue repair and angiogenesis by homing to sites of injury and releasing a broad range of paracrine factors, a capacity which has been referred to as trophic

activity (Caplan, 2007). The recognition of the immunomodulatory and trophic capacities has led to effective clinical employment of MSC in various cell-based therapies, such as the treatment of graft-versus-host-disease (Le Blanc *et al.*, 2004, 2008) and regenerative therapies, for example after myocardial infarction (Fisher *et al.*, 2013).

Similarly, MSC have been used in combination with biomaterials, or scaffolds, for the local regeneration of cardiovascular tissues in a one-step intervention, following the so-called *in situ* tissue engineering approach (Matsumura, Miyagawa-Tomita, *et al.*, 2003; Hibino *et al.*, 2005; Matsumura *et al.*, 2006; Vincentelli *et al.*, 2007; Emmert *et al.*, 2011, 2012; Weber *et al.*, 2013). Preseeding of scaffolds with either selected MSC or unfractionated bone marrow mononuclear cells (BM-MNC) has been shown to improve neotissue formation *in vivo* in various animal models, which has led to the first clinical trials using this approach for replacement of large-caliber arteries (Matsumura, Hibino, *et al.*, 2003; Shinoka *et al.*, 2005; Hibino *et al.*, 2010). Rather than terminally differentiating into functional tissue cells, it appeared that the preseeded BM-MNCs primarily ameliorate the regenerative process by paracrine signaling to recruit immune cells (Roh *et al.*, 2010). Accordingly, it was shown that static exposure of BM-MNCs to a synthetic scaffold significantly increased the secretion of several chemoattractants *in vitro* (Roh *et al.*, 2010). However, as the BM-MNCs are a highly heterogeneous population, the contribution of MSC to this process is not known. Since the amount of MSC is highly variable between patients, this may lead to high inter-patient variability in the clinical application of this approach, which warrants for a more systematic insight into these processes. Furthermore, the interactions between MSC and recruited leukocytes remain to be clarified. This is of importance as it is known that MSC only exhibit their immunosuppressive and trophic activities when in close cross-talk with leukocytes (Shi *et al.*, 2012). Moreover, the interactions between MSC and leukocytes may be influenced by the hemodynamic environment as it was shown that cyclic strain influences the synthetic and immunomodulatory behavior of MSC (Charoenpanich *et al.*, 2011; Colazzo *et al.*, 2011), as well as peripheral blood mononuclear cells (PBMC) (Ballotta *et al.*, 2014). Furthermore, we recently demonstrated that the recruitment of circulating PBMC is influenced by shear flow, which emphasizes the importance of the hemodynamic environment (unpublished data).

For safe and effective clinical translation of the promising *in situ* tissue engineering approach, our goal here was to systematically study the signaling factors secreted by preseeded cells in a biomaterial and their interaction with circulating leukocytes, in the presence of physiological biomechanical stimuli.

Fibrous poly(ϵ -caprolactone)-based scaffolds were seeded with human PBMC, bone marrow-derived mesenchymal stromal cells (BMSC), or adipose-derived mesenchymal stromal cells (ADSC), and the seeded scaffolds were analyzed for the production of immunomodulatory and trophic proteins under static conditions, as well as under cyclic strain. Subsequently, the cross-talk between seeded cells and circulating leukocytes was addressed by exposing the preseeded scaffolds to a suspension of PBMC in static transwells and in conditions of pulsatile flow.

4.2 Materials and methods

4.2.1 Cell culture and characterization

The BMSC were a generous gift from the Maastricht University, in cooperation with the Academic Hospital Maastricht, the Netherlands. Human ADSC were purchased from Invitrogen (Bleiswijk, the Netherlands). For both MSC types, α MEM (Gibco, Grand Island, NY) was used as the culture medium, supplemented with fetal bovine serum (10% v/v; FBS Gold, PAA Laboratories GmbH, Cölbe, Germany), L-glutamine (1% v/v; Sigma-Aldrich, St. Louis, MO), and penicillin/streptomycin (1% v/v; Lonza, Basel, Switzerland). After expansion, the MSC were frozen in α MEM, supplemented with Dimethyl Sulfoxide (DMSO; 10% v/v; Merck Millipore, Amsterdam, the Netherlands) and FBS Gold (20% v/v), and cryopreserved until use. Human PBMC were isolated from buffy coats (purchased from Sanquin, Nijmegen, the Netherlands) by density gradient centrifugation (Lymphoprep; Axis-Shield, Oslo, Norway). After isolation, PBMC were directly frozen in RPMI medium (RPMI 1640; Gibco), supplemented with FBS Gold (20% v/v) and DMSO (10% v/v). In total, PBMC from 6 healthy donors were used. Prior to use, the cell populations were characterized using flow cytometry, as described in 4.2.7.

4.2.2 Scaffold preparation

3D fibrous sheets were produced by electrospinning, using poly- ϵ -caprolactone bisurea (PCL-U4U) as the base material. PCL-U4U is an elastomeric polymer, custom-developed by SyMO-Chem (Eindhoven, the Netherlands), with Mw = 110 kDa. For electrospinning, the PCL-U4U was dissolved in chloroform (CHCl₃; amylene-stabilized, Sigma-Aldrich) at a concentration of 12.5 % (w/v) with addition of 1% (v/v) methanol. The polymer solution

was fed through a translating 14 G needle at high voltage (14 kV) and collected on a grounded, rotating cylindrical mandrel (\varnothing 29 mm, 100 rpm) at 15 cm distance. Temperature and relative humidity were kept constant at 23 °C and 30%, respectively, using an electrospinning climate chamber (EC-CLI, IME Technologies, Geldrop, the Netherlands). A coaxial flow of CHCl_3 -saturated air was applied around the needle to prevent excessive solvent evaporation. Scaffolds were kept under vacuum overnight to remove any solvent remnants. The resulting thickness of the scaffold sheet was determined using high-power digital microscopy (VHX-500FE, Keyence, Mechelen, Belgium) and the fiber diameter was measured using scanning electron microscopy (SEM; Quanta 600F, FEI, Eindhoven, the Netherlands).

4.2.3 Cell seeding

Scaffolds were cut to size from the electrospun sheets and sterilized using a 70% ethanol solution. Circular scaffolds (\varnothing 8 mm) were used for the chemotaxis assays and rectangular scaffolds were used for the flow and strain experiments (10 x 15 mm² and 5 x 35 mm², respectively). For the strain experiments, the scaffolds were glued onto non-coated BioFlex culture plates (FlexCell International Corporation, Hillsborough, NC) using silicone (Silastic MDX4-4210; Dow Corning, Midland, MI). After polymerization of the silicone glue, scaffolds were sterilized using 70% ethanol. Prior to cell seeding, the sterile scaffolds were washed using phosphate-buffered saline (PBS) and incubated in medium overnight to allow for protein adsorption. Cells were seeded using fibrin gel as a carrier (Mol, van Lieshout, *et al.*, 2005). BMSC and ADSC were used at passage 5 at a concentration of 8×10^3 cells/ μl . PBMC were seeded at a concentration of 1×10^5 cells/ μl . The cells were suspended in fibrinogen (10 mg/ml; Sigma-Aldrich), after which the suspension was mixed with thrombin (10 IU/ml; Sigma-Aldrich) and immediately seeded into the PCL-U4U scaffolds. The fibrin was allowed to polymerize for 15 minutes at 37 °C, before starting experiments. Four experimental conditions were applied to the seeded scaffolds: (I) static control, (II) cyclic strain, (III) chemotaxis assay, and (IV) shear flow conditions (Figure 4.1).

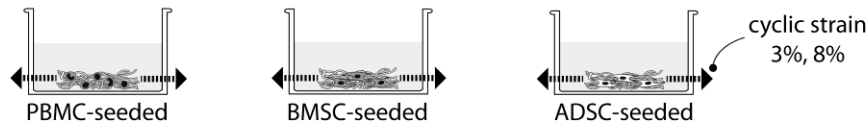
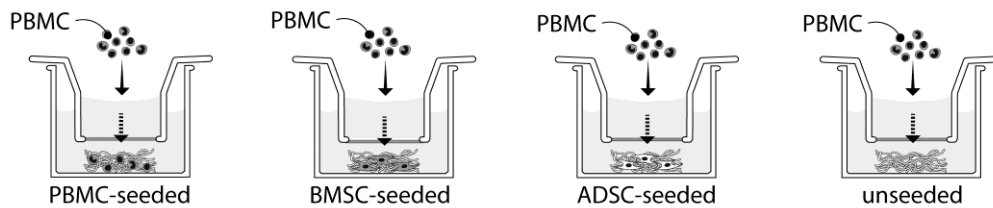
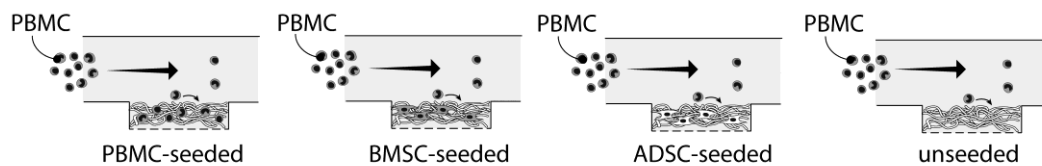
I. Static control**II. Cyclic strain****III. Chemotaxis****IV. Shear flow**

Figure 4.1 Drawing illustrating the experimental design. Scaffolds preseeded with PBMC, BMSC or ADSC were used as static control (I), or were subjected to 3% and 8% cyclic strain at 0.8 Hz (II). Scaffolds preseeded with PBMC, BMSC or ADSC and unseeded scaffolds were exposed to PBMC in suspension in a transwell chamber system (III) or in a fluidics setup to apply shear flow conditions (IV).

4.2.4 Strain experiments

Preseeded strips were subjected to cyclic stretch using the Flexcell system (FX-5000TM Tension System, FlexCell International Corporation) with maximum strain levels of 0%, 3%, and 8% at a frequency of 0.8 Hz. The strain distribution within the scaffolds was validated via digital imaging to correlate the applied stretch to the actual scaffold deformation, as previously described (Boerboom *et al.*, 2008). For this, a random dots pattern was sprayed onto the scaffolds and images were collected at 60 frames/sec with a high-speed camera (MotionScope, M5C, IDT, Tallahassee, FL). Images were analyzed with

ARAMIS DIC software (Gom GmbH, Braunschweig, Germany), resulting in the local strain distribution over the scaffold strips (data not shown).

BMSC- and ADSC-seeded scaffolds were cultured in complete α MEM culture medium, while PBMC-seeded strips were cultured in complete RPMI culture medium. Samples of the supernatant media were collected after 1, 4, and 24 hours for protein analyses. After 24 hours, the strips were released from the Bioflex plates, cut into small pieces, snap-frozen in liquid nitrogen and stored at $-80\text{ }^{\circ}\text{C}$ for qPCR analysis. Three experimental groups were tested: scaffolds seeded with PBMC, BMSC, and ADSC (N=9 per group).

4.2.5 Chemotaxis assay

Seeded scaffolds were placed in the lower compartment of a Boyden chamber, separated from the upper compartment by a membrane with $\varnothing\ 3\ \mu\text{m}$ pores (24-wells ThinCerts, Greiner Bio-One, Frickenhausen, Germany). Four experimental groups were tested: scaffolds seeded with PBMC, BMSC, ADSC, and fibrin only (N=9 per group). In all groups, PBMC were added into the upper compartment in complete RPMI medium at a concentration of 5×10^6 cells/ml. After 4 hours of incubation ($37\text{ }^{\circ}\text{C}$; 5% CO_2), the migrated cells were analyzed with flow cytometry and samples of the medium supernatant were obtained for protein analysis. The scaffolds and membranes were washed with PBS to include all non-adherent cells in the flow cytometric analysis. After washing, the scaffolds were cut into small pieces, snap-frozen in liquid nitrogen and stored at $-80\text{ }^{\circ}\text{C}$ for qPCR analysis.

4.2.6 Fluidics model

An in-house developed mesofluidics setup was used to investigate cell recruitment and interactions in bio-mimicking conditions of pulsatile flow, as previously described (Smits *et al.*, 2012). In brief, rectangular strips ($10 \times 15\ \text{mm}^2$) of the preseeded scaffolds were mounted into a parallel-plate flow chamber. PBMC were suspended in complete RPMI medium (5×10^6 cells/ml) and added to the syringes of a Fluidic Unit (ibidi GmbH, Martinsried, Germany) with a total volume of 10 ml per sample. The cell suspension was driven along the scaffold in a pulsatile flow using a modified pressure pump (ibidi GmbH).

Flow conditions were set at a frequency of 1 Hz, with peak shear stress and peak pressure of approximately 1.6 Pa and 100 mmHg, respectively, resembling typical hemodynamic conditions of human small-diameter arteries. Samples of the remaining cell suspension were taken during flow via in-line injection ports (ibidi GmbH) on the outlet port of the flow chambers (at 25 min, 1 hr and 4 hrs). These samples were analyzed using flow cytometry to quantify the remaining cell populations and the supernatant was analyzed for protein content. After 4 hours of exposure to the PBMC, the scaffolds were sacrificed. Approximately $\frac{1}{4}$ of the scaffold was fixated in formaldehyde (3.7% v/v; Merck Millipore, Amsterdam, the Netherlands) for immunofluorescent staining and the remainder was cut into small pieces, snap-frozen in liquid nitrogen and stored at -80 °C for qPCR analysis. Four experimental groups were tested: scaffolds seeded with PBMC, BMSC, ADSC, and fibrin only (N=9 per group).

4.2.7 Flow cytometry and gating strategy

For all experimental conditions, the cells collected for flow cytometric analysis were washed using a buffer of 0.6% (w/v) sodium citrate (Lonza) in PBS, and incubated in 10% (v/v) human serum (type AB; Lonza) in PBS to block non-specific binding. Subsequently, the cells were incubated for 30 minutes with the antibodies the following conjugated monoclonal antibodies: anti-CD105 (Alexa 488, clone SN6, AbD Serotec, Oxford, United Kingdom); anti-CD90 (PE, clone 5E10, BD Biosciences, San Jose, CA); anti-CD14 (FITC, clone TÜK4, AbD Serotec); anti-CD16 (Alexa 647, clone LNK-16, AbD Serotec); anti-CD4 (FITC, clone B-A1, Diaclone, Besançon, France); anti-CD8 (PE, clone B-Z31, Diaclone); anti-CD34 (PerCP-Cy5.5, clone 8G12, BD Biosciences); anti-CD45 (FITC, clone 2D1, BD Biosciences). Titration experiments were performed to determine optimal working concentrations and specificity was validated for all antibodies. The labelled cells were washed to remove background staining, and samples were measured using a bench-top flow cytometer (Guava easyCyte 6HT, Merck Millipore, Billerica, MA). Debris was excluded using a threshold on the forward scatter signal and at least 10,000 events were counted per sample. Data analysis was performed using the Guava Express Pro software package, combined with FCS Express (De Novo Software, Los Angeles, CA). MSC or PBMC were gated based on cell size and granularity (forward scatter and side scatter signals, respectively), all other events were excluded from analysis. The PBMC gate was subdivided into a monocyte gate and a lymphocyte gate. Within the monocyte gate, the

monocyte subsets were quantified based on expression of CD14 and CD16, with the classical CD14⁺/CD16⁻ monocytes designated as 'mon 1', intermediate CD14⁺/CD16⁺ monocytes as 'mon 2', and non-classical CD14^{dim}/CD16⁺ monocytes as 'mon 3' (Ziegler-Heitbrock, 2007; Shantsila *et al.*, 2011).

Table 4.1 Proteins and genes analyzed via Multiplex ELISA or qPCR, respectively.

Protein	Symbol	Function
Interleukin 4	IL-4	Stimulates repair, inhibits IFN- γ
Interleukin 12(p70)	IL-12	Pro-inflammatory factor
Interleukin 1 β	IL-1 β	Pro-inflammatory factor
Interferon γ	IFN- γ	Pro-inflammatory factor, induces MSC ^a apoptosis
Tumor necrosis factor α	TNF- α	Pro-inflammatory factor
Interleukin 10	IL-10	Anti-inflammatory factor, inhibits TNF- α , IFN- γ , IL-1 β
Matrix metalloproteinase 9	MMP-9	Extracellular matrix breakdown and remodeling
Interferon gamma-induced protein 10	IP-10	Inhibits angiogenesis
Macrophage inflammatory protein 1 β	MIP-1 β	Pro-inflammatory and chemotactic factor for M ϕ ^b
Macrophage inflammatory protein 1 α	MIP-1 α	Pro-inflammatory and chemotactic factor for M ϕ
Interleukin 6	IL-6	Both pro- and anti-inflammatory functions
Interleukin 8	IL-8	Chemotactic for neutrophils, pro-angiogenic
Monocyte chemoattractant protein 1	MCP-1	Chemotactic for monocytes/ M ϕ , stimulates healing
Basic fibroblast growth factor	bFGF	Pro-angiogenic, promotes scarless healing
Vascular endothelial growth factor	VEGF	Pro-angiogenic and vasculogenic, homing of EC ^c and MSC
Soluble vascular cell adhesion molecule	sICAM	Mediates cell adhesion and migration
Soluble intercellular adhesion molecule	sVCAM	Mediates cell adhesion and migration
Stromal cell-derived factor 1 (gene)	CXCL12	Chemotactic for MSC and progenitor cells

^aMSC = mesenchymal stromal cells, ^bM ϕ = macrophages, ^cEC = endothelial cells

4.2.8 Multiplex ELISA

Multiplex ELISA measurements were performed by the Multiplex core facility of the Laboratory for Translational Immunology of the University Medical Center Utrecht, the Netherlands, using an in-house developed and validated multiplex immunoassay based on

Luminex technology (Table 4.1). Samples were incubated with antibody-conjugated MagPlex microspheres (BioRad, Hercules, CA) for one hour at room temperature with continuous shaking, followed by one hour incubation with biotinylated antibodies, and 10 min incubation with phycoerythrin-conjugated streptavidin diluted in high performance ELISA (HPE) buffer (Sanquin). Acquisition was performed using a FLEXMAP 3D system controlled with xPONENT 4.1 software (Luminex, Austin, TX). Data was analyzed by 5-parametric curve fitting using Bio-Plex Manager software (version 6.1.1, Biorad). Protein measurements were corrected for the amount of seeded cells per volume of medium in each experimental condition. Heatmaps were created by averaging the data per experimental group and plotted according to a defined colour scale using the Sparklines application in Microsoft Excel.

4.2.9 qPCR

CXCL12 protein (also known as SDF-1 α) release was not detectable via ELISA. Therefore, the expression of the corresponding gene was analyzed. For all experimental conditions, the frozen scaffolds were disrupted with a microdismembrator (Sartorius, Goettingen, Germany) using RNase-free metal beads (\emptyset 3 mm, Sartorius, Goettingen, Germany) in Nalgene[®] cryogenic vials (Sigma-Aldrich). The disrupted cells were lysated using RLT buffer with β -mercaptoethanol (Sigma-Aldrich). RNA was isolated with Qiagen RNeasy kit (Qiagen) according to manufacturer's instructions, including a DNase incubation step. RNA quantity and purity were determined with a spectrophotometer (NanoDrop[®], ND-1000, Isogen Life Science, IJsselstein, the Netherlands). Absence of genomic contamination was checked using real-time PCR (CFX384 Touch Real-Time PCR Detection System, BioRad, Hercules, CA) with glyceraldehyde-3-phosphate dehydrogenase (GAPDH) primers. cDNA was synthesized starting from 200 ng RNA in a 15 μ l reaction volume consisting of 20 ng/ml random primers (Promega, Madison, WI), 5 mM dNTPs, 5X first strand buffer, 0.1 M DTT, 200 U/ μ l M-MLV Reverse Transcriptase (Invitrogen) and double autoclaved water (ddH₂O). cDNA synthesis was performed in a Thermal Cycler (C1000 Touch[™], BioRad) by subjecting the samples to a temperature cycle of 72°C for 6 minutes, 37°C for 5 minutes (with subsequent addition of M-MLV), 37°C for 60 minutes, and 95°C for 5 minutes. GAPDH was selected as the reference gene, as it represented the most stable gene throughout different experimental conditions according to GeNorm algorithm (Vandesompele *et al.*, 2002).

Gene expression of CXCL12 was determined by adding 20mM primer mix (5'-3' primer sequence: forward ATTCTCAACTCCAAACTGTGC; reverse CTTTCAGCCGGGCTACAATCTG, accession number NM_000609; Sigma-Aldrich) to the cDNA templates, together with SYBR Green Supermix (Bio-Rad) and ddH₂O. The real-time PCR reaction was carried out for 3 minutes at 95°C, 40x(20 seconds at 95°C, 20 seconds at 60°C, 30 seconds at 72), 1 minute at 65°C, followed by melting curve analysis (CFX384, Bio-Rad). C_t values were normalized to the reference gene to obtain the relative gene expression.

4.2.10 Immunostainings

For the flow experiments, the cells in the scaffolds were double-stained using antibodies against CD90 and CD45 to distinguish between MSC and PBMC. The formaldehyde-fixed samples were washed twice in PBS, followed by an antigen retrieval step of 30 minutes incubation with citrate buffer (pH 6, Target Retrieval Solution, Dako, Glostrup, Denmark) at 97 °C. Samples were permeabilized using 0.5% Triton X-100 (Merck Serono, Schiphol-Rijk, the Netherlands) in PBS for 15 minutes, followed by overnight incubation in 10% horse serum (Invitrogen) in PBS to block non-specific binding. Samples were incubated for 2 hours with a primary antibody mix of CD90 (1:200; monoclonal, rabbit anti-human IgG, Abcam, Cambridge, UK) and CD45 (1:200; monoclonal, mouse anti-human IgG₁, Abcam) with 1% bovine serum albumin and 0.1% Tween-20 in PBS, followed by washing with 0.1% Tween-20 and PBS. Fluorescent labeling was performed by 60 minutes incubation in 0.1% Tween-20 and PBS with a mix of Alexa fluor 555-conjugated goat anti-rabbit IgG (1:300) secondary antibody for CD90 and Alexa fluor 488-conjugated goat anti-mouse IgG₁ (1:300) secondary antibody for CD45 (Invitrogen). Excess antibody was removed by extensive washing with 0.1% Tween-20 and PBS, and cell nuclei were stained by 5 minutes incubation with 4',6-diamidino-2-phenylindole (DAPI; Sigma-Aldrich). After washing three times in PBS, scaffolds were mounted on slides with Mowiol (Calbiochem, San Diego, CA) and observed with confocal microscopy (TCS SP5X, Leica Microsystems, Wetzlar, Germany).

4.2.11 Statistical analysis

All data are expressed as mean \pm standard error of the mean. Differences in protein release and gene expression between control groups and chemotaxis or flow samples were analysed per cell type with a two-tailed t-test. To assess if synergistic effects existed between the preseeded cells and the PBMC in suspension (chemotaxis and flow), we directly compared the total amount of protein secreted in individual culture conditions with the total amount of protein secreted in the co-culture experiments. For this, the averages and variances of the single contributions were summed and the corresponding standard deviations were used in a two-way ANOVA. For all other analyses, one-way ANOVA was applied. All tests were followed by Bonferroni post hoc test and a P-value <0.05 was considered statistically significant. The analyses were performed using Prism software 5.0 (GraphPad Software, La Jolla, CA).

4.3 Results

4.3.1 Scaffold and cell characterization

The scaffolds obtained via electrospinning showed isotropic fiber distribution, with fiber diameter of $4.7 \pm 0.5 \mu\text{m}$ and overall thickness of $392 \pm 40 \mu\text{m}$. All cell types were characterized prior to seeding via flow cytometry, which revealed that ADSC and BMSC were positive for CD105 ($> 92\%$) and CD90 ($> 97\%$) and strictly negative for CD14, CD16, CD45, CD34, CD4, and CD8, indicating their phenotype of stem cells of non-hematopoietic origin (Figure 4.2). In contrast, PBMC stained predominantly negative for CD105 ($\sim 2.5\%$) and CD90 ($< 1\%$), while positive for the leukocyte marker CD45 ($\sim 98\%$). Among them, 60% was positive for CD4 and 27% for CD8, markers for T helper and T killer cells, respectively. Monocyte markers CD14 and CD16 were expressed by approximately 12% of total amount of PBMC, while only 6% stained positive for CD34, indicative of the hematopoietic progenitor lineage.

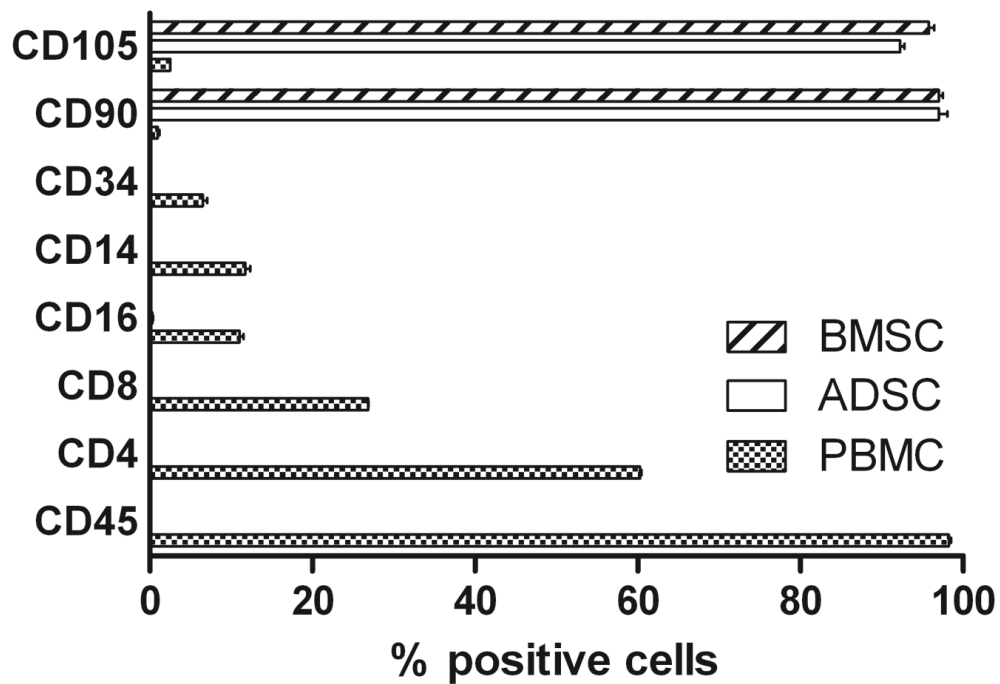


Figure 4.2 Flow cytometric characterization of MSC and PBMC after preculture/isolation, prior to seeding. MSC were positive to CD105 and CD90, but negative to CD34, displaying a profile of stem cells of non-hematopoietic origin. PBMC expressed the leukocyte marker CD45 and approximately 12% of population was positive to the monocyte markers CD14 and CD16.

4.3.2 Cell-scaffold interactions statically and under cyclic strain

In order to investigate the interplay between cells and scaffolds, the protein release and the gene expression of preseeded PBMC, BMSC, and ADSC were analyzed, both under static and cyclic strain conditions. The heatmap obtained for the static groups indicates that proteins involved in inflammatory and immunoregulatory processes were released conspicuously by PBMC, with increasing amounts over time (Figure 4.3).

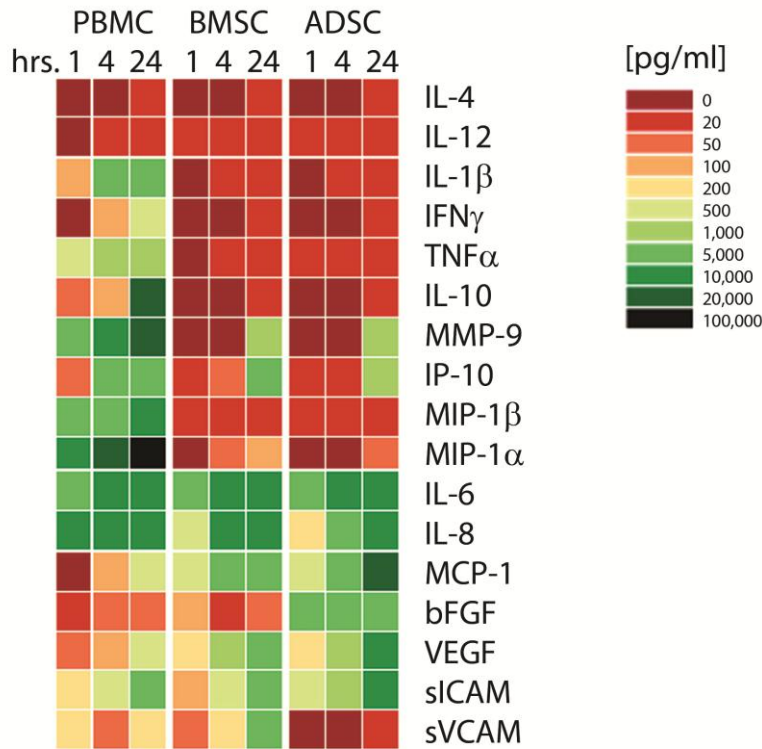


Figure 4.3 Heatmap of protein secretion over time by PBMC, BMSC and ADSC seeded into fibrous PCL-U4U scaffolds in static conditions. *Inflammatory and immunomodulatory proteins were predominantly released by PBMC, while synthesis of MCP-1, growth factors and adhesion molecules was associated with MSC. Overall protein release increased over time.*

The majority of these proteins were not synthesized by MSC or only minor release was observed, with a slight increase after 24 hours. Opposite tendency was observed for the chemokine MCP-1, the growth factors VEGF, and adhesion molecule sICAM, which were markedly secreted by both MSC types, and only to a little extent by PBMC, but increasingly over time for all cell types. The secretion profile of BMSC and ADSC was comparable, except for production of bFGF and sVCAM, which was markedly different between MSC types, with predominant secretion of bFGF by ADSC only and sVCAM by BMSC only. IL-4 and IL-12 were not detectable, whereas IL-6 and IL-8 were secreted by both PBMC and MSC, with no apparent differences between cell types. For most proteins, no clear effect of strain was observed for cyclic deformations up to 8%, with secretory profiles similar to the static condition (Figure 4.4A). A different behavior was exhibited by bFGF, which was released more considerably by MSC subjected to 3 and 8% strain, and in larger amount by ADSC.

Since CXCL12 protein release was not detectable via ELISA (data not shown), the expression of the corresponding gene was analyzed (Figure 4.4B, C, D). No difference in

CXCL12 expression was observed in either static or strained conditions for both BMSC and ADSC (Figure 4.4B, C). Expression of CXCL12 by the PBMC was considered minimal to absent, with expression levels values near the detectable threshold (Figure 4.4D).

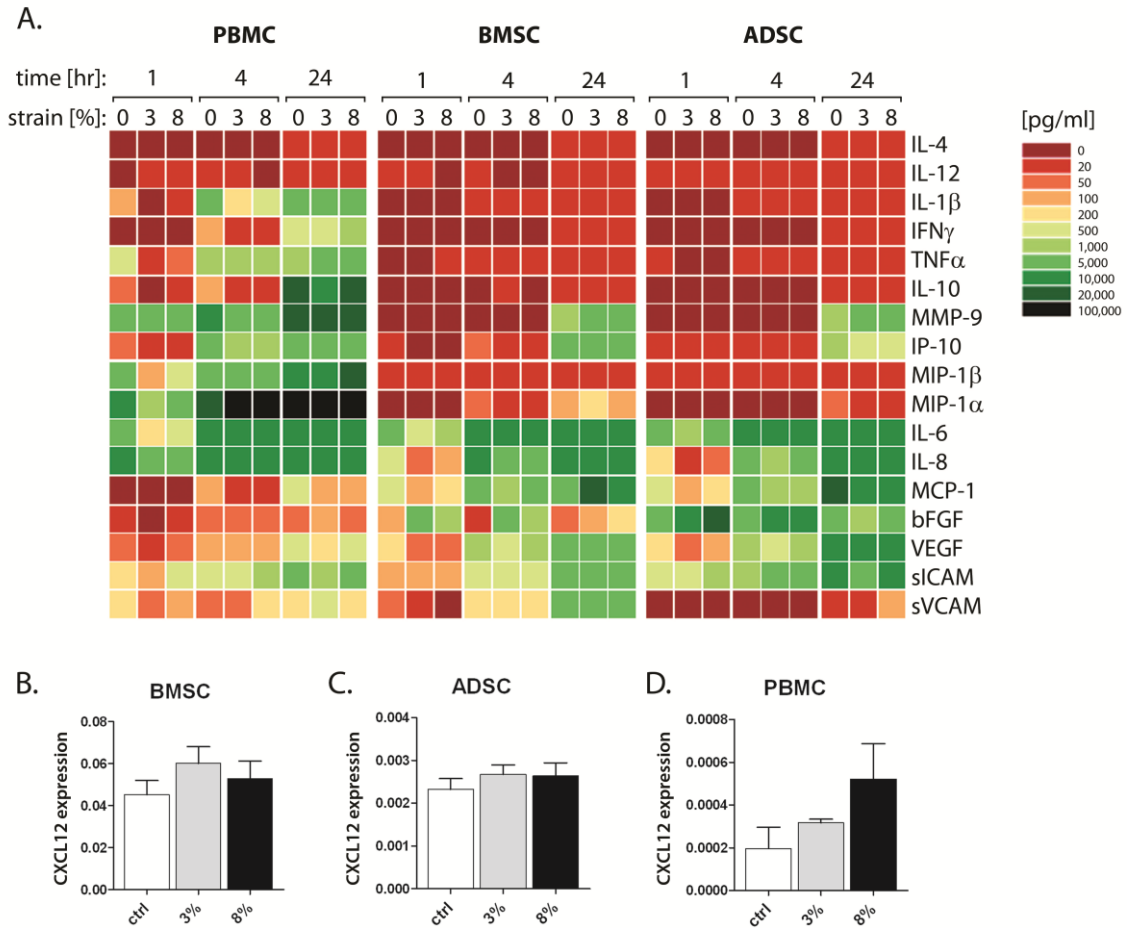


Figure 4.4 Protein secretion and gene expression by PBMC-, BMSC- and ADSC-seeded into fibrous PCL-U4U scaffold in conditions of cyclic strain, with maximum strain levels of 0, 3 or 8%, for up to 24 hours. The heatmap revealed no relevant effect of deformation on protein secretion was detected, except for bFGF release by BMSC and ADSC, which was amplified by cyclic strain (A). Gene expression of CXCL12 for BMSC (B), ADSC (C) and PBMC (D) for various strain levels, relative to GAPDH expression. No significant differences were detected among strain groups and controls.

4.3.3 Chemotaxis assays

The chemotactic effects of preseeded MSC in cross-talk with PBMC in suspension were examined with chemotaxis assays. Flow cytometric analysis of the migrated cells indicated an increase of the relative fraction of monocytes, as compared to the initial population (Figure 4.5A). Monocyte migration was significantly enhanced by scaffolds seeded with BMSC and ADSC, with respect to the unseeded scaffold, while no difference was observed for lymphocytes recruitment (Figure 4.5B, C). Concerning the monocyte subsets, it was

observed that MSC-seeded scaffolds elicited a significantly enhanced migration of the MCP-1-responsive subsets 'Mon1' and 'Mon2', as compared to unseeded scaffolds (Figure 4.5D, E, F).

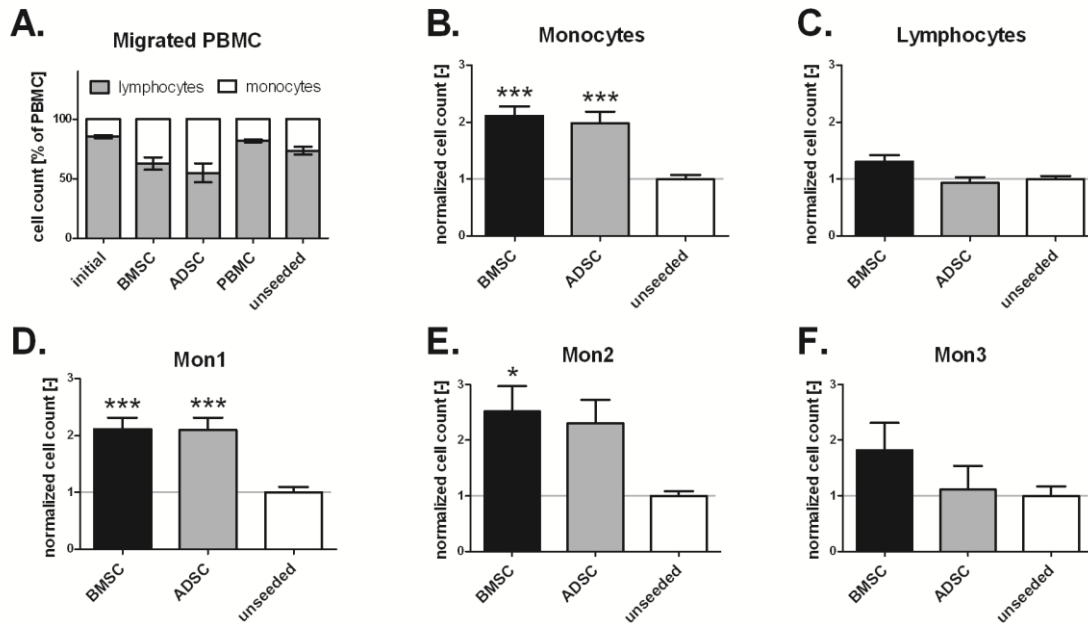


Figure 4.5 Analysis of PBMC migration towards MSC-seeded, PBMC-seeded or unseeded scaffolds after 4 hours of incubation. MSC-seeded scaffolds enhanced migration of monocytes, as compared to PBMC-seeded and unseeded constructs (A). With respect to the unseeded control, a two-fold increase in monocytes migration towards BMSC and ADSC was observed (B), while no significant difference was detected for lymphocytes (C). MSC induced relevant migration of Mon1 (D) and Mon2 (E) subsets, but not of Mon3 (F). Data was normalized per cell type on the unseeded control group. * and *** are representative of significant difference between the analyzed group and the unseeded control, for $p < 0.05$ and $p < 0.001$ respectively.

To analyze the effect of PBMC chemotaxis on the protein release by the preseeded cells, the protein levels in the chemotaxis assay were compared to the preseeded control samples in medium (Figure 4.6). Overall, the protein release by preseeded MSC exposed to the migrating PBMC fraction was increased, as compared to the control group. The only exception to this trend was represented by IL-4 and IL-12, which remained undetectable. In the chemotaxis samples, the amount of inflammatory and immunomodulatory species synthesized by preseeded PBMC, BMSC and ADSC did not differ notably from the corresponding amount detected for unseeded scaffolds. Different behavior was observed for the trophic factors (MCP-1, bFGF, VEGF), which were released substantially by MSC, but only to a little extent in PBMC- and unseeded groups.

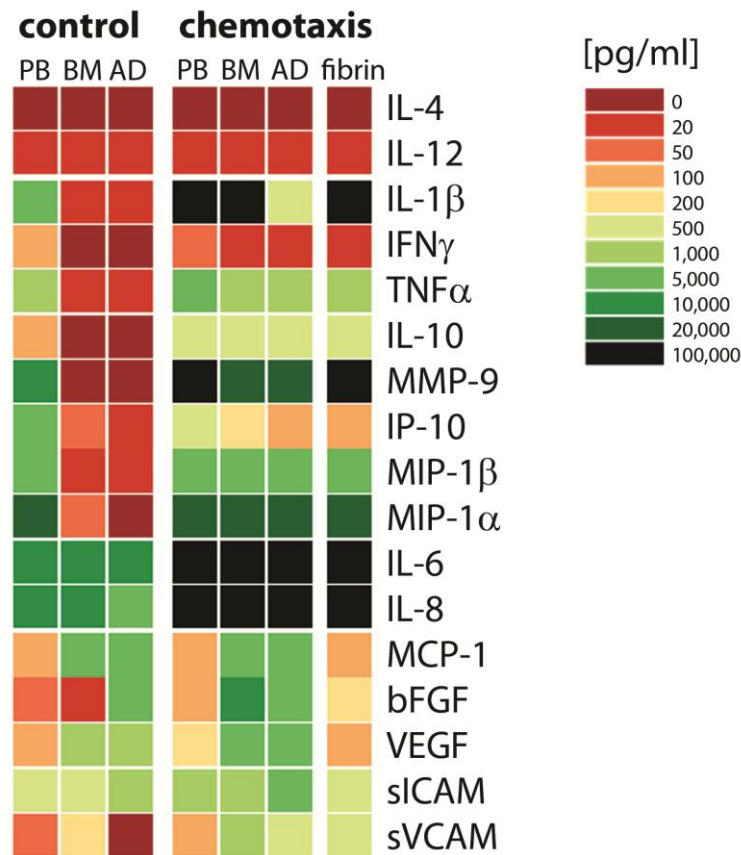


Figure 4.6 Heatmap of protein secretion by PBMC (PB)-, BMSC (BM)-, ADSC (AD)-seeded or unseeded (fibrin) PCL-U4U scaffolds exposed to PBMC in suspension in a transwell chamber, after 4 hours of incubation. Inflammatory and immunomodulatory protein release in MSC groups was enhanced in chemotaxis as compared to the control, but the total amount did not differ from the unseeded group. Inversely, MCP-1 and growth factors were substantially secreted in BMSC- and ADSC-seeded groups, and only in limited quantity in presence of PBMC-seeded and unseeded scaffolds.

Various proteins of particular interest were selected for quantitative and statistical analysis (Figure 4.7). The secretion of the pro-inflammatory cytokine TNF α and the immunomodulatory factors IL-10 and MMP9 was upregulated in all chemotaxis groups in comparison with the control scaffolds, but no significant differences were detected between cell-seeded and the unseeded control scaffolds, which indicates that these factors originated from the PBMC in suspension (Figure 4.7A, B, C). In contrast, MCP-1, VEGF and bFGF release was mainly associated to the preseeded MSC, rather than the PBMC (Figure 4.7D, E, F). In fact, MCP-1 and VEGF release by BMSC and ADSC and bFGF synthesis by ADSC were significantly upregulated, as compared to the unseeded scaffolds, while no difference was detected for PBMC-seeded scaffolds. Interestingly, VEGF was significantly upregulated for ADSC-seeded scaffolds in conditions of chemotaxis compared to the control.

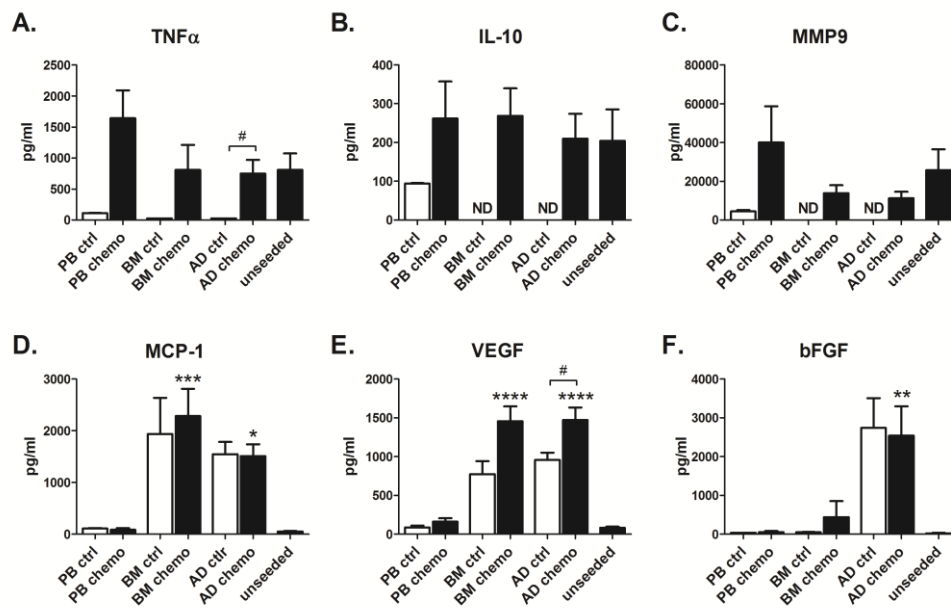


Figure 4.7 Protein release by PBMC- and MSC-seeded and unseeded PCL-U4U scaffolds in medium (ctrl) or exposed to PBMC in suspension in a transwell chamber (chemo). Constructs in chemotaxis conditions enhanced secretion of TNF α (A), IL-10 (B) and MMP9 (C), as compared to their respective controls, but no difference was detected between seeded and unseeded groups. Differently, MCP-1 (D), VEGF (E) and bFGF (F) release was upregulated for MSC groups with respect to PBMC-seeded and unseeded scaffolds. VEGF secretion by ADSC displayed a significant increase in chemotaxis conditions, as compared to the static control. ND=not detectable. *, **, ***, **** indicate significant differences of $p < 0.05$, $p < 0.01$, $p < 0.001$, and $p < 0.0001$, respectively, as compared to the unseeded group. # denotes a significant difference of $p < 0.05$ between chemotaxis and the respective control groups.

Gene expression of CXCL12 by cells adherent to the scaffold was not influenced by exposure to PBMC, as no significant differences were detected between the control groups and the chemotaxis samples per cell type (data not shown).

4.3.4 Cell behavior in pulsatile flow conditions

The experiments conducted in flow conditions aimed at establishing the influence of circulating PBMC and physiological shear stresses on seeded and unseeded scaffolds, in terms of cell recruitment and protein release. Flow cytometry, which was performed on the remaining circulating cell fraction, revealed a progressive depletion of monocytes over time, but no significant difference between cell-seeded and unseeded scaffolds was observed (Figure 4.8A). After 25 minutes, the amount of circulating lymphocytes remained relatively steady at approximately 50% of the initial fraction for all groups (Figure 4.8B). Migration of leukocytes into unseeded and MSC-seeded scaffolds was confirmed by the

presence of infiltrating CD45⁺ cells, which was displayed by immunostaining performed after 4 hours of flow (Figure 4.8C).

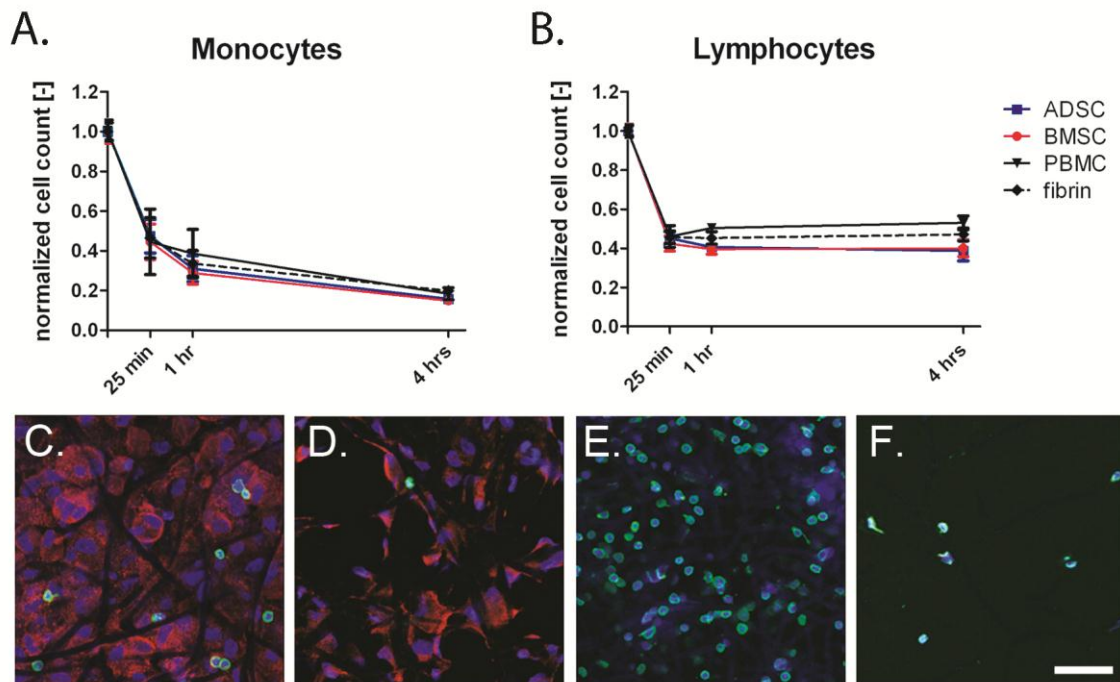


Figure 4.8 Flow cytometry of the remaining circulating cell fraction over time and immunostaining of pre-seeded and unseeded scaffolds after 4 hours of flow. Flow cytometric analysis revealed a gradual depletion of monocytes (A), while lymphocyte concentrations remained stable after an initial drop (B). Circulating PBMC adhered to the scaffold surface, either preseeded with ADSC (C), BMSC (D), PBMC (E) or unseeded (F), as demonstrated using immunofluorescent imaging after 4 hours of flow. CD45 is depicted in green, CD90 in red and DAPI in blue. Scale bar represents 50 μ m.

Protein synthesis under flow was quantified over time and compared to the static control, revealing an overall increase for samples exposed to circulating PBMC, accentuated after 4 hours (Figure 4.9). Similar to what was observed for the chemotaxis assays, the release of inflammatory and immunoregulatory factors was comparable for all groups, whereas the secretion of MCP-1, VEGF, bFGF, and sICAM was mainly associated with the preseeded MSC.

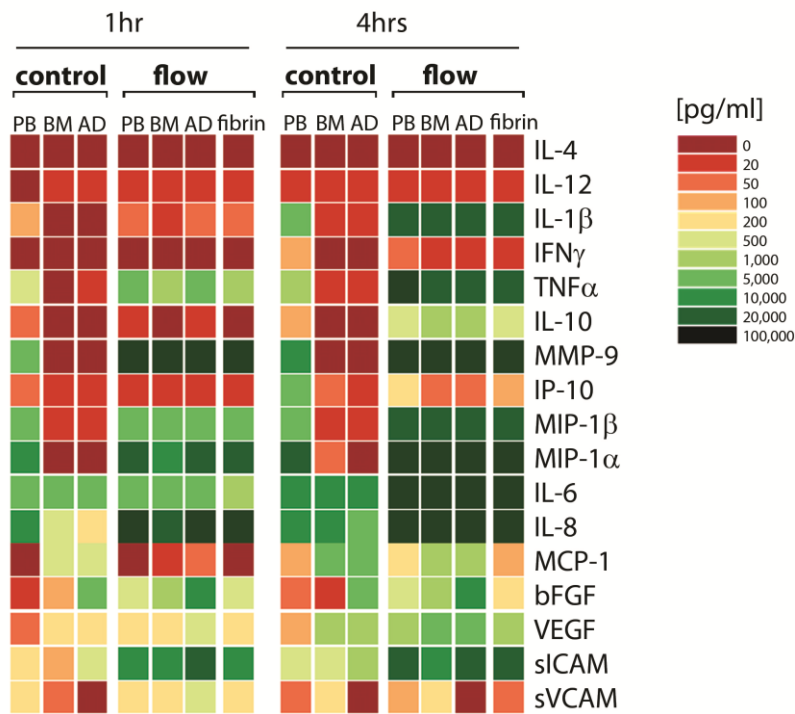


Figure 4.9 Heatmap of protein secretion by PBMC (PB), BMSC (BM), ADSC (AD)-seeded or unseeded (fibrin) PCL-U4U scaffolds exposed to circulating PBMC in shear flow, after 1 and 4 hours of incubation. Release of inflammatory and immunomodulatory species in MSC-seeded groups was enhanced in flow conditions with respect to the static control and the total amount of proteins was comparable to the unseeded group. Differently, synthesis of MCP-1 and growth factors was upregulated for BMSC- and ADSC-seeded scaffolds, as compared to PBMC-seeded and unseeded scaffolds. An overall increase in protein secretion was observed overtime.

Quantitative comparison of selected proteins after 4 hours revealed a marked increase of TNFα, IL-10 and MMP9 in the flow groups, in comparison with the static controls, with no relevant differences recorded among cell-seeded and unseeded scaffolds (Figure 4.10A, B, C). MCP-1 production was highest in the BMSC- and ADSC-seeded groups, although, surprisingly, the systemic MCP-1 levels were significantly decreased in conditions of flow, when compared to static controls (Figure 4.10D). VEGF and bFGF synthesis was enhanced for samples exposed to circulating PBMC in all groups (Figure 4.10E, F). Compared to unseeded samples, only the ADSC-seeded scaffolds exhibited a statistically significant increase in bFGF and VEGF. Interestingly, the bFGF levels in the ADSC groups were remarkably high, as compared to the other cell types and the unseeded group. Furthermore, exposure of MSC-seeded scaffolds to circulating PBMC in shear flow resulted in a significant increase in CXCL12 gene expression in comparison with their respective static control groups, while CXCL12 expression by seeded PBMC was unaffected (Figure 4.10G, H, I).

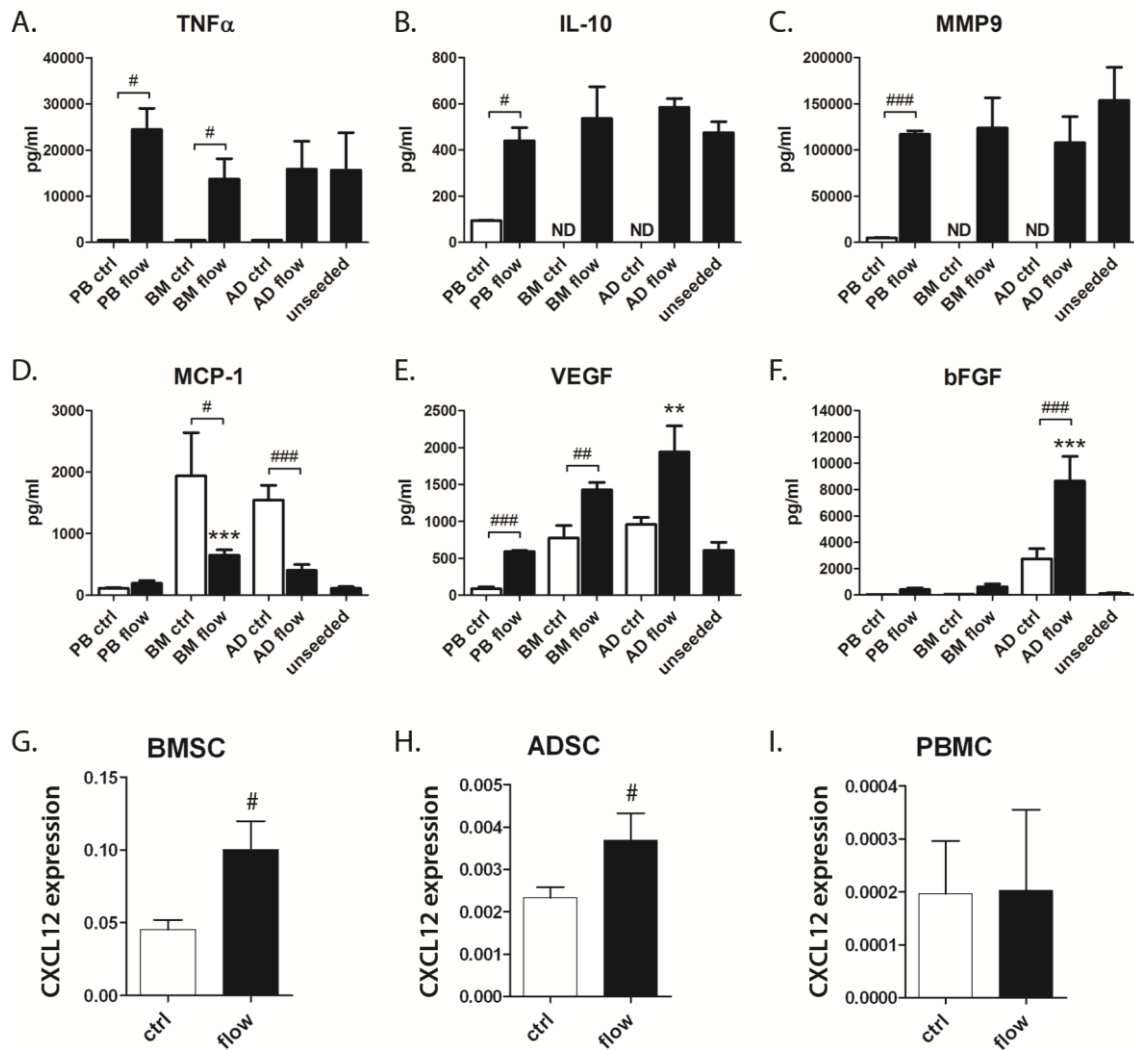


Figure 4.10 Protein release and gene expression by PBMC and MSC seeded into PCL-U4U scaffold in medium (ctrl) or exposed to circulating PBMC (flow) after 4 hours. *TNF α* (A), *IL-10*(B) and *MMP9*(C) secretion was increased in flow conditions as compared to the controls, but no significant difference was detected between seeded and unseeded groups. *MCP-1* synthesis was enhanced in MSC-seeded groups, but was significantly lower in presence of circulating PBMC, as compared to the static controls(D). Production of *VEGF*(E) and *bFGF*(F) was upregulated by seeded MSC exposed to flow, with a significant increase for ADSC in comparison with the unseeded group. A significant upregulation of *CXCL12* was observed for MSC(G, H) flow groups, but not PBMC(I), with respect to the static controls. ND=not detectable. **,*** indicate significant differences of $p<0.01$, $p<0.001$ between flow and unseeded groups. #,##,### indicate significant differences of $p<0.05$, $p<0.01$, $p<0.001$ between the flow groups and the respective controls.

4.3.5 Synergistic protein secretion

To examine if the combined culture of preseeded MSC with PBMC in suspension resulted in synergistic effects in terms of protein secretion, the individual amounts of protein secreted by the preseeded MSC and the circulating PBMC were summed, and this total

amount was directly compared to the protein levels measured in the combined cultures (chemotaxis and flow) (Figure 11).

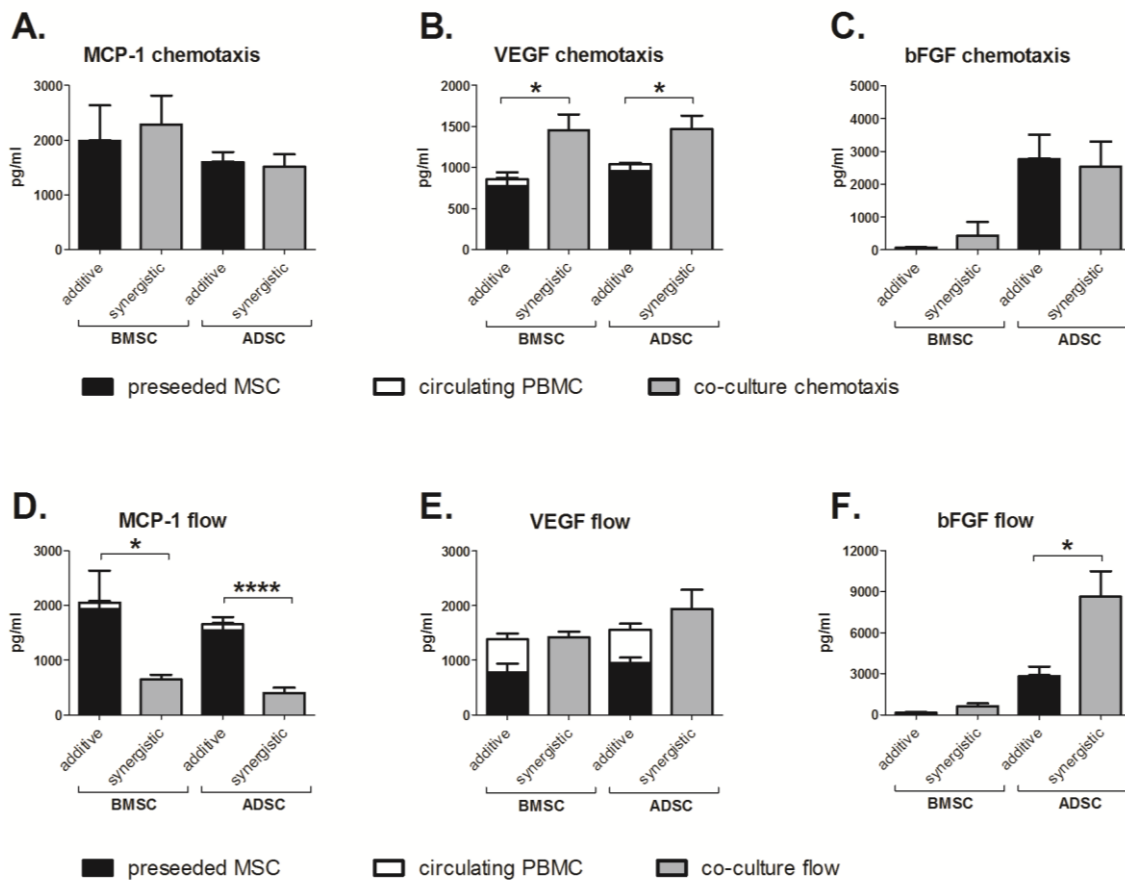


Figure 4.11 Synergistic effect of MSC and PBMC on MCP-1, VEGF and bFGF secretion in static and flow conditions. The synergistic effects on protein secretion between the preseeded MSC and the PBMC in suspension were examined by direct comparison of the sum of the individual contributions of each cell type (additive) with the protein secretion of the cell types together in combined culture (synergistic). No significant differences were detected in the chemotaxis assays, with respect to MCP-1 and bFGF levels, while VEGF exhibited a significant increase in the synergistic groups (A, B, C). In flow, there was a decrease in MCP-1 levels in the synergistic groups, while no significant differences were detected for VEGF secretion (D, E). In contrast, a strong synergistic effect was observed between circulating PBMC and preseeded ADSC on the production of bFGF (F). *, **** denote significant differences of $p < 0.05$ and $p < 0.0001$, respectively.

This comparison revealed a synergistic increase in VEGF production in static conditions, which was negated in pulsatile flow. MCP-1 showed a significant decrease in the synergistic group in flow conditions. On the other hand, a strong interdependent, rather than additive, increase in the production of bFGF was observed for ADSC-seeded scaffolds exposed to circulating PBMC in shear flow.

4.4 Discussion

In vivo, MSC play an important role in physiological wound healing by modulation of the immune response, in close cross-talk with the immune cells in the inflammatory environment (Bartholomew *et al.*, 2002; Di Nicola *et al.*, 2002). This characteristic has been exploited to modulate inflammation and harness healing, by implanting scaffolds preseeded with MSC (reviewed by (Shi *et al.*, 2012)). Concurrently, on-the-fly pre-seeding of autologous bone marrow-derived cell fractions into biodegradable synthetic cardiovascular grafts has been employed as a one-step intervention method to stimulate *in situ* regeneration of autologous neovessels and -valves (Hibino *et al.*, 2005; Weber *et al.*, 2011). However, the cross-talk between MSC, preseeded in a 3D synthetic scaffold, and leukocytes in the hemodynamic environment has not been clarified. Therefore, the aim of this study was to systematically study the signaling factors secreted by preseeded MSC in a fibrous synthetic scaffold, and the interaction of the MSC with circulating immune cells, in the presence of physiological mechanical loads (i.e. strain and shear flow). The results of this study elucidate an interdependent effect on the secretion of trophic factors by preseeded MSC and the inflammatory environment created by PBMC, in particular in conditions of shear flow.

Consistent with our results, it was proposed that inflammation induced by the exposure of a biomaterial to circulating leukocytes is a key factor for MSC activation (Groh *et al.*, 2005; Ren *et al.*, 2008). More specifically, release of TNF α , IL-1 β and IFN γ following acute inflammation activates MSC to secrete immunomodulatory and trophic factors, which suppress inflammation and promote secondary recruitment of reparative cell types (Shi *et al.*, 2012). The electrospun PCL-U4U scaffolds adopted in this study triggered an inflammatory reaction by PBMC, either preseeded or in shear flow, as illustrated by the distinct cytokine release profile of inflammatory mediators in both cell-seeded and unseeded groups. Protein mapping showed a mixed environment, containing strong pro-inflammatory cytokines, such as TNF α , IL-1 β , and MIP's, as well as anti-inflammatory species, such as IL-10 and MMP9. IL-12, a protagonist for the inflammatory protein IFN γ , was not detected, which is in accordance to observations in mice studies (Maggini *et al.*, 2010). Concurrently, IFN γ , which is known to reduce the viability of MSC and induce production of the anti-angiogenic factor IP-10 (Freytes *et al.*, 2013), was only marginally detected. Interestingly, IP-10 was downregulated in conditions of flow, compared to the static controls, which may be attributed to the lack of IFN γ . This environment of pro- and

anti-inflammatory factors was instituted by the PBMC in response to the scaffold, generally indifferent to the presence or absence of preseeded MSC. Furthermore, the application of moderate cyclic strain (up to 8%) did not have a marked effect on the protein release by either preseeded PBMC or MSC. In contrast to the other inflammatory factors, IL-6 and IL-8 were not only secreted by PBMC, but also produced in great amount by the preseeded MSC. Substantial production of IL-6 and IL-8 was suggested to induce BMSC, previously exposed to TNF α , to stimulate angiogenesis and tissue repair through increased homing of endothelial progenitor cells (Kwon *et al.*, 2013). Moreover, IL-6 production by BMSC was shown to be instrumental to prevent the differentiation of monocytes into antigen-presenting immunogenic cells and skew differentiation towards an anti-inflammatory, IL-10-producing cell type (Melief *et al.*, 2013). Overall, these results suggests that the electrospun PCL-U4U substrate can serve to trigger a positive immune response and that preseeded MSC in the scaffold are activated by this PBMC-induced environment.

Previous studies have shown that inflammation-activated MSC can act upon cells involved in both the adaptive (T cells, B cells) and innate immunity (neutrophils, natural killer cells, dendritic cells) (Shi *et al.*, 2012). Contact-dependent mechanisms and soluble factors both participate to induce MSC-mediated immunosuppression and tissue repair, but the exact mechanisms are still unclear (Groh *et al.*, 2005; Puissant *et al.*, 2005; Uccelli *et al.*, 2008). Ren *et al.* established that the suppression of immune cells by MSC is orchestrated by the release of chemokines as well as by upregulation of the adhesion molecules ICAM and VCAM (Ren *et al.*, 2008, 2010). It has also been suggested that preseeded MSC can mediate the differentiation of monocytes towards M1 or M2 type macrophages, the pro- and anti-inflammatory phenotypes, respectively (Mosser & Edwards, 2008; Kim & Hematti, 2009; Hanson *et al.*, 2011). With respect to MSC-induced repair, it was shown that intramyocardial injection of MSC could partially restore the functionality of infarcted porcine hearts, while conditioned medium could not, suggesting that paracrine factors alone could not mimic the beneficial effect of MSC (Hatzistergos *et al.*, 2010). Similarly, injection of MSC-conditioned medium (containing VEGF, bFGF, MCP-1) did enhance the proliferation of endothelial and smooth muscle cells in murine ischemic peripheral muscles. Though the beneficial effects, in terms of reperfusion and limb remodeling, were less pronounced, with lower levels of systemic VEGF and bFGF, as compared to injected MSC (Kinnaird *et al.*, 2004). This interdependent effect of MSC and leukocytes is in line with our current findings, which suggest a synergistic rather than additive upregulation of bFGF when preseeded ADSC were subjected to PBMC in pulsatile

shear flow. Furthermore, both BMSC and ADSC subjected to shear stress showed enhanced gene expression of CXCL12, a factor involved in the mobilization and homing of progenitor cells into the target tissue (Askari *et al.*, 2003; Sordi *et al.*, 2005).

Clearly, VEGF, bFGF and CXCL12 are important trophic factors in physiological wound healing. All three factors function as chemoattractant factors for bone marrow-derived stem cells and progenitor cells. MSC were shown to enhance wound healing in mice by recruitment of macrophages and endothelial progenitor cells via secretion of angiogenic factors, including VEGF and CXCL12 (Chen *et al.*, 2008). VEGF is not only involved in endothelial cells proliferation and MSC migration, but it is also associated with immunosuppression. A study by Willenborg *et al.* established that time of release and the secreted amount of VEGF play a crucial role for the healing process. Moreover, they appointed macrophages as the main source for VEGF release during the early phase of tissue repair (Willenborg 2012). Interestingly, this correlates to the VEGF secretion we observed by circulating PBMC in shear flow in response to the unseeded scaffolds. The presence of MSC further contributed to the levels of VEGF in conditions of pulsatile flow. CXCL12, VEGF and bFGF were shown to increase migratory activity of MSC, with the most pronounced effect in the presence of bFGF (Willenborg *et al.*, 2012). Remarkably, it was shown that a low dose of bFGF induced migration, while a high dose led to MSC repulsion (Schmidt *et al.*, 2006). bFGF can also enhance proliferation of endothelial cells and smooth muscle cells (Kinnaird *et al.*, 2004) and is involved in scarless healing processes (Abe *et al.*, 2012).

MCP-1 plays an essential role in physiological wound healing and tissue regeneration (Shireman *et al.*, 2007; Capoccia *et al.*, 2008). Moreover, MCP-1 has been prompted as a pivotal factor for the success of *in situ* regeneration of vascular grafts in rodents (Roh *et al.*, 2010). This was attributed to its ability to enhance the early recruitment of monocytes, followed by increased downstream homing of circulating CD34+ cells (unpublished data). Preseeded ADSC and BMSC produced markedly higher levels of MCP-1 compared to PBMC, resulting in a strong chemotaxis of monocytes, with a preferred attraction of MCP-1-responsive monocyte subsets. However, this selective recruitment was negated in conditions of flow and systemic levels of MCP-1 were significantly lower in conditions of shear flow compared to static. This reduction in MCP-1 levels under flow possibly represents the effect of rapid internalization of the MCP-1 protein by the circulating monocytes, as previously described (Volpe *et al.*, 2012). This is in correspondence with our previous study, in which we demonstrated a similar

differential effect on monocyte recruitment in shear flow compared to static conditions, in response to a burst-release of MCP-1 from electrospun PCL scaffolds (unpublished data).

Implanted biomaterials can effectively modulate stem cell fate, enhancing their engraftment and angiogenesis and directing differentiation with mechanical and biochemical signaling (Segers & Lee, 2011). Concurrently, preseeding of synthetic scaffolds with unselected BM-MNCs has been adopted for application in *in situ* cardiovascular tissue engineering therapies as a means to functionalize scaffolds prior to implantation (Hibino *et al.*, 2005; Roh *et al.*, 2010). Although we did not perform a direct comparison between BM-MNC and BMSC, these *in vitro* results illustrate that the MSC fraction within the heterogeneous BM-MNC population is responsible for the production of trophic factors. Moreover, we demonstrate that PBMC cannot serve as an alternative cell source for preseeding, as they displayed a distinctly different protein secretion profile. ADSC, on the other hand, were shown to release higher amounts of bFGF when exposed to PBMC in flow, in comparison with the more widely used BMSC. This is in correspondence with previous profiling studies, which demonstrated that, although BMSC and ADSC have similar immunomodulatory potentials, distinct differences exist between cell types and the tissue of origin remains retraceable (Puissant *et al.*, 2005; Yoo *et al.*, 2009).

A potential limitation of this study lies in the use of allogenic combinations of leukocytes and MSC, rather than autologous cell combinations. However, MSC are immune-privileged and tolerance of immune cells to MSC in allogenic transplantation is recognized, which may overcome the use of non-autologous cells (Puissant *et al.*, 2005; Williams & Hare, 2011).

It is obvious that MSC-preseeding represents a valid approach to create immunomodulatory scaffolds that can initiate a regenerative healing response. Nevertheless, the use of MSC inherently carries several risks. For example, MSC can enhance tumour development in animal models due to their immunosuppressive potential and their intrinsic ability to convert into fibroblasts (Djouad *et al.*, 2003; Spaeth *et al.*, 2009). Though a recent small-scale observational study by Ren *et al.* showed absence of tumour-development in patients treated with BMSC (Ren *et al.*, 2013). For safe and effective clinical therapy, any intrinsic risk from the use of MSC may be circumvented by the use of instructive acellular biomaterials, capable of mimicking the beneficial effects of preseeded MSC. Roh *et al.* recently proposed the use of microsphere-encapsulated MCP-1 instead of BM-MNC preseeding to trigger a favourable regenerative response (Roh *et al.*, 2010). In the current study, we identified CXCL12 and bFGF as trophic factors, respectively expressed and released exclusively by preseeded MSC. Therefore, these factors represent

evident candidates to create acellular pro-regenerative scaffolds for application in *in situ* cardiovascular tissue engineering therapies.

Acknowledgments

We would like to thank Esther Potier for providing the MSC, in cooperation with the Maastricht University and the Academic Hospital Maastricht, the Netherlands, and for her excellent help regarding the MSC culture. SyMO-Chem and Serge Söntjens are acknowledged for providing the PCL-U4U and Tina Thakkar for electrospinning of the fibrous meshes and Marloes Janssen-van den Broek for the technical support. The multiplex immunoassays were in-house developed, validated and performed by the Multiplex core facility of the Laboratory for Translational Immunology (LTI) of the University Medical Center Utrecht (UMCU).

This research forms part of the iValve project of the research program of the BioMedical Materials institute, co-funded by the Dutch Ministry of Economic Affairs, Agriculture and Innovation. The financial contribution of the Nederlandse Hartstichting is gratefully acknowledged.

5

General discussion

New approaches for prompt and effective regeneration of cardiovascular tissues have been proposed within the field of tissue engineering. A promising strategy that has been successfully applied in clinical trials comprises the implantation of a biodegradable scaffold seeded “on-the-fly” with autologous cells (Hibino *et al.*, 2010). However, the cell harvesting procedure is invasive and time consuming, and the entailed risk of infection, represents an additional hindrance. The ultimate goal of *in situ* tissue engineering is to offer cell-free, off-the-shelf constructs able to positively interact with the host upon implantation towards functional tissue formation and remodeling and complete integration with the host tissue. The essential requirement for such an approach is the development of scaffolds capable of modulating the regenerative process, in synergy with the complex physiological milieu. The primary focus of this thesis was to investigate the influence of mechanical forces on the host response to biomaterials, in order to provide inputs for the design of novel, instructive scaffolds for *in situ* regeneration of load-bearing cardiovascular tissues.

5.1 Summary and main findings

The implantation of a biomaterial initiates an immune response, which can induce and support tissue repair via a wound healing-like mechanism. The recruitment of monocyte-derived macrophages and their differentiation towards a reparative phenotype is believed to play a major role in the positive outcome of the implant with functional tissue formation (Hibino *et al.*, 2011). Monocyte chemoattractant protein-1 (MCP-1) was indicated as a key player in the regeneration via synthetic scaffolds, by enhancing the initial recruitment of monocytes (Roh *et al.*, 2010). The first part of this thesis aimed at elucidating the chemotactic role of MCP-1-loaded scaffolds subjected to shear stress (chapter 2). We hypothesized that such scaffolds would selectively recruit angiogenic and reparative monocyte subsets, with enhanced expression of CCR2 receptor. A static migration assay was performed to verify the chemotactic effect triggered by MCP-1, while monocyte recruitment under flow conditions was assessed using a previously developed fluidic set-up (Smits *et al.*, 2012). For both studies, electrospun polycaprolactone (PCL) scaffolds, either as pristine material or functionalized with exogenous MCP-1, were exposed to a suspension of human peripheral blood mononuclear cells (PBMC). Enhanced migration of CCR2⁺ population towards MCP-1-loaded scaffolds was observed under static conditions, whereas no selective recruitment of monocyte subsets was recorded for scaffolds exposed

to pulsatile flow. On the other hand, a marked increase in monocyte infiltration was observed during the short pulse of MCP-1 in flow, indicating that monocyte infiltration directly correlates to release kinetics of MCP-1, also in the presence of shear stresses. These results suggest that timely release of chemokines is a crucial factor to trigger cell infiltration into the scaffolds under shear flow. Moreover, we rejected the hypothesis that MCP-1-mediated regeneration *in vivo* is due to local recruitment of CCR2⁺ cells, as selective attraction of monocytes is overruled by shear stress. The role of MCP-1 might rather be related to the mobilization of specific monocyte subsets from other regions of the body, such as bone marrow or splenic reservoirs.

The PCL scaffolds exposed to circulating immune cells were infiltrated with monocyte-derived macrophages, with mixed inflammatory (M1) and immune-modulating (M2) phenotype, regardless of MCP-1 presence. Macrophage phenotype is considered a critical determinant of scaffold remodeling (Brown *et al.*, 2012). Therefore, we decided to examine in depth the polarization state of macrophages adherent on electrospun PCL scaffolds, while taking into account the additional effect of local deformations mimicking physiological loads acting *in vivo* on cardiovascular tissues (chapter 3). A PCL-derived material consisting of a PCL soft segment and two urea groups, PCL-U4U, was selected for its elastic behavior under tensile forces and processed into isotropic fibrous scaffolds via electrospinning. PBMC, representative of the recruited cell population, were seeded into the scaffolds and differentiation of monocytes into macrophages was observed upon contact with the scaffold. By applying a range of cyclic deformations with the FlexCell[®] tension system, we demonstrated that moderate tensile strains (below 7%) promote polarization of macrophages towards an anti-inflammatory, pro-tissue-healing macrophage phenotype in electrospun PCL-U4U scaffold. In contrast, higher deformations induced expression of genes and surface markers typical of inflammatory macrophages, which have been associated with detrimental long-term tissue remodeling (Badylak *et al.*, 2008).

Using the same model system, we investigated the contribution of adherent PBMC to extracellular matrix synthesis, which would gradually replace the mechanical support of the biodegradable constructs. Infiltrated monocytes have earlier been shown to remain within the scaffolds until full scaffold degradation in animal models (Roh *et al.*, 2010), but there is only limited knowledge about their role in tissue deposition (Chang *et al.*, 2012). We provided experimental evidence that PBMC secrete glycosaminoglycans and collagen, main constituents of the heart valves extracellular matrix, one week after seeding and with no substantial differences for strains between 0 and 12%. Besides offering mechanical

support, the synthesized matrix promotes cell adhesion and binds important cytokines involved in resolution of inflammation and angiogenesis (Franz *et al.*, 2011).

Monocyte infiltration associated with long-term remodeling was shown to be enhanced by bioactive molecules incorporated into the scaffolds, such as MCP-1, or by on-the-fly seeding of autologous mononuclear cells isolated from the bone marrow (Roh *et al.*, 2010). Among these cells, mesenchymal stem cell fraction (MSC) was indicated responsible for the secretion of important immunomodulating factors, thus harnessing the immune response in a paracrine fashion. However, neither the signaling actors and pathways involved in regeneration, nor the cross-talk between MSC and circulating immune cells, have been fully documented. Such knowledge would provide a benchmark for the functionalization of cell-free substrates able to positively interact with the immune system. In order to gain insight into this mechanism, we analyzed the signaling molecules released by MSC (from bone marrow and adipose tissue) and PBMC seeded in PCL-U4U scaffolds and exposed to circulating PBMC in the presence of mechanical stimuli (i.e. strain and shear stresses) (chapter 4). We showed that unseeded PCL-U4U scaffolds were sufficient to trigger an inflammatory reaction by PBMC, inducing release of a mix of immunomodulatory cytokines such as TNF α , IL-10 and MMP9, which were not secreted by MSC. On the other hand, important trophic factors involved in physiological wound healing, such as MCP-1, VEGF and bFGF were almost exclusively released by MSC. Interestingly, gene expression of CXCL12 and secretion of bFGF, proteins associated with angiogenesis and scar-less healing, were significantly upregulated by MSC exposed to circulating PBMC. This synergistic behavior was more marked for adipose-derived mesenchymal cells and was observed only in the presence of shear flow. In contrast, cyclic deformations within the range beneficial for macrophage differentiation indicated in chapter 3, did not hamper protein release by MSC. In terms of monocyte recruitment, the MSC preseeded scaffolds exhibited a similar behavior to MCP-1 loaded scaffolds as described in chapter 2. When exposed statically to PBMC in suspension, MSC elicited enhanced migration of monocytes and selective recruitment of CCR2⁺ subsets. Under pulsatile flow conditions, on the contrary, PCL-U4U scaffolds allowed for monocyte infiltration, but no significant differences were detected between seeded and unseeded groups. Although pre-seeded cells should represent a source of sustained, local release of MCP-1, we observed a diminished systemic level of this chemokine when pre-seeded scaffolds were exposed to flow, probably due to sequestration by circulating PBMC (Volpe *et al.*, 2012).

In summary, we demonstrated that shear stress plays a major role in early inflammatory response, by influencing selective monocyte recruitment and release of bioactive molecules. In particular, we proved that MCP-1 elicits accelerated infiltration of monocytes, but, in conditions of shear flow, the chemotactic effect declines rapidly and is not associated with recruitment of specific monocyte subsets. Furthermore, only in the presence of shear stress it was possible to detect the up-regulation of bFGF and CXCL12, important trophic factors secreted by MSC that might represent valuable targets for scaffold functionalization. Lastly, we showed that mechanical strain can modulate the phenotype of infiltrated cells towards reparative or inflammatory subsets. Taken together, these results emphasize the importance of the hemodynamic forces for *in situ* regeneration and are instructive for tailoring scaffolds for *in situ* cardiovascular regeneration.

5.2 Towards the design of immunomodulatory scaffolds

The overall goal of this work was to elucidate the effects exerted by mechanical forces on the inflammation that naturally occurs when biomaterials are implanted into a living host as vascular replacements. Our experimental observations suggest that mechanical forces can profoundly influence the early immune response and provide practical cues for the design of responsive substrates. The following section will translate some of the main findings of this thesis into concrete directions towards the design of immunomodulatory substrates.

5.2.1 Design of synthetic scaffolds

The first step towards the optimal design of a scaffold is the choice of the appropriate material. The material we selected for the first study was PCL, a slow-degrading elastomer shown to enhance *in vitro* tissue formation of cardiovascular substrates seeded with human cells (Brugmans *et al.*, 2013). The surface exposed for cell adhesion by PCL scaffolds is hydrophobic, but it can be effectively conditioned with serum proteins to increase the overall hydrophilicity of the construct and offer binding sites for the cells. In chapter 2, it was shown that PCL scaffolds allowed for adhesion of circulating cells and could trigger an initial response with mixed inflammatory and immunomodulatory

signaling by the infiltrating leukocytes. However, our PCL scaffolds exhibited plastic deformation when cyclically strained, therefore these experiments were performed with PCL-U4U, a PCL derived polymer with enhanced elasticity, custom-developed by SyMO-Chem (Eindhoven, the Netherlands). This material was shown to positively interact with circulating immune cells, promoting their adhesion and release of pro- and anti-inflammatory cytokines, as indicated in chapter 4. Both PCL-based elastomers can be processed by electrospinning, thereby allowing for direct regulation of several scaffold properties, such as overall thickness, fiber diameter and alignment, by tuning the spinning time, the polymer-to-solvent ratio and the rotational speed of the collector, respectively. A fine control of the scaffold architecture and microstructure is an essential requirement for *in situ* applications, as fiber density, dimension and alignment directly influence infiltration and biological response of the cells (Saino *et al.*, 2011; Garg *et al.*, 2013). In our studies, PCL-U4U scaffolds with an average fiber diameter of 5 μ m and thickness around 350 μ m were chosen, resulting in uniform cell distribution throughout the whole thickness after static seeding of PBMC (Figure 3.1). Nevertheless, in order to verify how scaffold properties can influence blood-borne cell infiltration and behavior, it is important to test the constructs under physiological conditions of blood flow and pressure.

5.2.2 Synthetic scaffolds under mechanical forces

Shear stress acting on cardiovascular tissues *in vivo* is a determinant for local recruitment of circulating cells (Ley *et al.*, 2007). The experimental setup described in chapter 4 demonstrated that fibrous PCL-U4U scaffolds permit the infiltration of immune cells under unidirectional, pulsatile shear flow, representative of physiological forces acting on blood vessels. Heart valve hemodynamics is more complex, with pulsatile and high shear stresses on the ventricular side, and lower, but oscillatory ones on the pulmonary and aortic side. *In vitro* platforms able to reproduce accurately these forces while exposing the substrates to circulating and perpetually replenished cells are yet to be developed, therefore animal models represent, so far, the sole opportunity for testing heart valve leaflets in fully physiological conditions. In an ongoing study of *in situ* tissue regeneration performed within the BMM iValve project, unseeded heart valve-shaped scaffolds in PCL-U4U have been implanted into sheep in the pulmonary position. Preliminary results at 5 weeks after implantation indicated leaflet repopulation by the host cells, as indicated by DNA assay (Figure 5.1A) and immunostaining analyses revealed a major presence of cells

on the pulmonary side, where the oscillatory flow results in lower shear stresses (data not shown). However, verifying whether such cells infiltrated from the bloodstream or from adjacent tissues is not trivial, and is currently under investigation. Within the same animal study, deposition of the main components of heart valve extracellular matrix, i.e. sulphated glycosaminoglycans (sGAG) and collagen (HYP), was observed (Figure 5.1B, C).

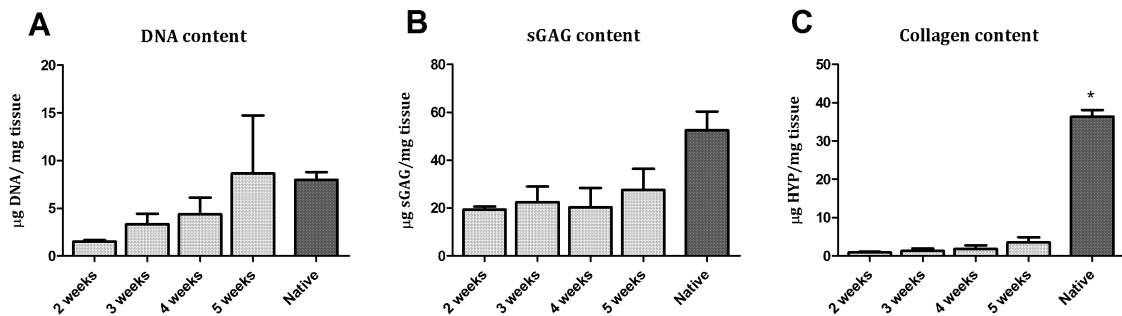


Figure 5.1 DNA, sGAG and HYP content in scaffolds implanted in pulmonary position in sheep. Biochemical assays performed on scaffolds explanted after 2, 3, 4 and 5 weeks revealed presence of cells (A) and matrix constituents (B, C). Native control was obtained from 3 ovine pulmonary valves (courtesy of Bart Sanders). * denotes a significant difference for $p < 0.0001$.

Biaxial tensile tests performed on explants after 5 weeks showed a progressive modification of the mechanical properties of the construct, with a shift from a stiff, isotropic scaffold, towards a more anisotropic, elastic structure, closer to the one of native valves (Figure 5.2). Such alterations might be due to the observed increase of biological tissue content, as well as to the degradation of the synthetic fibers that naturally occurs *in vivo*.

Besides allowing for cellular infiltration and adhesion under physiological forces, scaffolds for *in situ* regeneration should also appropriately transfer such forces to the adherent cells. In chapter 3, we demonstrated that immune cells adherent on fibrous scaffolds could sense the different strain levels applied and responded by modulating their gene and surface marker expression. In particular, we stated that local strain around 7-8% would promote polarization of the infiltrated macrophages towards an anti-inflammatory, reparative phenotype. Geometrical and mechanical properties of the scaffolds should therefore be tuned to induce deformations within this range, when subjected to physiological pressure loads upon implantation. In order to provide cues for the scaffold design, numerical simulations of heart valve-shaped scaffolds subjected to pulmonary pressure difference were carried out by dr. Sandra Loerakker, as described in Appendix A.

The curves obtained by plotting strain against k_1 , a material parameter associated with the fiber stiffness, revealed that pulmonary loads result in strains below 8% in presence of isotropic scaffolds with $k_1 > 5$ MPa or of anisotropic scaffolds with $k_1 > 2$ MPa (Figure 5.3A-C). Furthermore, scaffold anisotropy does not represent an essential specification to obtain low strains when the selected material exhibits adequate stiffness. Nevertheless, a preferred orientation of fibers along the circumferential direction was shown to lead to larger radial stretch and better leaflet coaptation, therefore anisotropy of the scaffold should be pursued (Loerakker *et al.*, 2013).

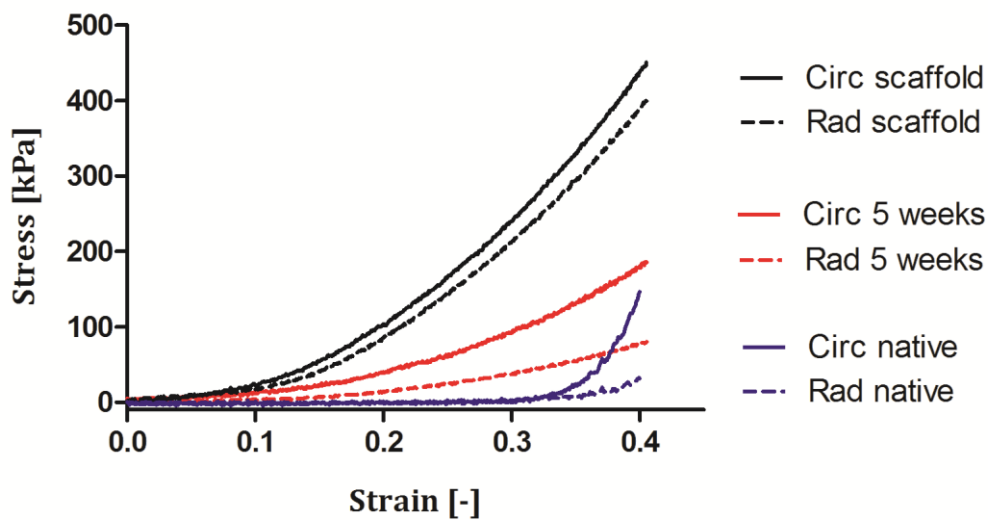


Figure 5.2 Mechanical characterization of PCL-U4U scaffolds before and after implantation. Biaxial tensile test on circumferential (Circ, solid line) and radial (Rad, dashed line) directions of scaffolds before (black lines) and after (red lines) being implanted into sheep in pulmonary positions, compared to native ovine valves (blue lines). After 5 weeks, the scaffold behaves more similarly to the native valve in response to tensile forces, especially in the radial direction. Native control data was obtained as courtesy of Bart Sanders.

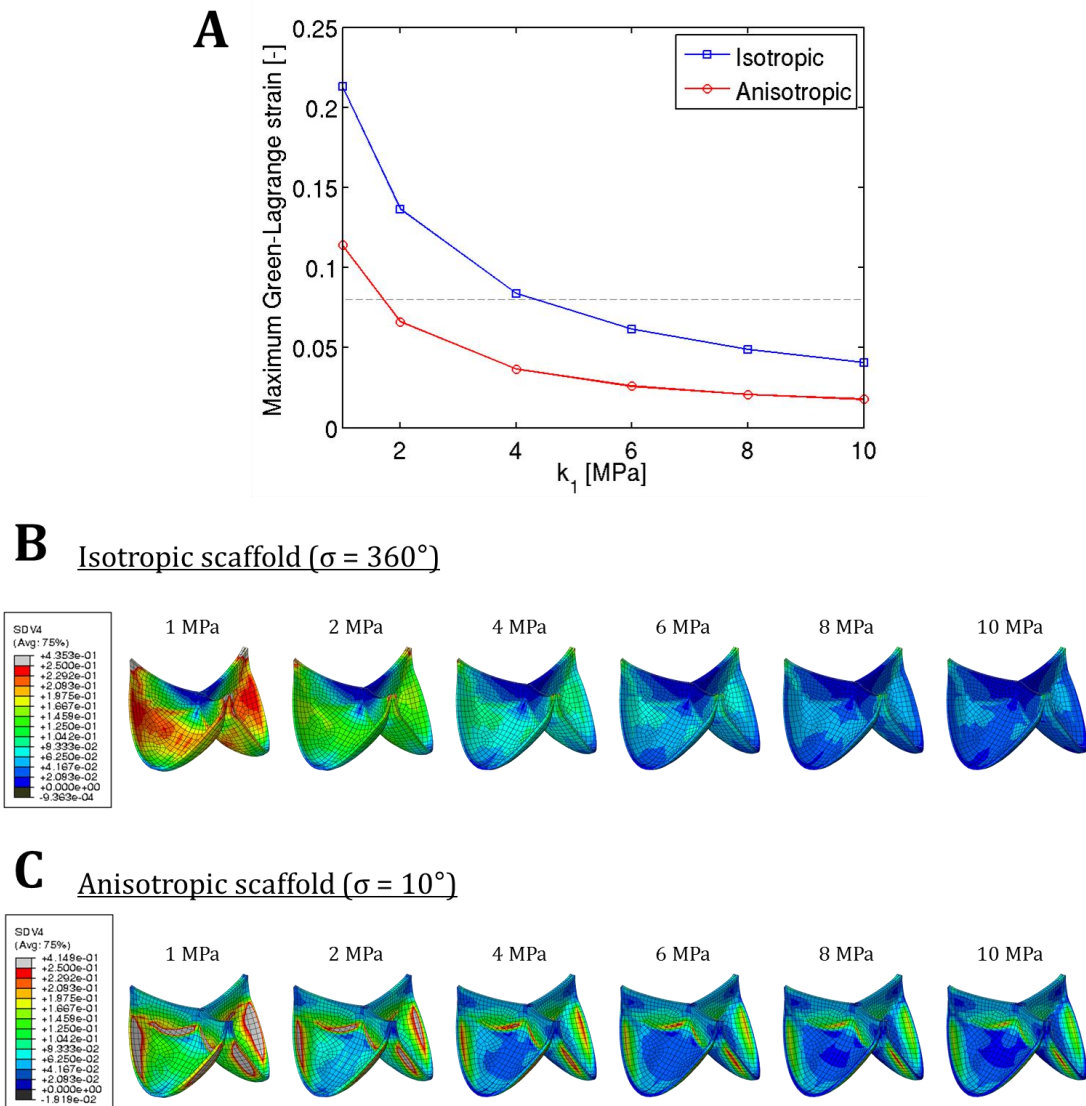


Figure 5.3 Effect of scaffold material properties on local deformations under physiological pulmonary pressure. (A) Maximum strain of the scaffold fibers calculated in the central elements of the leaflet belly for increasing k_1 , a material parameter. Strains below the threshold of 8%, indicated by the dashed line, are obtained for $k_1 > 5$ MPa and $k_1 > 2$ MPa for isotropic and anisotropic scaffolds, respectively. Maximum fiber strain distribution over the leaflet for (B) isotropic and (C) anisotropic scaffolds, resulting in lower deformations in the belly regions for increasing values of k_1 . All data, results and figures we kindly provided by dr. Sandra Loerakker, Eindhoven University of Technology.

5.2.3 Unseeded vs seeded scaffold

The ambitious *in situ* approach of tissue engineering relies on the delivery of cell-free, instructive scaffolds that could lead to complete regeneration avoiding the isolation and culturing of autologous cells. The ideal scaffold for this approach should be able to allow for cellular infiltration and tissue deposition, while timely degrading. To this end, the

development of bioactive, acellular scaffolds has been proposed. Incorporation of molecules able to accelerate cellular infiltration and promote selective recruitment of specific cell populations would provide a promising, off-the-shelf solution for *in situ* regeneration. However, the identification of the appropriate bioactive compounds and of their interaction with the host cells is still to be unraveled. Besides MCP-1, which has been previously indicated as a valuable target (Roh *et al.*, 2010), in chapter 4 we indicated bFGF and SDF1 α as additional moieties for scaffold functionalization. Another important parameter to be finely tuned within the scaffold design is the controlled release of such molecules over time. As observed in chapter 2, a prolonged release of MCP-1 might represent a crucial factor to obtain sufficient scaffold repopulation. However, a highly controlled spatio-temporal delivery of bioactive molecules remains elusive, therefore some research groups have been pursuing the avoidance of bioactive moieties incorporation, suggesting that the choice of appropriate material and geometry of the scaffold could be sufficient to prompt tissue remodeling. In fact, synthetic scaffolds tailored to enable rapid cell recruitment and fast degradation were proven to endorse remodeling of vascular, cell-free grafts within 3 months in rats (Wu *et al.*, 2012) and 12 months in canine models (Matsumura *et al.*, 2013).

Since not all the factors orchestrating the *in situ* cardiovascular regeneration process have been acknowledged, the use of cells still represents a clinically relevant option to create immunomodulatory scaffolds. Seeded cells exposed to the blood interact synergistically with the circulating blood cells and secrete factors for the mobilization of stem cells from bone marrow, angiogenesis and repair. Moreover, they can also contribute to the initial deposition of matrix, thus providing not only mechanical support to the scaffold, but also a binding site for immunomodulating molecules (Franz *et al.*, 2011). Early matrix synthesis is particularly interesting for clinical applications, as clearance of pre-seeded cells from the scaffold might be delayed in human, as compared to small animals. In fact, slower depletion of pre-seeded cells from the implanted scaffolds was observed for animal models with increasing size and lifespan, as discussed in chapter 3 (Sales *et al.*, 2007; Roh *et al.*, 2010). The so-called “one-step approach” consists of the isolation of the patient’s cells with a minimally invasive procedure, such as aspiration of bone marrow or adipose tissue, seeding onto a scaffold and delivery to the implant site, within a single surgical session. Mononuclear cells are widely used for this approach and can be isolated from different tissues, e.g. bone marrow, adipose tissue, blood. We investigated the potentiality of pre-seeding blood mononuclear cells (PBMC), which can be easily harvested via a routine blood sampling, but encompass only a limited fraction of

stem cells. PBMC showed positive response under mechanical loads, exhibiting expression of immunomodulating genes and secretion of matrix components, as shown in chapter 3, but resulted in limited release of proteins involved in angiogenesis and tissue repair (chapter 4).

Mononuclear cells isolated from bone marrow or adipose tissue represent promising cell sources, due to the higher percentage of multipotent cells present in the total cell fraction. In chapter 4, we demonstrated that seeding mesenchymal stromal cells from bone marrow or adipose tissue into PCL-U4U fibrous scaffolds enhanced the synthesis of important immunomodulatory factors, such as the chemokine MCP-1, the trophic factors VEGF and bFGF, and sVCAM and sICAM, that mediate cell adhesion and migration. In particular, adipose derived stem cells (ADSC) were associated with extensive release of bFGF, fundamental for appropriate tissue repair, when exposed to circulating leukocytes in shear flow. Furthermore, previous findings indicated ADSC as a promising cell source for cardiovascular tissue engineering, due to their capability of synthesizing and remodel collagen and elastin (Colazzo *et al.*, 2011). In order to test their behavior under mechanical strain, we seeded ADSC onto PCL and PCL-U4U fibrous scaffolds and we exposed them to pulmonary pressure loads in a pulse duplicator, adapted from Mol *et al.* (Mol, Driessen, *et al.*, 2005). PCL scaffolds exhibit higher stiffness than PCL-U4U scaffolds, thus resulting in lower deformation when subjected to the same pressure difference. After 48 hours, ADSC subjected to cyclic strain in PCL-U4U displayed up-regulated gene expression of matrix components (collagen I and III), crosslink (LOX) and smooth muscle actine (α -SMA), as compared to the static control (set at a baseline of 1, Figure 5.4). The differential gene expression of cells seeded on PCL and PCL-U4U, and therefore subjected to different deformations demonstrated that ADSC are responsive to variation of the strains transferred by the scaffolds.

ADSC under cyclic load

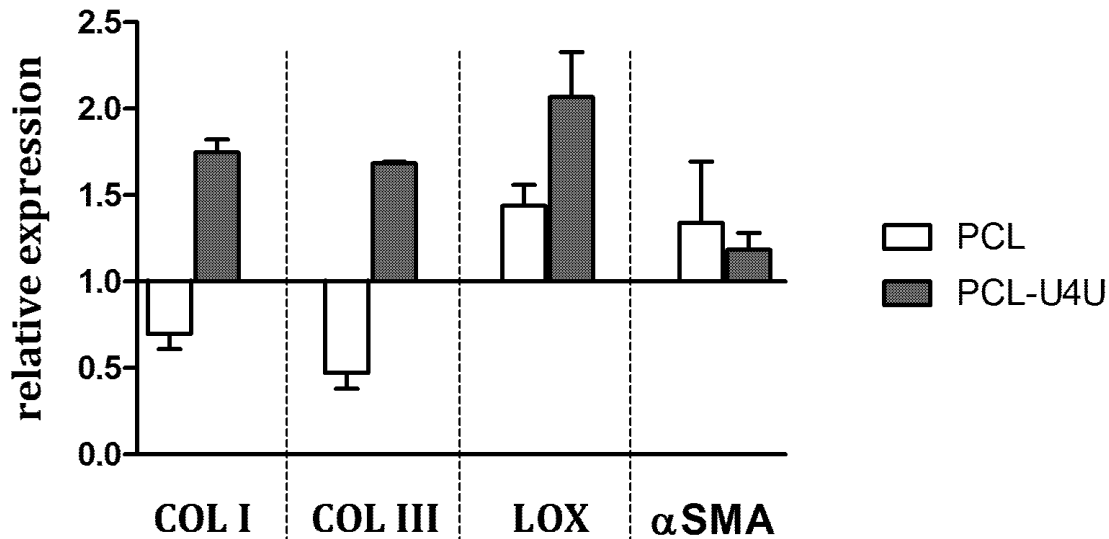


Figure 5.4 Relative expression of collagen I and III, LOX and α SMA for ADSC subjected to cyclic loads. ADSC were seeded on PCL and PCL-U4U electrospun scaffolds and exposed to cyclic loads of 2 kPa in a pulse duplicator for 2 days. The higher stiffness of PCL scaffolds resulted in lower deformations in presence of the pressure loads, as compared to PCL-U4U constructs. Expression of the genes per each group was normalized on the respective static control, which was set at a value of 1. Relative expression above 1 indicates up-regulation, whereas expression below 1 denotes down-regulation of the gene. The higher strains induced by the pressure loads in the PCL-U4U scaffolds resulted in up-regulation of Collagen I and III expression, while these genes were down-regulated for ADSC seeded on PCL, as compared to the respective static controls. Up-regulation of LOX and α SMA was observed for both scaffold types subjected to cyclic loads.

Additional evidences of ADSC responsiveness to mechanical deformations were provided by immunostainings performed one day after seeding on PCL-U4U scaffolds subjected to 0, 3 and 8% cyclic strain in a FlexCell™ tension system. ADSC in static conditions were shown to express the contractile protein α -SMA (in green), but exhibited round shape and absence of stress fibers (Figure 5.5A). In contrast, increasing strain magnitudes resulted in improved α -SMA organization, with extensive presence of stress fibers and elongated cellular structure in the 8% group (Figure 5.5B, C).

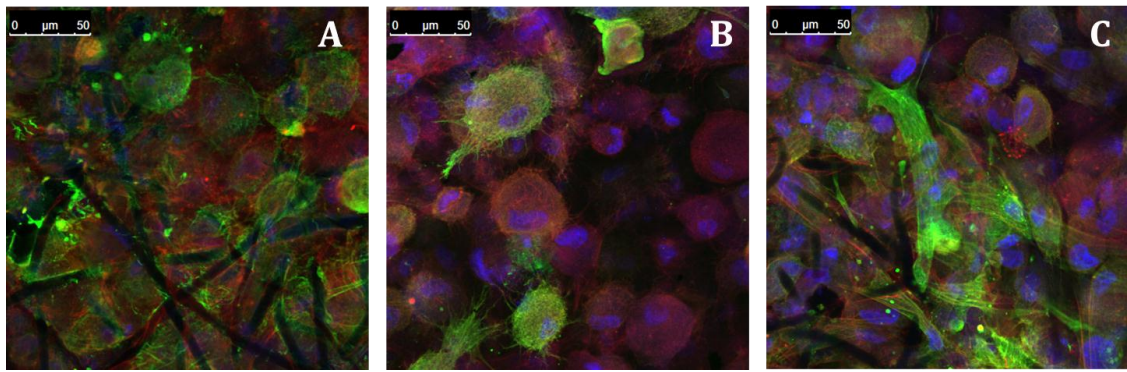


Figure 5.5 Immunofluorescent images of ADSC seeded in PCL-U4U and subjected to 0% (A), 3% (B) and 8% (C) cyclic strain for 1 day. ADSC expressed α -SMA marker (in green) in all groups, but exhibited elongates cell structure and organized stress fibers only when subjected to strain. DAPI (in blue) and phalloidin (in red) indicate cell nuclei and cytoskeleton, respectively.

Taken together, these results indicate that the pre-seeding of ADSC might harbor great potential for cardiovascular tissue engineering. One of the major challenges posed by this approach is the availability of effective and reproducible seeding techniques. However, a standardized, operator-independent seeding method for vascular applications has been recently proposed and validated in large animal models, achieving highly consistent seeding patterns (Udelsman *et al.*, 2011). On the other hand, the pre-seeded approach still implies several disadvantages, such as the risk of infection and viability loss entailed by the cell harvesting procedure. Therefore, the development of cell-free, instructive substrates might reduce the existing barriers to the clinical use of cardiovascular tissue engineered constructs.

5.3 Study limitations and future perspectives

The exact mechanism of cell repopulation of the scaffolds remains elusive, and the ideal experimental model to investigate it has yet to be developed. Animal experiments offer the possibility to study the immune response to a biomaterials in a physiological environment, but they can provide only limited insight into the mechanism of cell recruitment. Firstly, ethical reasons prevent the sacrifice of animals at frequent time points shortly after implantation to verify the phenotype and distribution of infiltrated cells, while non-invasive (imaging) techniques to monitor cell and tissue immunomodulatory responses to scaffolds are not yet far advanced. Furthermore, transanastomotic ingrowth is the main source of host tissue cells in animals, but this phenomenon is extremely limited in human (Zilla *et al.*, 2007). In order to enhance the clinical relevance of *in vivo* studies, modified

animal models with “humanized” features were developed. Looped interposition (Pennel *et al.*, 2013) and highly shielded grafts (Talacua *et al.*, 2014) providing scaffold isolation sufficient to prevent the transanastomotic migration when implanted into rats. Based on observation from these studies, the development of an appropriate, “humanized” *in vitro* model would not only solve the ethical issues, but also allow for direct analysis of the key phenomena taking place in human, thus providing a valid tool to unravel the mechanism of cell recruitment.

In the present work, *in vitro* platforms were used to separately evaluate the contribution of mechanical forces to cell recruitment, differentiation and signaling, in order to identify the role played by each condition in immunomodulation. *In vivo*, cardiovascular constructs are subjected to simultaneous tensile and shear stresses, which may result in more complex interplays between implanted scaffolds and host cells. The development of a novel platform able to expose scaffolds to fully physiological conditions of loading would allow for a deeper understanding of the combined effect of local shear and tensile stress on *in situ* regeneration.

Another limitation of our model system is that circulating cells are rapidly depleted from the blood flow upon adhesion onto the scaffolds, thus impeding long-term studies on cell recruitment. Under physiological conditions, circulating cells are continuously replenished by natural reservoirs represented by the bone marrow and the spleen. Including *in vitro* equivalents of such reservoirs to fluidic setups would provide not only constant replenishment of depleted cells, but also the opportunity to assess the chemotactic effectiveness of bioactive scaffolds. With a similar system, the contribution of MCP-1 in mobilization of specific cell population from other regions, as hypothesized in chapter 2, could be further investigated. Additionally, sorting and labelling of monocyte subsets beforehand would provide a potent tool to track cellular mobilization, recruitment and differentiation over time.

In the present work, the flow setup has been used exclusively for the observation of mononuclear cells isolated from buffy coats, with a main focus on the leukocytic fraction. In future studies, it could be relevant to investigate the behavior of other cell types present in the blood, like neutrophils and dendritic cells, which may participate to the immune response and interact with the biomaterials (Hume *et al.*, 2012; Wantha *et al.*, 2013). The adaptation of current *in vitro* platforms towards more realistic models is essential to limit the need of animal trials and to ensure safer clinical translation.

The deformation resulting from mechanical loads applied to the scaffold were proven to be sensed by the infiltrating cells, but the activation thresholds and modalities

of force transmission remain incompletely understood. Recent studies showed that fiber diameter can affect cell adhesion and induce differential rearrangement of the cytoskeleton, with potential implications for mechanotransduction (Fioretta *et al.*, 2014). Moreover, Garg *et al.* correlated macrophage polarization with scaffolds microstructure, in particular with fibers and pores dimension (Garg *et al.*, 2013). In chapter 3, we observed that macrophages subjected to high strains exhibit preferentially M1 phenotype, but the correlation between cytoskeleton and macrophage polarization has not been deeply investigated. Associating M1 and M2 phenotype with specific cytoskeleton rearrangements, such as actin remodeling, may explain the differential behavior of macrophage in varying strain conditions and would provide important cues for the design of responsive scaffolds.

Another factor that might influence cell behavior when exposed to mechanical loads is the presence of fibrin. In the current study, a fibrin gel was used to incorporate MCP-1 into the scaffold (chapter 2) or to allow for a uniform distribution of seeded cells (chapter 3 and 4). Seeded and infiltrating cells can migrate through the dense matrix formed by fibrin, but the extensive presence of such gel within the pores may partially shield the effect of local forces and cover the tridimensional, fibrous microstructure of the scaffold, altering the early immune response to the biomaterial. Moreover, preparation of autologous fibrin for clinical applications would limit immunogenic reactions, but would require an additional, time-consuming step with the intrinsic infection risks involved in any laboratory process. Therefore, avoidance of fibrin utilization would be preferred, but a deeper awareness of its role in *in situ* regeneration is necessary.

The distribution of recruited cells throughout the scaffold thickness was not deeply investigated in the present thesis, but it represents an important parameter towards appropriate regeneration. We believe that extensive infiltration of macrophages throughout the scaffold might result in positive signaling for recruitment of matrix-producing cells and lead to well-organized matrix deposition. Scaffold architecture plays a crucial role into this process, as it can facilitate cellular infiltration and tune polarization of cell phenotype. Flat surfaces were shown to induce a more intense inflammatory reaction *in vitro*, as compared to porous biomaterials (Saino *et al.*, 2011), which were also proven to heal with less encapsulation (Brown *et al.*, 2012). Garg *et al.* demonstrated that larger pores are usually associated with positive signaling by infiltrating macrophages and hypothesized that offering more space for spreading and orientation to the cells results in preferred differentiation towards immunoregulatory M2 phenotype (Garg *et al.*, 2013). In the experimental studies presented in chapter 3 and 4, we used PCL-U4U scaffolds with an

average fiber diameter of 6 μm , which resulted in a porosity sufficient for leukocyte infiltration. Structures characterized by larger pores might induce not only positive signaling by adherent macrophages, but could also facilitate migration of bigger cells, such as stem cells and fibroblasts, throughout the whole scaffold depth. In order to validate this hypothesis, a wider range of fiber diameters and, subsequently, scaffold porosities should be tested with different cell types in the presence of mechanical loads, which were proven to affect cell recruitment (chapter 2) and differentiation (chapter 3). Since varying scaffold microstructure can result in differential response to mechanical forces, combining the experimental sessions with numerical modeling might represent a valuable tool to assist in the design of responsive substrates.

5.4 Conclusions

The present work provides insight into the interactions between circulating immune cells and synthetic scaffolds for cardiovascular regeneration, in the presence of mechanical forces. We demonstrated that highly porous electrospun PCL-based scaffolds can allow for the infiltration of monocytes in the presence of shear stress and that the infiltrated cells, when subjected to moderate deformations, can be activated into immunomodulatory macrophages. Furthermore, we suggested that cell recruitment and regeneration can be ameliorated by incorporation of bioactive species into the scaffold, namely MCP-1, bFGF and CXCL12. Taken together, these observations indicate that tailoring substrates able to trigger infiltration of immune cells and to expose them to the desired deformations represents a decisive strategy towards the regeneration of vital tissues. In particular, uniform distribution of cells throughout the scaffold depth can be achieved with highly porous scaffolds, eventually functionalized with chemoattractants able to guide cell infiltration. In addition, fibers with the appropriate stiffness can transfer in a controlled fashion the mechanical loads to the adherent monocytes. Their differentiation into healing macrophages will initiate a positive immunomodulatory cascade and lead to recruitment of matrix-producing cells, with scaffold fibers serving as core structures for progressive tissue deposition and remodeling. Merging the advanced polymer research with the *in situ* tissue engineering experience would lead to the development of instructive substrates able to tune the balance between homogeneous matrix deposition and scaffold degradation in physiological conditions, towards full tissue regeneration.

Appendix A

Numerical simulations of heart valve-shaped scaffolds subjected to pulmonary pressure difference were conducted with Abaqus 6.10 (Simulia, Providence, RI) by dr. Sandra Loerakker. Scaffold parameters previously determined by Argento et al. (Argento *et al.*, 2012) were adopted, and applied to both isotropic and anisotropic fiber distributions, where parameter k_1 was varied to adjust the strains. K_1 is a coefficient of the fiber material law (eq. 2) and is representative of the fiber stiffness:

$$\psi_f = k_1 \lambda_f^2 \left[e^{k_2(\lambda_f^2 - 1)} - 1 \right] \quad (2)$$

with ψ_f and λ_f indicating fiber stress and stretch, respectively, and k_2 as an adimensional material parameter. The standard deviation of the fiber angle was $\sigma=360^\circ$ for isotropic scaffolds and $\sigma=10^\circ$ for anisotropic ones, with fibers oriented mainly circumferentially. The fibers were embedded in a matrix with 10 kPa shear modulus, providing initial stability to the construct and signifying the contribution of the fibrin gel. The overall valve design was inspired by Hamid et al., where the geometrical parameter values were chosen as in Loerakker et al. ("shape H3c") (Hamid *et al.*, 1986; Loerakker *et al.*, 2013). The maximum strain along all fiber directions was calculated in the central elements of the leaflet belly, which was statically loaded with 2 kPa. Maximum strain of the scaffold fibers was calculated in the central elements of the leaflet belly for increasing k_1 .

Bibliography

- Abe, M., Yokoyama, Y., & Ishikawa, O. (2012) A possible mechanism of basic fibroblast growth factor-promoted scarless wound healing: the induction of myofibroblast apoptosis. *Eur. J. Dermatology*, **22**, 46–53.
- Abe, R., Donnelly, S.C., Peng, T., Bucala, R., & Metz, C.N. (2001) Peripheral blood fibrocytes: differentiation pathway and migration to wound sites. *J. Immunol.*, **166**, 7556–7562.
- Aggarwal, S. & Pittenger, M.F. (2005) Human mesenchymal stem cells modulate allogeneic immune cell responses. *Blood*, **105**, 1815–1822.
- Ancuta, P., Rao, R., Moses, A., Mehle, A., Shaw, S.K., Luscinskas, F.W., & Gabuzda, D. (2003) Fractalkine preferentially mediates arrest and migration of CD16+ monocytes. *J. Exp. Med.*, **197**, 1701–1707.
- Anderson, J.M. & McNally, A.K. (2011) Biocompatibility of implants: lymphocyte/macrophage interactions. *Semin. Immunopathol.*, **33**, 221–233.
- Anderson, J.M., Rodriguez, A., & Chang, D.T. (2008) Foreign body reaction to biomaterials. *Semin. Immunol.*, **20**, 86–100.
- Ando, J., Tsuboi, H., Korenaga, R., Takada, Y., Toyama-Sorimachi, N., Miyasaka, M., & Kamiya, A. (1994) Shear stress inhibits adhesion of cultured mouse endothelial cells to lymphocytes by downregulating VCAM-1 expression. *Am. J. Physiol.*, **267**, C679–87.
- Argento, G., Simonet, M., Oomens, C.W.J., & Baaijens, F.P.T. (2012) Multi-scale mechanical characterization of scaffolds for heart valve tissue engineering. *J. Biomech.*, **45**, 2893–2898.
- Arjunon, S., Rathan, S., Jo, H., & Yoganathan, A.P. (2013) Aortic valve: mechanical environment and mechanobiology. *Ann. Biomed. Eng.*, **41**, 1331–1346.
- Askari, A.T., Unzek, S., Popovic, Z.B., Goldman, C.K., Forudi, F., Kiedrowski, M., Rovner, A., Ellis, S.G., Thomas, J.D., DiCorleto, P.E., Topol, E.J., & Penn, M.S. (2003) Effect of stromal-cell-derived factor 1 on stem-cell homing and tissue regeneration in ischaemic cardiomyopathy. *Lancet*, **362**, 697–703.
- Auffray, C., Sieweke, M.H., & Geissmann, F. (2009) Blood monocytes: development, heterogeneity, and relationship with dendritic cells. *Annu. Rev. Immunol.*, **27**, 669–692.
- Badylak, S.F., Valentin, J.E., Ravindra, A.K., McCabe, G.P., & Stewart-Akers, A.M. (2008) Macrophage phenotype as a determinant of biologic scaffold remodeling. *Tissue Eng. Part A*, **14**, 1835–1842.
- Balguid, A., Mol, A., van Marion, M.H., Bank, R.A., Bouten, C.V.C., & Baaijens, F.P.T. (2009) Tailoring fiber diameter in electrospun poly(epsilon-caprolactone) scaffolds for optimal cellular infiltration in cardiovascular tissue engineering. *Tissue Eng. Part A*, **15**, 437–444.
- Ballotta, V., Driessen-Mol, A., Bouten, C.V.C., & Baaijens, F.P.T. (2014) Strain-dependent modulation of macrophage polarization within scaffolds. *Biomaterials*, 1–10.

Bibliography

- Bao, X., Lu, C., & Frangos, J.A. (1999) Temporal gradient in shear but not steady shear stress induces PDGF-A and MCP-1 expression in endothelial cells: role of NO, NF kappa B, and egr-1. *Arterioscler. Thromb. Vasc. Biol.*, **19**, 996–1003.
- Bartholomew, A., Sturgeon, C., Siatskas, M., Ferrer, K., McIntosh, K., Patil, S., Hardy, W., Devine, S., Ucker, D., Deans, R., Moseley, A., & Hoffman, R. (2002) Mesenchymal stem cells suppress lymphocyte proliferation in vitro and prolong skin graft survival in vivo. *Exp. Hematol.*, **30**, 42–48.
- Bellini, A. & Mattoli, S. (2007) The role of the fibrocyte, a bone marrow-derived mesenchymal progenitor, in reactive and reparative fibroses. *Lab. Invest.*, **87**, 858–870.
- Bianchi, M.E. (2007) DAMPs, PAMPs and alarmins: all we need to know about danger. *J. Leukoc. Biol.*, **81**, 1–5.
- Boerboom, R. a, Rubbens, M.P., Driessen, N.J.B., Bouten, C.V.C., & Baaijens, F.P.T. (2008) Effect of strain magnitude on the tissue properties of engineered cardiovascular constructs. *Ann. Biomed. Eng.*, **36**, 244–253.
- Bouten, C.V.C., Dankers, P.Y.W., Driessen-Mol, A., Pedron, S., Brizard, a M. a, & Baaijens, F.P.T. (2011) Substrates for cardiovascular tissue engineering. *Adv. Drug Deliv. Rev.*, **63**, 221–241.
- Breuer, C.K. (2009) NCT01034007: a pilot study investigating the clinical use of tissue engineered vascular grafts in congenital heart surgery. [WWW Document].
- Brown, B.N. & Badylak, S.F. (2013) Expanded applications, shifting paradigms and an improved understanding of host-biomaterial interactions. *Acta Biomater.*, **9**, 4948–4955.
- Brown, B.N., Ratner, B.D., Goodman, S.B., Amar, S., & Badylak, S.F. (2012) Macrophage polarization: an opportunity for improved outcomes in biomaterials and regenerative medicine. *Biomaterials*, **33**, 3792–3802.
- Brown, B.N., Valentin, J.E., Stewart-Akers, A.M., McCabe, G.P., & Badylak, S.F. (2009) Macrophage phenotype and remodeling outcomes in response to biologic scaffolds with and without a cellular component. *Biomaterials*, **30**, 1482–1491.
- Brugmans, M.M.C.P., Driessen-Mol, A., Rubbens, M.P., Cox, M.A.J., & Baaijens, F.P.T. (2013) Poly-ε-caprolactone scaffold and reduced in vitro cell culture: beneficial effect on compaction and improved valvular tissue formation. *J. Tissue Eng. Regen. Med.*,
- Butcher, J.T., Mahler, G.J., & Hockaday, L. a (2011) Aortic valve disease and treatment: the need for naturally engineered solutions. *Adv. Drug Deliv. Rev.*, **63**, 242–268.
- Butcher, J.T. & Nerem, R.M. (2006) Valvular endothelial cells regulate the phenotype of interstitial cells in co-culture: effects of steady shear stress. *Tissue Eng.*, **12**, 905–915.
- Caplan, A.I. (2007) Adult mesenchymal stem cells for tissue engineering versus regenerative medicine. *J. Cell. Physiol.*, **213**, 341–347.
- Capoccia, B.J., Gregory, A.D., & Link, D.C. (2008) Recruitment of the inflammatory subset of monocytes to sites of ischemia induces angiogenesis in a monocyte chemoattractant protein-1-dependent fashion. *J. Leukoc. Biol.*, **84**, 760–768.

- Cesarone, C.F., Bolognesi, C., & Santi, L. (1979) Improved microfluorometric DNA determination in biological material using 33258 Hoechst. *Anal. Biochem.*, **100**, 188–197.
- Chan, J.R., Hyduk, S.J., & Cybulsky, M.I. (2001) Chemoattractants induce a rapid and transient upregulation of monocyte alpha4 integrin affinity for vascular cell adhesion molecule 1 which mediates arrest: an early step in the process of emigration. *J. Exp. Med.*, **193**, 1149–1158.
- Chang, M.Y., Chan, C.K., Braun, K.R., Green, P.S., O'Brien, K.D., Chait, A., Day, A.J., & Wight, T.N. (2012) Monocyte-to-macrophage differentiation: synthesis and secretion of a complex extracellular matrix. *J. Biol. Chem.*, **287**, 14122–14135.
- Charoenpanich, A., Wall, M.E., Tucker, C.J., Andrews, D.M.K., Lalush, D.S., & Lobo, E.G. (2011) Microarray analysis of human adipose-derived stem cells in three-dimensional collagen culture: osteogenesis inhibits bone morphogenetic protein and Wnt signaling pathways, and cyclic tensile strain causes upregulation of proinflammatory cytokine regulators. *Tissue Eng. Part A*, **17**, 2615–2627.
- Chen, L., Tredget, E.E., Wu, P.Y.G., & Wu, Y. (2008) Paracrine factors of mesenchymal stem cells recruit macrophages and endothelial lineage cells and enhance wound healing. *PLoS One*, **3**, e1886.
- Choon Hwai Yap, Hee-Sun Kim, Kartik Balachandran, Michael Weiler, Rami Haj-Ali, A.P.Y. (2010) Dynamic deformation characteristics of porcine aortic valve leaflet under normal and hypertensive conditions. *Am. J. ...*, 395–405.
- Cochain, C., Rodero, M.P., Vilar, J., Récalde, A., Richart, A.L., Loinard, C., Zougari, Y., Guérin, C., Duriez, M., Combadière, B., Poupel, L., Lévy, B.I., Mallat, Z., Combadière, C., & Silvestre, J.-S. (2010) Regulation of monocyte subset systemic levels by distinct chemokine receptors controls post-ischaemic neovascularization. *Cardiovasc. Res.*, **88**, 186–195.
- Colazzo, F., Sarathchandra, P., Smolenski, R.T., Chester, A.H., Tseng, Y.-T., Czernuszka, J.T., Yacoub, M.H., & Taylor, P.M. (2011) Extracellular matrix production by adipose-derived stem cells: implications for heart valve tissue engineering. *Biomaterials*, **32**, 119–127.
- Cros, J., Cagnard, N., Woollard, K., Patey, N., Zhang, S.-Y., Senechal, B., Puel, A., Biswas, S.K., Moshous, D., Picard, C., Jais, J.-P., D'Cruz, D., Casanova, J.-L., Trouillet, C., & Geissmann, F. (2010) Human CD14^{dim} monocytes patrol and sense nucleic acids and viruses via TLR7 and TLR8 receptors. *Immunity*, **33**, 375–386.
- d'Arcy, J.L., Prendergast, B.D., Chambers, J.B., Ray, S.G., & Bridgewater, B. (2011) Valvular heart disease: the next cardiac epidemic. *Heart*, **97**, 91–93.
- Dankers, P.Y.W., Harmsen, M.C., Brouwer, L. a, van Luyn, M.J. a, & Meijer, E.W. (2005) A modular and supramolecular approach to bioactive scaffolds for tissue engineering. *Nat. Mater.*, **4**, 568–574.
- De Valence, S., Tille, J.-C., Mugnai, D., Mrowczynski, W., Gurny, R., Möller, M., & Walpoth, B.H. (2012) Long term performance of polycaprolactone vascular grafts in a rat abdominal aorta replacement model. *Biomaterials*, **33**, 38–47.
- Deshmane, S.L., Kremlev, S., Amini, S., & Sawaya, B.E. (2009) Monocyte chemoattractant protein-1 (MCP-1): an overview. *J. Interferon Cytokine Res.*, **29**, 313–326.

Bibliography

- Di Nicola, M., Carlo-Stella, C., Magni, M., Milanese, M., Longoni, P.D., Matteucci, P., Grisanti, S., & Gianni, A.M. (2002) Human bone marrow stromal cells suppress T-lymphocyte proliferation induced by cellular or nonspecific mitogenic stimuli. *Blood*, **99**, 3838–3843.
- Dijkman, P.E., Driessen-Mol, A., Frese, L., Hoerstrup, S.P., & Baaijens, F.P.T. (2012) Decellularized homologous tissue-engineered heart valves as off-the-shelf alternatives to xeno- and homografts. *Biomaterials*, **33**, 4545–4554.
- Djouad, F., Plence, P., Bony, C., Tropel, P., Apparailly, F., Sany, J., Noël, D., & Jorgensen, C. (2003) Immunosuppressive effect of mesenchymal stem cells favors tumor growth in allogeneic animals. *Blood*, **102**, 3837–3844.
- Driessen-Mol, A., Emmert, M.Y., Dijkman, P.E., Frese, L., Sanders, B., Weber, B., Cesarovic, N., Sidler, M., Leenders, J., Jenni, R., Grünenfelder, J., Falk, V., Baaijens, F.P.T., & Hoerstrup, S.P. (2013) Transcatheter implantation of homologous “off-the-shelf” tissue engineered heart valves with self-repair capacity: long term functionality and rapid in vivo remodeling in sheep. *J. Am. Coll. Cardiol.*,
- Emmert, M.Y., Weber, B., Behr, L., Frauenfelder, T., Brokopp, C.E., Grünenfelder, J., Falk, V., & Hoerstrup, S.P. (2011) Transapical aortic implantation of autologous marrow stromal cell-based tissue-engineered heart valves: first experiences in the systemic circulation. *JACC. Cardiovasc. Interv.*, **4**, 822–823.
- Emmert, M.Y., Weber, B., Wolint, P., Behr, L., Sammut, S., Frauenfelder, T., Frese, L., Scherman, J., Brokopp, C.E., Templin, C., Grünenfelder, J., Zünd, G., Falk, V., & Hoerstrup, S.P. (2012) Stem cell-based transcatheter aortic valve implantation: first experiences in a pre-clinical model. *JACC. Cardiovasc. Interv.*, **5**, 874–883.
- Farndale, R.W., Buttle, D.J., & Barrett, a J. (1986) Improved quantitation and discrimination of sulphated glycosaminoglycans by use of dimethylmethylene blue. *Biochim. Biophys. Acta*, **883**, 173–177.
- Favre, J., Terborg, N., & Horrevoets, A.J.G. (2013) The diverse identity of angiogenic monocytes. *Eur. J. Clin. Invest.*, **43**, 100–107.
- Fioletta, E.S., Simonet, M., Smits, A.I.P.M., Baaijens, F.P.T., & Bouten, C.V.C. (2014) Differential response of endothelial and endothelial colony forming cells on electrospun scaffolds with distinct microfiber diameters. *Biomacromolecules*, **15**, 821–829.
- Fisher, S. a, Dorée, C., Brunskill, S.J., Mathur, A., & Martin-Rendon, E. (2013) Bone Marrow Stem Cell Treatment for Ischemic Heart Disease in Patients with No Option of Revascularization: A Systematic Review and Meta-Analysis. *PLoS One*, **8**, e64669.
- Franz, S., Rammelt, S., Scharnweber, D., & Simon, J.C. (2011) Immune responses to implants - a review of the implications for the design of immunomodulatory biomaterials. *Biomaterials*, **32**, 6692–6709.
- Freytes, D.O., Kang, J.W., Marcos-Campos, I., & Vunjak-Novakovic, G. (2013) Macrophages modulate the viability and growth of human mesenchymal stem cells. *J. Cell. Biochem.*, **114**, 220–229.
- Friedewald, V.E., Bonow, R.O., Borer, J.S., Carabello, B. a, Kleine, P.P., Akins, C.W., & Roberts, W.C. (2007) The Editor’s Roundtable: cardiac valve surgery. *Am. J. Cardiol.*, **99**, 1269–1278.

- Garg, K., Pullen, N. a, Oskeritzian, C. a, Ryan, J.J., & Bowlin, G.L. (2013) Macrophage functional polarization (M1/M2) in response to varying fiber and pore dimensions of electrospun scaffolds. *Biomaterials*, **34**, 4439–4451.
- Germani, A., Di Campli, C., Pompilio, G., Biglioli, P., & Capogrossi, M.C. (2009) Regenerative therapy in peripheral artery disease. *Cardiovasc. Ther.*, **27**, 289–304.
- Gerszten, R.E., Garcia-Zepeda, E.A., Lim, Y.C., Yoshida, M., Ding, H.A., Gimbrone, M.A., Luster, A.D., Lusinskas, F.W., & Rosenzweig, A. (1999) MCP-1 and IL-8 trigger firm adhesion of monocytes to vascular endothelium under flow conditions. *Nature*, **398**, 718–723.
- Gieni, R.S. & Hendzel, M.J. (2008) Mechanotransduction from the ECM to the genome: are the pieces now in place? *J. Cell. Biochem.*, **104**, 1964–1987.
- Godwin, J.W., Pinto, A.R., & Rosenthal, N. a (2013) Macrophages are required for adult salamander limb regeneration. *Proc. Natl. Acad. Sci. U. S. A.*, **110**, 9415–9420.
- Gonzalez-simon, A.L. & Eniola-adeso, O. (2012) *Engineering Biomaterials for Regenerative Medicine*. Springer New York, New York, NY.
- Gordon, S. & Taylor, P.R. (2005) Monocyte and macrophage heterogeneity. *Nat. Rev. Immunol.*, **5**, 953–964.
- Green, S.R., Han, K.H., Chen, Y., Almazan, F., Charo, I.F., Miller, Y.I., & Quehenberger, O. (2006) The CC chemokine MCP-1 stimulates surface expression of CX3CR1 and enhances the adhesion of monocytes to fractalkine/CX3CL1 via p38 MAPK. *J. Immunol.*, **176**, 7412–7420.
- Groh, M.E., Maitra, B., Szekely, E., & Koç, O.N. (2005) Human mesenchymal stem cells require monocyte-mediated activation to suppress alloreactive T cells. *Exp. Hematol.*, **33**, 928–934.
- Guyton, A.C. & Hall, J.E. (2000) *Textbook of Medical Physiology*, Textbook of medical physiology. Philadelphia.
- Halka, A.T., Turner, N.J., Carter, A., Ghosh, J., Murphy, M.O., Kirton, J.P., Kielty, C.M., & Walker, M.G. (2008) The effects of stretch on vascular smooth muscle cell phenotype in vitro. *Cardiovasc. Pathol.*, **17**, 98–102.
- Hamid, M.S., Sabbah, H.N., & Stein, P.D. (1986) Influence of stent height upon stresses on the cusps of closed bioprosthetic valves. *J. Biomech.*, **19**, 759–769.
- Hanson, S.E., King, S.N., Kim, J., Chen, X., Thibeault, S.L., & Hematti, P. (2011) The effect of mesenchymal stromal cell-hyaluronic acid hydrogel constructs on immunophenotype of macrophages. *Tissue Eng. Part A*, **17**, 2463–2471.
- Hatzistergos, K.E., Quevedo, H., Oskouei, B.N., Hu, Q., Feigenbaum, G.S., Margitich, I.S., Mazhari, R., Boyle, A.J., Zambrano, J.P., Rodriguez, J.E., Dulce, R., Pattany, P.M., Valdes, D., Revilla, C., Heldman, A.W., McNiece, I., & Hare, J.M. (2010) Bone marrow mesenchymal stem cells stimulate cardiac stem cell proliferation and differentiation. *Circ. Res.*, **107**, 913–922.
- Hibino, N., McGillicuddy, E., Matsumura, G., Ichihara, Y., Naito, Y., Breuer, C., & Shinoka, T. (2010) Late-term results of tissue-engineered vascular grafts in humans. *J. Thorac. Cardiovasc. Surg.*, **139**, 431–6, 436.e1–2.

Bibliography

- Hibino, N., Shinoka, T., Matsumura, G., Ikada, Y., Kurosawa, H., & Shin'oka, T. (2005) The tissue-engineered vascular graft using bone marrow without culture. *J. Thorac. Cardiovasc. Surg.*, **129**, 1064–1070.
- Hibino, N., Yi, T., Duncan, D.R., Rathore, A., Dean, E., Naito, Y., Dardik, A., Kyriakides, T., Madri, J., Pober, J.S., Shinoka, T., & Breuer, C.K. (2011) A critical role for macrophages in neovessel formation and the development of stenosis in tissue-engineered vascular grafts. *FASEB J.*, **25**, 4253–4263.
- Hristov, M., Schmitz, S., Nauwelaers, F., & Weber, C. (2012) A flow cytometric protocol for enumeration of endothelial progenitor cells and monocyte subsets in human blood. *J. Immunol. Methods*, **381**, 9–13.
- Huang, A.H. & Niklason, L.E. (2014) Engineering of arteries in vitro. *Cell. Mol. Life Sci.*,
- Huenecke, S., Behl, M., Fadler, C., Zimmermann, S.Y., Bochennek, K., Tramsen, L., Esser, R., Klarmann, D., Kamper, M., Sattler, A., von Laer, D., Klingebiel, T., Lehrnbecher, T., & Koehl, U. (2008) Age-matched lymphocyte subpopulation reference values in childhood and adolescence: application of exponential regression analysis. *Eur. J. Haematol.*, **80**, 532–539.
- Hume, P.S., He, J., Haskins, K., & Anseth, K.S. (2012) Strategies to reduce dendritic cell activation through functional biomaterial design. *Biomaterials*, **33**, 3615–3625.
- Huszar, G., Maiocco, J., & Naftolin, F. (1980) Monitoring of collagen and collagen fragments in chromatography of protein mixtures. *Anal. Biochem.*, **105**, 424–429.
- Hyduk, S.J. & Cybulsky, M.I. (2009) Role of alpha4beta1 integrins in chemokine-induced monocyte arrest under conditions of shear stress. *Microcirculation*, **16**, 17–30.
- Hynes, R.O. (2002) Integrins: bidirectional, allosteric signaling machines. *Cell*, **110**, 673–687.
- Ingersoll, M.A., Spanbroek, R., Lottaz, C., Gautier, E.L., Frankenberger, M., Hoffmann, R., Lang, R., Haniffa, M., Collin, M., Tacke, F., Habenicht, A.J.R., Ziegler-Heitbrock, L., & Randolph, G.J. (2010) Comparison of gene expression profiles between human and mouse monocyte subsets. *Blood*, **115**, e10–9.
- Jaipersad, A.S., Lip, G.Y.H., Silverman, S., & Shantsila, E. (2014) The role of monocytes in angiogenesis and atherosclerosis. *J. Am. Coll. Cardiol.*, **63**, 1–11.
- Jay, S.M., Shepherd, B.R., Andrejcsk, J.W., Kyriakides, T.R., Pober, J.S., & Saltzman, W.M. (2010) Dual delivery of VEGF and MCP-1 to support endothelial cell transplantation for therapeutic vascularization. *Biomaterials*, **31**, 3054–3062.
- Jonge, N. De, Foolen, J., Brugmans, M.C.P., & So, S.H.M. (2014) Degree of Scaffold Degradation Influences Collagen (re) Orientation in Engineered Tissues **00**, 1–11.
- Kajahn, J., Franz, S., Rueckert, E., Forstreuter, I., Hintze, V., Moeller, S., & Simon, J.C. (2012) Artificial extracellular matrices composed of collagen I and high sulfated hyaluronan modulate monocyte to macrophage differentiation under conditions of sterile inflammation. *Biomatter*, **2**, 226–236.
- Kim, J. & Hematti, P. (2009) Mesenchymal stem cell-educated macrophages: a novel type of alternatively activated macrophages. *Exp. Hematol.*, **37**, 1445–1453.

- Kinnaird, T., Stabile, E., Burnett, M.S., Shou, M., Lee, C.W., Barr, S., Fuchs, S., & Epstein, S.E. (2004) Local delivery of marrow-derived stromal cells augments collateral perfusion through paracrine mechanisms. *Circulation*, **109**, 1543–1549.
- Kobayashi, S.D., Voyich, J.M., Burlak, C., & DeLeo, F.R. (2005) Neutrophils in the innate immune response. *Arch. Immunol. Ther. Exp. (Warsz)*, **53**, 505–517.
- Koh, T.J. & DiPietro, L.A. (2011) Inflammation and wound healing: the role of the macrophage. *Expert Rev. Mol. Med.*, **13**, e23.
- Kränkell, N., Kuschnerus, K., Madeddu, P., Lüscher, T.F., & Landmesser, U. (2011) A novel flow cytometry-based assay to study leukocyte-endothelial cell interactions in vitro. *Cytometry. A*, **79**, 256–262.
- Kwon, Y.W., Heo, S.C., Jeong, G.O., Yoon, J.W., Mo, W.M., Lee, M.J., Jang, I.-H., Kwon, S.M., Lee, J.S., & Kim, J.H. (2013) Tumor necrosis factor- α -activated mesenchymal stem cells promote endothelial progenitor cell homing and angiogenesis. *Biochim. Biophys. Acta*, **1832**, 2136–2144.
- Langille, B.L. & O'Donnell, F. (1986) Reductions in arterial diameter produced by chronic decreases in blood flow are endothelium-dependent. *Science*, **231**, 405–407.
- Larsen, G., Spretz, R., & Velarde-Ortiz, R. (2004) Use of Coaxial Gas Jackets to Stabilize Taylor Cones of Volatile Solutions and to Induce Particle-to-Fiber Transitions. *Adv. Mater.*, **16**, 166–169.
- Laudanna, C. & Alon, R. (2006) Right on the spot. Chemokine triggering of integrin-mediated arrest of rolling leukocytes. *Thromb. Haemost.*, **95**, 5–11.
- Le Blanc, K., Frassoni, F., Ball, L., Locatelli, F., Roelofs, H., Lewis, I., Lanino, E., Sundberg, B., Bernardo, M.E., Remberger, M., Dini, G., Egeler, R.M., Bacigalupo, A., Fibbe, W., & Ringdén, O. (2008) Mesenchymal stem cells for treatment of steroid-resistant, severe, acute graft-versus-host disease: a phase II study. *Lancet*, **371**, 1579–1586.
- Le Blanc, K., Rasmusson, I., Sundberg, B., Götherström, C., Hassan, M., Uzunel, M., & Ringdén, O. (2004) Treatment of severe acute graft-versus-host disease with third party haploidentical mesenchymal stem cells. *Lancet*, **363**, 1439–1441.
- Leibovich, S.J. & Ross, R. (1975) The role of the macrophage in wound repair. A study with hydrocortisone and antimacrophage serum. *Am. J. Pathol.*, **78**, 71–100.
- Ley, K., Laudanna, C., Cybulsky, M.I., & Nourshargh, S. (2007) Getting to the site of inflammation: the leukocyte adhesion cascade updated. *Nat. Rev. Immunol.*, **7**, 678–689.
- Loerakker, S., Argento, G., Oomens, C.W.J., & Baaijens, F.P.T. (2013) Effects of valve geometry and tissue anisotropy on the radial stretch and coaptation area of tissue-engineered heart valves. *J. Biomech.*, **46**, 1792–1800.
- Madden, L.R., Mortisen, D.J., Sussman, E.M., Dupras, S.K., Fugate, J. a, Cuy, J.L., Hauch, K.D., Laflamme, M. a, Murry, C.E., & Ratner, B.D. (2010) Proangiogenic scaffolds as functional templates for cardiac tissue engineering. *Proc. Natl. Acad. Sci. U. S. A.*, **107**, 15211–15216.
- Maggini, J., Mirkin, G., Bognanni, I., Holmberg, J., Piazzón, I.M., Nepomnaschy, I., Costa, H., Cañones, C., Raiden, S., Vermeulen, M., & Geffner, J.R. (2010) Mouse bone marrow-derived mesenchymal stromal cells turn activated macrophages into a regulatory-like profile. *PLoS One*, **5**, e9252.

Bibliography

- Mantovani, A., Sica, A., Sozzani, S., Allavena, P., Vecchi, A., & Locati, M. (2004) The chemokine system in diverse forms of macrophage activation and polarization. *Trends Immunol.*, **25**, 677–686.
- Mantovani, A., Sozzani, S., Locati, M., Allavena, P., & Sica, A. (2002) Macrophage polarization: tumor-associated macrophages as a paradigm for polarized M2 mononuclear phagocytes. *Trends Immunol.*, **23**, 549–555.
- Marieb, E.N. (2001) *Human Anatomy and Physiology*, 5th editio. edn. San Franisco.
- Mascarenhas, J. V, Albayati, M.A., Shearman, C.P., & Jude, E.B. (2014) Peripheral Arterial Disease. *Endocrinol. Metab. Clin. North Am.*, **43**, 149–166.
- Matsumura, G., Hibino, N., Ikada, Y., Kurosawa, H., & Shinoka, T. (2003) Successful application of tissue engineered vascular autografts: clinical experience. *Biomaterials*, **24**, 2303–2308.
- Matsumura, G., Isayama, N., Matsuda, S., Taki, K., Sakamoto, Y., Ikada, Y., & Yamazaki, K. (2013) Long-term results of cell-free biodegradable scaffolds for in situ tissue engineering of pulmonary artery in a canine model. *Biomaterials*, **34**, 6422–6428.
- Matsumura, G., Ishihara, Y., Miyagawa-Tomita, S., Ikada, Y., Matsuda, S., Kurosawa, H., & Shinoka, T. (2006) Evaluation of tissue-engineered vascular autografts. *Tissue Eng.*, **12**, 3075–3083.
- Matsumura, G., Miyagawa-Tomita, S., Shin'oka, T., Ikada, Y., & Kurosawa, H. (2003) First evidence that bone marrow cells contribute to the construction of tissue-engineered vascular autografts in vivo. *Circulation*, **108**, 1729–1734.
- Matsumura, G., Nitta, N., Matsuda, S., Sakamoto, Y., Isayama, N., Yamazaki, K., & Ikada, Y. (2012) Long-term results of cell-free biodegradable scaffolds for in situ tissue-engineering vasculature: in a canine inferior vena cava model. *PLoS One*, **7**, e35760.
- Maus, U., Henning, S., Wenschuh, H., Mayer, K., Seeger, W., & Lohmeyer, J. (2002) Role of endothelial MCP-1 in monocyte adhesion to inflamed human endothelium under physiological flow. *Am. J. Physiol. Heart Circ. Physiol.*, **283**, H2584–91.
- Meier, L. a, Syedain, Z.H., Lahti, M.T., Johnson, S.S., Chen, M.H., Hebbel, R.P., & Tranquillo, R.T. (2014) Blood outgrowth endothelial cells alter remodeling of completely biological engineered grafts implanted into the sheep femoral artery. *J. Cardiovasc. Transl. Res.*, **7**, 242–249.
- Melgarejo, E., Medina, M.A., Sánchez-Jiménez, F., & Urdiales, J.L. (2009) Monocyte chemoattractant protein-1: a key mediator in inflammatory processes. *Int. J. Biochem. Cell Biol.*, **41**, 998–1001.
- Melief, S.M., Geutskens, S.B., Fibbe, W.E., & Roelofs, H. (2013) Multipotent stromal cells skew monocytes towards an anti-inflammatory interleukin-10-producing phenotype by production of interleukin-6. *Haematologica*, **98**, 888–895.
- Mol, A., Driessen, N.J.B., Rutten, M.C.M., Hoerstrup, S.P., Bouten, C.V.C., & Baaijens, F.P.T. (2005) Tissue engineering of human heart valve leaflets: a novel bioreactor for a strain-based conditioning approach. *Ann. Biomed. Eng.*, **33**, 1778–1788.
- Mol, A., Rutten, M.C.M., Driessen, N.J.B., Bouten, C.V.C., Zünd, G., Baaijens, F.P.T., & Hoerstrup, S.P. (2006) Autologous human tissue-engineered heart valves: prospects for systemic application. *Circulation*, **114**, I152–8.

- Mol, A., Smits, A.I.P.M., Bouten, C.V.C., & Baaijens, F.P.T. (2009) Tissue engineering of heart valves: advances and current challenges. *Expert Rev. Med. Devices*, **6**, 259–275.
- Mol, A., van Lieshout, M.I., Dam-de Veen, C.G., Neuenschwander, S., Hoerstrup, S.P., Baaijens, F.P.T., & Bouten, C.V.C. (2005) Fibrin as a cell carrier in cardiovascular tissue engineering applications. *Biomaterials*, **26**, 3113–3121.
- Moore, B.B., Kolodsick, J.E., Thannickal, V.J., Cooke, K., Moore, T.A., Hogaboam, C., Wilke, C.A., & Toews, G.B. (2005) CCR2-mediated recruitment of fibrocytes to the alveolar space after fibrotic injury. *Am. J. Pathol.*, **166**, 675–684.
- Mosser, D.M. & Edwards, J.P. (2008) Exploring the full spectrum of macrophage activation. *Nat. Rev. Immunol.*, **8**, 958–969.
- Mrówczyński, W., Mugnai, D., de Valence, S., Tille, J.-C., Khabiri, E., Cikirikcioglu, M., Möller, M., & Walpoth, B.H. (2013) Porcine carotid artery replacement with biodegradable electrospun poly-ε-caprolactone vascular prosthesis. *J. Vasc. Surg.*, 1–10.
- Nathan, C. (2008) Metchnikoff's Legacy in 2008. *Nat. Immunol.*, **9**, 695–698.
- Niu, J. & Kolattukudy, P.E. (2009) Role of MCP-1 in cardiovascular disease: molecular mechanisms and clinical implications. *Clin. Sci. (Lond.)*, **117**, 95–109.
- Otto, C.M. (2001) Clinical practice. Evaluation and management of chronic mitral regurgitation. *N. Engl. J. Med.*, **345**, 740–746.
- Palsson, B.O. & Bhatia, S.N. (2004) *Tissue Engineering*. Upper Saddle River.
- Patel, N.R., Bole, M., Chen, C., Hardin, C.C., Kho, A.T., Mih, J., Deng, L., Butler, J., Tschumperlin, D., Fredberg, J.J., Krishnan, R., & Koziel, H. (2012) Cell elasticity determines macrophage function. *PLoS One*, **7**, e41024.
- Pektok, E., Nottelet, B., Tille, J.-C., Gurny, R., Kalangos, A., Moeller, M., & Walpoth, B.H. (2008) Degradation and healing characteristics of small-diameter poly(ε-caprolactone) vascular grafts in the rat systemic arterial circulation. *Circulation*, **118**, 2563–2570.
- Pennel, T., Zilla, P., & Bezuidenhout, D. (2013) Differentiating transmural from transanastomotic prosthetic graft endothelialization through an isolation loop-graft model. *J. Vasc. Surg.*, **58**, 1053–1061.
- Pham, Q.P., Sharma, U., & Mikos, A.G. (2006) Electrospun poly(ε-caprolactone) microfiber and multilayer nanofiber/microfiber scaffolds: characterization of scaffolds and measurement of cellular infiltration. *Biomacromolecules*, **7**, 2796–2805.
- Pittenger, M.F., Mackay, a M., Beck, S.C., Jaiswal, R.K., Douglas, R., Mosca, J.D., Moorman, M. a, Simonetti, D.W., Craig, S., & Marshak, D.R. (1999) Multilineage potential of adult human mesenchymal stem cells. *Science*, **284**, 143–147.
- Polverini, P.J., Cotran, P.S., Gimbrone, M.A., & Unanue, E.R. (1977) Activated macrophages induce vascular proliferation. *Nature*, **269**, 804–806.
- Puissant, B., Barreau, C., Bourin, P., Clavel, C., Corre, J., Bousquet, C., Taureau, C., Cousin, B., Abbal, M., Laharrague, P., Penicaud, L., Casteilla, L., & Blancher, A. (2005) Immunomodulatory effect of

Bibliography

- human adipose tissue-derived adult stem cells: comparison with bone marrow mesenchymal stem cells. *Br. J. Haematol.*, **129**, 118–129.
- Rai, R., Tallawi, M., Grigore, A., & Boccaccini, A.R. (2012) Synthesis, properties and biomedical applications of poly(glycerol sebacate) (PGS): A review. *Prog. Polym. Sci.*, **37**, 1051–1078.
- Ratner, B.D. (2011) The biocompatibility manifesto: biocompatibility for the twenty-first century. *J. Cardiovasc. Transl. Res.*, **4**, 523–527.
- Reilkoff, R. a, Bucala, R., & Herzog, E.L. (2011) Fibrocytes: emerging effector cells in chronic inflammation. *Nat. Rev. Immunol.*, **11**, 427–435.
- Ren, C., Geng, R.-L., Ge, W., Liu, X.-Y., Chen, H., Wan, M.-R., & Geng, D.-Q. (2013) An Observational Study of Autologous Bone Marrow-Derived Stem Cells Transplantation in Seven Patients with Nervous System Diseases: A 2-Year Follow-Up. *Cell Biochem. Biophys.*.
- Ren, G., Zhang, L., Zhao, X., Xu, G., Zhang, Y., Roberts, A.I., Zhao, R.C., & Shi, Y. (2008) Mesenchymal stem cell-mediated immunosuppression occurs via concerted action of chemokines and nitric oxide. *Cell Stem Cell*, **2**, 141–150.
- Ren, G., Zhao, X., Zhang, L., Zhang, J., L'Huillier, A., Ling, W., Roberts, A.I., Le, A.D., Shi, S., Shao, C., & Shi, Y. (2010) Inflammatory cytokine-induced intercellular adhesion molecule-1 and vascular cell adhesion molecule-1 in mesenchymal stem cells are critical for immunosuppression. *J. Immunol.*, **184**, 2321–2328.
- Robbins, C.S. & Swirski, F.K. (2010) The multiple roles of monocyte subsets in steady state and inflammation. *Cell. Mol. Life Sci.*, **67**, 2685–2693.
- Roh, J.D., Sawh-Martinez, R., Brennan, M.P., Jay, S.M., Devine, L., Rao, D. a, Yi, T., Mirensky, T.L., Nalbandian, A., Udelsman, B., Hibino, N., Shinoka, T., Saltzman, W.M., Snyder, E., Kyriakides, T.R., Pober, J.S., & Breuer, C.K. (2010) Tissue-engineered vascular grafts transform into mature blood vessels via an inflammation-mediated process of vascular remodeling. *Proc. Natl. Acad. Sci. U. S. A.*, **107**, 4669–4674.
- Sacks, M.S., Merryman, W.D., & Schmidt, D.E. (2009) On the biomechanics of heart valve function. *J. Biomech.*, **42**, 1804–1824.
- Safar, M.E. (2010) Arterial aging--hemodynamic changes and therapeutic options. *Nat. Rev. Cardiol.*, **7**, 442–449.
- Saino, E., Focarete, M.L., Gualandi, C., Emanuele, E., Cornaglia, A.I., Imbriani, M., & Visai, L. (2011) Effect of electrospun fiber diameter and alignment on macrophage activation and secretion of proinflammatory cytokines and chemokines. *Biomacromolecules*, **12**, 1900–1911.
- Sales, V.L., Mettler, B. a, Lopez-Illasaca, M., Johnson, J. a, & Mayer, J.E. (2007) Endothelial progenitor and mesenchymal stem cell-derived cells persist in tissue-engineered patch in vivo: application of green and red fluorescent protein-expressing retroviral vector. *Tissue Eng.*, **13**, 525–535.
- Schmidt, A., Ladage, D., Schinköthe, T., Klausmann, U., Ulrichs, C., Klinz, F.-J., Brixius, K., Arnhold, S., Desai, B., Mehlhorn, U., Schwinger, R.H.G., Staib, P., Addicks, K., & Bloch, W. (2006) Basic fibroblast growth factor controls migration in human mesenchymal stem cells. *Stem Cells*, **24**, 1750–1758.

- Schober, A. & Zerneck, A. (2007) Chemokines in vascular remodeling. *Thromb. Haemost.*, **97**, 730–737.
- Schober, A., Zerneck, A., Liehn, E. a, von Hundelshausen, P., Knarren, S., Kuziel, W. a, & Weber, C. (2004) Crucial role of the CCL2/CCR2 axis in neointimal hyperplasia after arterial injury in hyperlipidemic mice involves early monocyte recruitment and CCL2 presentation on platelets. *Circ. Res.*, **95**, 1125–1133.
- Schoen, F.J. (2012) Mechanisms of function and disease of natural and replacement heart valves. *Annu. Rev. Pathol.*, **7**, 161–183.
- Segers, V.F.M. & Lee, R.T. (2011) Biomaterials to enhance stem cell function in the heart. *Circ. Res.*, **109**, 910–922.
- Serbina, N. V & Pamer, E.G. (2006) Monocyte emigration from bone marrow during bacterial infection requires signals mediated by chemokine receptor CCR2. *Nat. Immunol.*, **7**, 311–317.
- Shantsila, E., Tapp, L.D., Wrigley, B.J., Montoro-García, S., & Lip, G.Y.H. (2013) CXCR4 positive and angiogenic monocytes in myocardial infarction. *Thromb. Haemost.*, **109**, 255–262.
- Shantsila, E., Wrigley, B., Tapp, L., Apostolakis, S., Montoro-Garcia, S., Drayson, M.T., & Lip, G.Y.H. (2011) Immunophenotypic characterization of human monocyte subsets: possible implications for cardiovascular disease pathophysiology. *J. Thromb. Haemost.*, **9**, 1056–1066.
- Shi, C. & Pamer, E.G. (2011) Monocyte recruitment during infection and inflammation. *Nat. Rev. Immunol.*, **11**, 762–774.
- Shi, Y., Su, J., Roberts, A.I., Shou, P., Rabson, A.B., & Ren, G. (2012) How mesenchymal stem cells interact with tissue immune responses. *Trends Immunol.*, **33**, 136–143.
- Shinoka, T., Matsumura, G., Hibino, N., Naito, Y., Watanabe, M., Konuma, T., Sakamoto, T., Nagatsu, M., & Kurosawa, H. (2005) Midterm clinical result of tissue-engineered vascular autografts seeded with autologous bone marrow cells. *J. Thorac. Cardiovasc. Surg.*, **129**, 1330–1338.
- Shireman, P.K., Contreras-Shannon, V., Ochoa, O., Karia, B.P., Michalek, J.E., & McManus, L.M. (2007) MCP-1 deficiency causes altered inflammation with impaired skeletal muscle regeneration. *J. Leukoc. Biol.*, **81**, 775–785.
- Simon, P. (2003) Early failure of the tissue engineered porcine heart valve SYNERGRAFT™ in pediatric patients. *Eur. J. Cardio-Thoracic Surg.*, **23**, 1002–1006.
- Simonet, M., Stingelin, N., Wismans, J.G.F., Oomens, C.W.J., Driessen-Mol, A., & Baaijens, F.P.T. (2014) Tailoring the void space and mechanical properties in electrospun scaffolds towards physiological ranges. *J. Mater. Chem. B*, **2**, 305.
- Skrzeczyńska-Moncznik, J., Bzowska, M., Loseke, S., Grage-Griebenow, E., Zembala, M., & Pryjma, J. (2008) Peripheral blood CD14^{high} CD16⁺ monocytes are main producers of IL-10. *Scand. J. Immunol.*, **67**, 152–159.
- Smits, A., Driessen-Mol, A., Bouten, C.V.C., & Baaijens, F.P.T. (2012) A mesofluidics-based test platform for systematic development of scaffolds for in situ cardiovascular tissue engineering. *Tissue Eng. Part C Methods*, **18**, 1–34.

Bibliography

- Sordi, V., Malosio, M.L., Marchesi, F., Mercalli, A., Melzi, R., Giordano, T., Belmonte, N., Ferrari, G., Leone, B.E., Bertuzzi, F., Zerbini, G., Allavena, P., Bonifacio, E., & Piemonti, L. (2005) Bone marrow mesenchymal stem cells express a restricted set of functionally active chemokine receptors capable of promoting migration to pancreatic islets. *Blood*, **106**, 419–427.
- Soulis, J. V., Farmakis, T.M., Giannoglou, G.D., & Louridas, G.E. (2006) Wall shear stress in normal left coronary artery tree. *J. Biomech.*, **39**, 742–749.
- Spaeth, E.L., Dembinski, J.L., Sasser, A.K., Watson, K., Klopp, A., Hall, B., Andreeff, M., & Marini, F. (2009) Mesenchymal stem cell transition to tumor-associated fibroblasts contributes to fibrovascular network expansion and tumor progression. *PLoS One*, **4**, e4992.
- Spiller, D., Mirtelli, C., Losi, P., Briganti, E., Sbrana, S., Counoupas, S., Kull, S., Tonlorenzi, S., & Soldani, G. (2009) In vitro evaluation of the PETU-PDMS material immunocompatibility: the influence of surface topography and PDMS content. *J. Mater. Sci. Mater. Med.*, **20**, 2511–2520.
- Talacua, H., Smits, A.I.P.M., Muylaert, D.E.P., van Rijswijk, J.W., Vink, A., Verhaar, M.C., Driessen-Mol, A., van Herwerden, L.A., Bouten, C.V.C., Kluin, J., & Baaijens, F.P.T. (2014) Improved in situ tissue engineering of functional small-diameter arteries by circulating cells mediated by Monocyte Chemotactic Protein-1. *Prep.*.
- Tendera, M., Aboyans, V., Bartelink, M.-L., Baumgartner, I., Clément, D., Collet, J.-P., Cremonesi, A., De Carlo, M., Erbel, R., Fowkes, F.G.R., Heras, M., Kownator, S., Minar, E., Ostergren, J., Poldermans, D., Rimbau, V., Roffi, M., Röther, J., Sievert, H., van Sambeek, M., & Zeller, T. (2011) ESC Guidelines on the diagnosis and treatment of peripheral artery diseases: Document covering atherosclerotic disease of extracranial carotid and vertebral, mesenteric, renal, upper and lower extremity arteries: the Task Force on the Diagnosis and Treatm. *Eur. Heart J.*, **32**, 2851–2906.
- Thevenot, P.T., Baker, D.W., Weng, H., Sun, M.-W., & Tang, L. (2011) The pivotal role of fibrocytes and mast cells in mediating fibrotic reactions to biomaterials. *Biomaterials*, **32**, 8394–8403.
- Thevenot, P.T., Nair, A.M., Shen, J., Lotfi, P., Ko, C.-Y., & Tang, L. (2010) The effect of incorporation of SDF-1alpha into PLGA scaffolds on stem cell recruitment and the inflammatory response. *Biomaterials*, **31**, 3997–4008.
- Throm Quinlan, A.M., Sierad, L.N., Capulli, A.K., Firstenberg, L.E., & Billiar, K.L. (2011) Combining dynamic stretch and tunable stiffness to probe cell mechanobiology in vitro. *PLoS One*, **6**, e23272.
- Tsou, C., Peters, W., Si, Y., Slaymaker, S., Aslanian, A.M., Weisberg, S.P., Mack, M., & Charo, I.F. (2007) Critical roles for CCR2 and MCP-3 in monocyte mobilization from bone marrow and recruitment to inflammatory sites. *J. Clin. Invest.*, **117**, 902–909.
- Tsujioka, H., Imanishi, T., Ikejima, H., Kuroi, A., Takarada, S., Tanimoto, T., Kitabata, H., Okochi, K., Arita, Y., Ishibashi, K., Komukai, K., Kataiwa, H., Nakamura, N., Hirata, K., Tanaka, A., & Akasaka, T. (2009) Impact of heterogeneity of human peripheral blood monocyte subsets on myocardial salvage in patients with primary acute myocardial infarction. *J. Am. Coll. Cardiol.*, **54**, 130–138.
- Uccelli, A., Moretta, L., & Pistoia, V. (2008) Mesenchymal stem cells in health and disease. *Nat. Rev. Immunol.*, **8**, 726–736.

- Udelsman, B., Hibino, N., Villalona, G.A., McGillicuddy, E., Nieponice, A., Sakamoto, Y., Matsuda, S., Vorp, D.A., Shinoka, T., & Breuer, C.K. (2011) Development of an operator-independent method for seeding tissue-engineered vascular grafts. *Tissue Eng. Part C. Methods*, **17**, 731–736.
- Van Andel, C.J., Pisteccky, P. V. & Borst, C. (2003) Mechanical properties of porcine and human arteries: implications for coronary anastomotic connectors. *Ann. Thorac. Surg.*, **76**, 58–64; discussion 64–5.
- Van der Laan, A.M., Ter Horst, E.N., Delewi, R., Begieneman, M.P. V, Krijnen, P.A.J., Hirsch, A., Lavaei, M., Nahrendorf, M., Horrevoets, A.J., Niessen, H.W.M., & Piek, J.J. (2013) Monocyte subset accumulation in the human heart following acute myocardial infarction and the role of the spleen as monocyte reservoir. *Eur. Heart J.*,
- Van Loon, S.L.M., Smits, A.I.P.M., Driessen-Mol, A., Baaijens, F.P.T., & Bouten, C.V.C. (2013) The immune response in in situ tissue engineering of aortic heart valves. In Aikawa, E. (ed), *Calcific Aortic Valve Disease*. InTech, Rijeka, pp. 207–245.
- Vandesompele, J., De Preter, K., Pattyn, F., Poppe, B., Van Roy, N., De Paepe, A., & Speleman, F. (2002) Accurate normalization of real-time quantitative RT-PCR data by geometric averaging of multiple internal control genes. *Genome Biol.*, **3**, research0034.1.
- Vesely, I. (1998) The role of elastin in aortic valve mechanics. *J. Biomech.*, **31**, 115–123.
- Vincentelli, A., Wautot, F., Juthier, F., Fouquet, O., Corseaux, D., Marechaux, S., Le Tourneau, T., Fabre, O., Susen, S., Van Belle, E., Mouquet, F., Decoene, C., Prat, A., & Jude, B. (2007) In vivo autologous recellularization of a tissue-engineered heart valve: are bone marrow mesenchymal stem cells the best candidates? *J. Thorac. Cardiovasc. Surg.*, **134**, 424–432.
- Volpe, S., Cameroni, E., Moepps, B., Thelen, S., Apuzzo, T., & Thelen, M. (2012) CCR2 acts as scavenger for CCL2 during monocyte chemotaxis. *PLoS One*, **7**, e37208.
- Wantha, S., Alard, J.-E., Megens, R.T.A., van der Does, A.M., Döring, Y., Drechsler, M., Pham, C.T.N., Wang, M.-W., Wang, J.-M., Gallo, R.L., von Hundelshausen, P., Lindbom, L., Hackeng, T., Weber, C., & Soehnlein, O. (2013) Neutrophil-derived cathelicidin promotes adhesion of classical monocytes. *Circ. Res.*, **112**, 792–801.
- Weber, B., Dijkman, P.E., Scherman, J., Sanders, B., Emmert, M.Y., Grünenfelder, J., Verbeek, R., Bracher, M., Black, M., Franz, T., Kortsmid, J., Modregger, P., Peter, S., Stampanoni, M., Robert, J., Kehl, D., van Doeselaar, M., Schweiger, M., Brokopp, C.E., Wälchli, T., Falk, V., Zilla, P., Driessen-Mol, A., Baaijens, F.P.T., & Hoerstrup, S.P. (2013) Off-the-shelf human decellularized tissue-engineered heart valves in a non-human primate model. *Biomaterials*, **34**, 7269–7280.
- Weber, B., Scherman, J., Emmert, M.Y., Gruenenfelder, J., Verbeek, R., Bracher, M., Black, M., Kortsmid, J., Franz, T., Schoenauer, R., Baumgartner, L., Brokopp, C., Agarkova, I., Wolint, P., Zund, G., Falk, V., Zilla, P., & Hoerstrup, S.P. (2011) Injectable living marrow stromal cell-based autologous tissue engineered heart valves: first experiences with a one-step intervention in primates. *Eur. Heart J.*, **32**, 2830–2840.
- Weber, K.S., von Hundelshausen, P., Clark-Lewis, I., Weber, P.C., & Weber, C. (1999) Differential immobilization and hierarchical involvement of chemokines in monocyte arrest and transmigration on inflamed endothelium in shear flow. *Eur. J. Immunol.*, **29**, 700–712.

Bibliography

- Willenborg, S., Lucas, T., van Loo, G., Knipper, J. a, Krieg, T., Haase, I., Brachvogel, B., Hammerschmidt, M., Nagy, A., Ferrara, N., Pasparakis, M., & Eming, S. a (2012) CCR2 recruits an inflammatory macrophage subpopulation critical for angiogenesis in tissue repair. *Blood*, **120**, 613–625.
- Williams, A.R. & Hare, J.M. (2011) Mesenchymal stem cells: biology, pathophysiology, translational findings, and therapeutic implications for cardiac disease. *Circ. Res.*, **109**, 923–940.
- Williams, D.F. (1987) European society for biomaterials, definitions in biomaterials. In Williams, D.F. (ed), *Proceeding of a Consensus Conference of the European Society for Biomaterial*. Elsevier, Chester, England.
- Wisse, E., Govaert, L.E., Meijer, H.E.H., & Meijer, E.W. (2006) Unusual Tuning of Mechanical Properties of Thermoplastic Elastomers Using Supramolecular Fillers. *Macromolecules*, **39**, 7425–7432.
- Wong, K.L., Tai, J.J.-Y., Wong, W.-C., Han, H., Sem, X., Yeap, W.-H., Kourilsky, P., & Wong, S.-C. (2011) Gene expression profiling reveals the defining features of the classical, intermediate, and nonclassical human monocyte subsets. *Blood*, **118**, e16–31.
- Wu, W., Allen, R.A.R.A., & Wang, Y. (2012) Fast-degrading elastomer enables rapid remodeling of a cell-free synthetic graft into a neoartery. *Nat. Med.*, **18**, 1148–1153.
- Xeltis (2014) World’s first study of spontaneous tissue growth technology [WWW Document].
- Yap, C.H., Saikrishnan, N., Tamilselvan, G., & Yoganathan, A.P. (2012) Experimental measurement of dynamic fluid shear stress on the aortic surface of the aortic valve leaflet. *Biomech. Model. Mechanobiol.*, **11**, 171–182.
- Yokota, T., Ichikawa, H., Matsumiya, G., Kuratani, T., Sakaguchi, T., Iwai, S., Shirakawa, Y., Torikai, K., Saito, A., Uchimura, E., Kawaguchi, N., Matsuura, N., & Sawa, Y. (2008) In situ tissue regeneration using a novel tissue-engineered, small-caliber vascular graft without cell seeding. *J. Thorac. Cardiovasc. Surg.*, **136**, 900–907.
- Yoo, K.H., Jang, I.K., Lee, M.W., Kim, H.E., Yang, M.S., Eom, Y., Lee, J.E., Kim, Y.J., Yang, S.K., Jung, H.L., Sung, K.W., Kim, C.W., & Koo, H.H. (2009) Comparison of immunomodulatory properties of mesenchymal stem cells derived from adult human tissues. *Cell. Immunol.*, **259**, 150–156.
- Zgair, A.K. (2012) The effect of high temperature on the kinetics of lipopolysaccharide (LPS)-induced human monocytes activity in vitro. *Cell. Immunol.*, **275**, 55–60.
- Ziegler-Heitbrock, L. (2007) The CD14+ CD16+ blood monocytes: their role in infection and inflammation. *J. Leukoc. Biol.*, **81**, 584–592.
- Ziegler-Heitbrock, L., Ancuta, P., Crowe, S., Dalod, M., Grau, V., Hart, D.N., Leenen, P.J.M., Liu, Y.-J., MacPherson, G., Randolph, G.J., Scherberich, J., Schmitz, J., Shortman, K., Sozzani, S., Strobl, H., Zembala, M., Austyn, J.M., & Lutz, M.B. (2010) Nomenclature of monocytes and dendritic cells in blood. *Blood*, **116**, e74–80.
- Zilla, P., Bezuidenhout, D., & Human, P. (2007) Prosthetic vascular grafts: wrong models, wrong questions and no healing. *Biomaterials*, **28**, 5009–5027.

Nederlandse samenvatting

Er zijn verscheidene methodes ontwikkeld volgens het zogenaamde *tissue engineering* principe om cardiovasculaire implantaten te produceren die in staat zijn tot integratie en regeneratie in het menselijk lichaam. Binnen het principe van tissue engineering is er een nieuw en klinisch relevant concept voor de vervanging van cardiovasculaire defecten in ontwikkeling waarbij het immuunsysteem van de patient gestimuleerd wordt om een bioafbreekbare synthetische prothese, al dan niet voorgezaaid met lichaamseigen cellen, succesvol in het lichaam te laten integreren, het zogenaamde *in situ* tissue engineering. Het doel van dit proefschrift is om een beter inzicht te verkrijgen in het reguleren van de immuunrespons door de mechanische belastingen die bepaalde cardiovasculaire weefsels, zoals hartkleppen en arteriën, dragen. Er is hierbij specifiek onderzocht wat de effecten zijn van rek en schuifspanning op de aantrekking, differentiatie en signalering van immuuncellen in synthetische protheses.

Monocyte Chemotactic Protein-1 (MCP-1) is een signaaleiwit dat wordt gezien als een van de hoofdpersonen in de regeneratie van synthetische protheses. Het eerste deel van dit proefschrift is erop gericht om de respons van specifieke immuuncellen in de bloedbaan op een prothese geladen met MCP-1 uit te lichten. Door gebruik te maken van migratie assays hebben we aangetoond dat MCP-1 selectief pro-angiogene en reparatieve monocyt en fibrocyten aantrekt. In een pulsatiele vloeistofstroom, daarentegen, zagen we wel een initiële toename van monocyt en, maar was er geen duidelijke selectiviteit in de aangetrokken monocyte subpopulaties. Dit suggereert dat de selectiviteit in de aantrekking van dergelijke cellen afhankelijk is van de snelheid waarmee het MCP-1 uit de prothese afgescheiden wordt, aangezien dit in een pulsatiele vloeistofstroom, na de initiële golf van MCP-1, overstemd wordt door de schuifspanning.

Na het bestuderen van de aantrekking van cellen, hebben we ons gericht op het effect van cyclische rek op de aangetrokken cellen in de prothese. Daarbij hebben we gebruik gemaakt van de mononucleaire celfractie uit humaan perifeer bloed, ofwel PBMC, als zijnde een bron van immuuncellen representatief voor de cellen die een synthetische prothese in het lichaam infiltreren. Deze PBMC werden gezaaid op electrogesponnen protheses van polycaprolactone (PCL) en vervolgens onderworpen aan cyclische rekken in het FlexCell® reksysteem. We hebben aangetoond dat de PBMC in het prothesemateriaal differentiëren naar macrofagen en dat gematigde rek (onder de 7%) de polarisatie van deze macrofagen naar een anti-inflammatoir, pro-wondgenezingstype stimuleert. Deze

resultaten suggereren dat macrofaagpolarisatie gecontroleerd kan worden door de mechanische eigenschappen van het prothesemateriaal, en daarmee de resulterende rekbelasting, aan te passen.

Het is aangetoond dat de infiltratie van monocyte-afgeleide macrofagen verbeterd wordt door het opnemen van lichaamseigen cellen in een synthetische prothese voor de implantatie. Het mechanisme dat hieraan ten grondslag ligt is echter niet bekend. In het laatste deel van dit proefschrift hebben we voorgezaaide cellen in de synthetische protheses opgenomen om de signaalfactoren die een rol spelen in de immuunrespons en wondgenezing en die uitgescheiden worden door deze cellen onder invloed van fysiologische rek en schuifspanning, te identificeren. We hebben aangetoond dat humane mesenchymale stamcellen (MSC) gezaaid in een PCL-gebaseerde prothese verantwoordelijk zijn voor de synthese van de eiwitten MCP-1, *Vascular Endothelial Growth Factor* (VEGF) en *basic Fibroblast Growth Factor* (bFGF) en dat deze synthese niet beïnvloed wordt door rekbelasting. Daarbij werd er een synergetische toename in bFGF synthese geobserveerd als de MSC blootgesteld werden aan circulerende PBMC in een pulsatiele vloeistofstroming. Vergelijkbaar hieraan vertoonde de expressie van het gen *Stromal cell-Derived Factor-1 α* (SDF-1 α), een factor die belangrijk is voor wondgenezing, een synergetische toename in MSC die blootgesteld waren aan PBMC.

Ter conclusie kunnen we stellen dat de factoren MCP-1, SDF-1 α en bFGF een veelbelovende en voorname rol spelen in het sturen van de immuunrespons. Voor het produceren van a-cellulaire synthetische protheses zouden deze factoren derhalve als bioactieve componenten opgenomen kunnen worden in de prothese, mits de snelheid waarmee de factoren afgescheiden worden op de plek van implantatie nauwkeurig gereguleerd kunnen worden in samenspel met de effecten ten gevolge van schuifspanning. Daarnaast is het raadzaam de mechanische eigenschappen van de prothese zo af te stemmen dat aangetrokken cellen blootgesteld worden aan gematigde rekbelasting (ongeveer 7%). De resultaten behaald in dit proefschrift dragen bij aan de verder ontwikkeling van instructieve synthetische protheses voor *in situ* regeneratieve therapieën voor cardiovasculaire weefsels.

Acknowledgements

As a modern poet used to sing, dedication and devotion are prerequisites for any commitment in the walk of life, and a significant dose of both was needed to get this thesis done. But since the most important tasks in human life cannot be accomplished by a single person, my personal effort would have been fruitless without the help of several people, and now it is the time to thank them.

The first people I wish to acknowledge are my promoters, Frank and Carlijn, who gave me the chance to join their group and supported my research with both practical and intellectual means. I will always be grateful to you for the freedom and trust you granted me during these years, being always available when I needed your advice. Frank, I owe you special thanks for encouraging me to stick to my Italian roots and to keep practicing my gesture skills.

Anita, working with you has been pleasant from the first moment and, over these years, I have been learning a lot from you about science, heart valves, statistics and kindness. You have been a brilliant mentor. Moniek, thanks for your help in and out of the Cellab, all the fruitful discussions and the short, but intense period in which you were my supervisor. Sandra, I deeply appreciated your last-minute help, my manuscript definitely gained an increased value after your numerical touch!

The STBE group offers such a great environment to talk about science, that it made sustainable even the meetings on Monday morning, with a little help from the coffee of the Mate corner. But what made really unique my time at TUE is the legendary 4.12 office: with the old glories and the new members, it is always the place to be on the 4th floor. Thanks for the candies, cakes, borrels, uitjes and concerts (hup Seasons, hup!).

After all the time spent together, many colleagues have inevitably become friends and the person that better embodies this overlay is Anthal(e). Music, football and beer have always been our glue. Way before becoming my lab-mate, you have been my foosball buddy and a precious guide into the peculiar beauty of the Dutch culture. Together with Linda(ke) and Daphne, you took me to the exotic Volendam and the beautiful beaches of Schiermonnikoog (I can maybe write it, but still cannot pronounce it!). Now only the mystery of Limburg is waiting to be unveiled by our group of adventurers.

Manu, you have been the most trustworthy friend I could imagine. We have been sharing office, cabinets, lunches and hotel rooms for so long, establishing new records of non-stop chatting. You and Valerio offered me shelter and food (much food!) when I was in

Acknowledgements

need and staying with you always feels like home. You have been great friends and travel companions and I wish you all the best for the big step(s)!

The due credits should be given also to the people that made these years in Eindhoven just great. First of all my housemates and neighbours, that lived happily in the beautiful mansion of NS29&31. Because of you, I have never felt alone and my knowledge of fashion, salsa, skating, electronic music, Mediterranean cuisine, Sicilian and Piemontese dialects has extremely improved. Dani, friendship sometimes can be a struggle, but in our case I believe it is totally worth it. Rubi, I have been missing our herbal-tea-night-chats and the white tissue debris on the carpet of the third floor (or maybe not: nostalgia can play bad tricks to the mind sometimes). Agny, coming across such a generous and tolerant person is a rare fortune: thanks for your patience and contagious positivity. Rocco, from Eindhoven to Basilicata, our paths are insolubly linked and I hope they will keep on crossing. Anna, our sangria-sprinkled chats are still one of my favourite summer night dreams. Rugge, having you popping up at every party with my pin button on your jacket is a habit I would never like to break. Claudia, Chiara and Luca, our reunions get more and more complicated to arrange, but we still make memorable time out of them: thanks for always being there, we rock! Vale and Emma, no matter how far we are, I always feel you very close. Marc, Piz and Véro, when we started hanging out together we were young and full of energy. Now we tend to prefer cosy dinners, but Stratum is still out there waiting for us!

My family deserves special thanks for helping me laying the foundations for this thesis. Mamma e papà, la serenità che avete sempre costruito attorno a me e il solido supporto nella scelta di seguire i miei interessi sono stati un dono meraviglioso. Porzia, sorella tuttodore, sei la mia stella fissa: anche da lontano sei sempre la semplificatrice maxima della mia vita.

Albe, questa tesi è dedicata a te perché più di tutti hai contribuito alla sua stesura e finalizzazione, credendo in essa più di quanto ci abbia talvolta creduto io stessa. Se dovessi ringraziarti qui ed ora per la pazienza con cui hai affrontato gli ultimi mesi insieme, non basterebbe lo spazio che ho a disposizione e saresti costretto ad impaginare nuovamente la tesi, quindi te lo risparmierei. Mi impegno invece a starti accanto come lo sei stato tu a me, da sempre, with all my loving.

Curriculum vitae

Virginia Ballotta was born on November 30th, 1984 in Milan, Italy. After completing high school in 2003 at “Liceo Classico Niccolò Machiavelli” in Segrate, Italy, she studied Biomedical Engineering at Politecnico di Milano, Italy. In 2009, she graduated with a thesis based on the development of a bioreactor for vascular tissue engineering, in collaboration with the Mario Negri Institute for Pharmacological Research in Bergamo, Italy. From 2009, she started a PhD project at the Eindhoven University of Technology, the Netherlands, in the division of Soft Tissue Biomechanics and Engineering. Her research concerned the *in vitro* evaluation of substrates for *in situ* cardiovascular tissue engineering subjected to physiological stimuli. The results of her efforts within this topic are presented in this dissertation. Since 2014 she is employed as Research Engineer in the Orthopaedic Biomechanics department at TU/e.

List of publications

Ballotta V.*, Smits AIPM*, Driessen-Mol A, Bouten CVC, Baaijens FPT (2014) "Shear flow affects selective monocyte recruitment into MCP-1-loaded scaffolds". *Journal of Cellular and Molecular Medicine*. In press.

*these authors contributed equally

Ballotta V., Driessen-Mol A, Bouten CVC, Baaijens FPT (2014) "Strain-dependent modulation of macrophage polarization within scaffolds". *Biomaterials*, 35(18):4919-28.

Ballotta V.*, Smits A.I.P.M.*, Driessen-Mol A, Bouten CVC, Baaijens FPT (2014) "Synergistic protein secretion by mesenchymal stromal cells seeded in 3D scaffolds and circulating leukocytes in physiological flow". *Biomaterials*, 35(33):9100-13.

*these authors contributed equally